Tampere University

KABEER HUSSAIN SHAH

ELECTRICALLY CONTROLLED HYDRAULIC ROCK DRILL

Master of Science Thesis

Faculty of Engineering and Natural Sciences
Master's Degree Thesis
November 2018

ABSTRACT

KABEER HUSSAIN SHAH: ELECTRICALLY CONTROLLED HYDRAULIC ROCK DRILL
Tampere University
Master of Science Thesis, 61 pages, 12 Appendix pages
November 2018
Master's Degree Program in Hydraulics and Automation
Major: Fluid Power Automation
Examiner: Professor Seppo Tikkanen, Professor Kalevi Huhtala

Keywords: Hydraulics, Simulation, Rock drill, Percussion mechanism, Valve Controller

Epiroc Rock Drills AB is a recognized around the world as a leading manufacturer and supplier of mining machinery and tools for surface drilling and underground drilling operations. This thesis work is an investigative study to find the possibilities to use electric valves in current hydraulic rock drills. The primary requirement for this purpose is the modelling of a controller to regulate valve in a percussion mechanism. The controller should control the valve operation and also, piston motion by adjusting the piston stroke length. To model and implement the controller in a percussion mechanism, knowledge of the operation of valves in current rock drills is necessary. The other requirement is the simulation model of an electric valve to work along controller.

The master thesis has resulted in a conceptual design of an electrically controlled hydraulic rock drill. The design is based on the percussion mechanism of the rock drill. The functionality of the system has been proven in a simulation model, and possible operational range, efficiency and control strategy has been studied in several analysis.

The results of the simulation analysis agree with the specified requirements. Furthermore, these results point out the capability of the controller to operate valve, adjust piston stroke length and percussion pressure and the use of two input signals simultaneously for better control and performance of the percussion mechanism.

The recommendation on the basis of this investigative study is to thoroughly investigate the implementation of the controller in a current rock drill. If the system meets the specified requirements, it is recommended then to build the controller in order to further evaluate its capabilities.

PREFACE

I am thankful to ALLAH TA'ALA and Prophet Mohammad (SAW) for all of their blessings through my entire life. I am thankful to Epiroc for giving me the opportunity to work on this thesis, especially thankful to my supervisor *Maria Pettersson* for the guidance, support and availability during this work. I am also thankful to Prof. Seppo Tikkanen for supervising this thesis work.

I am very grateful to my *Baba g*, *parents, sister, Jabeer* and *Arif sab* for their endless support, encouragement and help in my life.

Örebro, 12.11.2018

Kabeer Hussain Shah

TABLE OF CONTENTS

LIST OF FIGURES

LIST OF SYMBOLS AND ABBREVIATIONS

Symbol	Quantity	SI-Units
a	Acceleration	[m/s^2]
F	Force	[N]
m	Piston Mass	[kg]
D_1	Diameter, piston	[m]
D_2	Diameter, piston	[m]
D_3	Diameter, piston	[m]
A_1	Piston driving Area from shank	[m^2]
A_2	Piston driving Area towards shank	[m^2]
v_1	Piston Backward velocity at valve switching	[m/s]
v_2	Piston Impact Velocity	[m/s]
P	Supply Pressure	[Pa]
x_p	Piston position	[m]
S	Piston Stroke	[m]
R	Rebound coefficient	[-]
z	Piston position at valve switching	[m]
z_2	Deceleration Motion	[m]
z_3	Piston position at valve switching before impact	[m]
z_4	Piston position at valve switching	[m]
v_3	Piston velocity at valve switching before impact	[m]
v_4	Piston velocity at valve switching	[m]
z_1	Piston position during valve delay	[m]
p_o	Pressure driving piston towards shank	[Pa]
p_u	Pressure driving piston from shank	[Pa]
ΔP	Pressure loss	[Pa]
ao	Valve opening between supply pressure and p_o	[m^2]
ra	Valve opening between Chamber A and Tank	[m^2]
au	Valve opening between p_u and tank pressure	[m^2]
ru	Valve opening between Chamber B and Tank	[m^2]
C_q	Flow Coefficient	[-]
ρ	rho, Fluid Density	[kg/m^3]
A_v	Maximum Opening area of the valve	[m^2]
t_d	Valve delay	[s]
t_1	Time taken by piston for backward motion (Ideal valve operation)	[s]
t_2	Time for deceleration motion (Ideal valve operation)	[s]
t_3	Time taken by piston to reach impact position (Ideal valve operation)	[s]
T_1	Time for piston backward motion before valve delay	[s]
T_2	Time for deceleration motion	[s]
T_3	Time to move piston towards shank before valve delay	[s]

1. INTRODUCTION

A hydraulic rock drill is used to generate sufficient amount of energy to break the rock. A piston repeatedly hits the drill string in a rock drill. The kinetic energy generated by the piston is converted into a stress wave transmitted to the drill string. The current hydraulic rock drill designs cannot provide the control of simultaneous frequency and energy. The concept of electrically controlled hydraulic rock drills can be a potential solution to this problem. This thesis work investigates the possibility to use electric valves in these rock drills to improve the controllability, performance and operational range of the rock drill. This can provide the opportunity to simultaneously control the energy and frequency of the rock drill.

1.1 Background

Epiroc Rock Drills AB is a globally recognized as a leading manufacturer and supplier of percussive rock drilling machinery for surface and underground applications. The current rock drills machines are based on hydraulic/mechanical feedback systems and their impact data is linked to the mechanics of the machine. The motion of the percussive piston in common rock drills is controlled hydro-mechanically by a valve.

Figure 1. *Epiroc Boomer 282 [1]*

To drill holes (ϕ 20-200mm), so-called percussive rock drilling is most commonly used. In a rock drill, a percussive piston is used to repeatedly hit the drill string. The kinematic energy is transformed to elastic energy, as a stress wave which propagates through the drill string towards the drill bit, where it is used to crush the rock. By rotating the drill bit, the inserted tungsten carbide buttons will crush the rock in a new position for each piston stroke. A hydraulic motor is used for the rotation, which is transferred through gears, acting at splines on the first part of the drill string, called the shank adapter. The rotation torque needed to overcome the forces at the bit and drill rod is also used to keep the threads on the drill string tightened.

1.2 Goals and Methods

The motion of the percussive piston in common rock drills is controlled hydro-mechanically by a valve. In this work the possibility to use electrically controlled valves is investigated. Can electrically controlled valve control the rock drill operation? The analytical investigation is required to derive the desired equations for the piston motion. These equations will be utilized in the development of controller. The desired controller will be used to control the operation of a percussion mechanism in a rock drill. The performance of the controller will be tested by using it in the simulation model of the rock drill. Performance concerning operational range, adjustable percussion energy and frequency and efficiency should be analyzed (using simulation). Simulation models of electrically controlled valves should be developed and used in a rock drill model. Possible operational range, efficiency and control strategy should be mapped. Also, the task involves the possibility of controlling both the frequency and energy.

1.3 Delimitations and Challenges

Percussive Rock Drills utilize four main functions (percussion, rotation, flushing, feed) while operating to crush a rock. The percussion mechanism consists of two main functions. First percussive motion used for the purpose of crushing the rock, while the other rotational motion of the drill rod to reposition the crushing tool. This thesis work focuses solely on the percussive motion while designing a controller for the rock drill. The controller is designed to match a general model of a rock drill. It should be adaptable for a range of different rock drills, but as a starting point for the simulation work done, a basic percussive model is built with values of the rock drill. One challenge is the availability of high-speed electric valves with high flow rates but Johannes et al. (2010) showed that the technology is fast approaching towards the availability of these valves. Also, the swift variations in noise levels and force due to rapid rise in pressure rates in hydraulically controlled solutions can be compensated by using fast speed on/off solenoid valves [12].

1.4 Approach to the Research

The first few weeks were spent familiarizing with the HOPSAN software ad studying the basic methodology of rock drilling theory and various rock drilling techniques. The functioning of the valve and its operation in the percussion mechanism was studied, and existing control strategies were analyzed using the simulation.

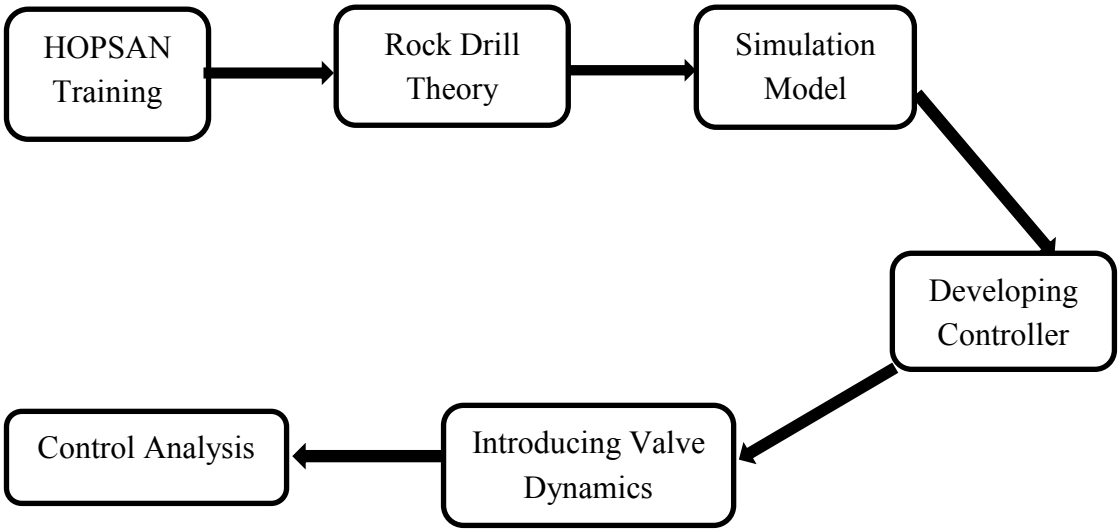

First phase was mostly about knowing the Hopsan software environment and libraries used by Epiroc to develop simulation models followed by the theory of current rock drills. The study involves the operation of the valve in the current rock drills, the control strategies of piston/valve motion, timing the motion of piston in relation to the valve openings and the stroke length settings. This knowledge is utilized to build a simulation model of a percussion mechanism to be used during the development of various controllers.

Theoretical valve switching positions can be derived by measuring piston position to obtain a desired striking velocity. The properties of solenoid valves were added to the model for investigation of the performance of the percussion mechanism. Control strategies to compensate for valve dynamics were developed. The possibility to control both frequency and energy of the system were also studied.

1.5 Outline

In chapter 1, background and limitations are described. The theory of the rock drills and percussion mechanism were discussed in the chapter 2. Chapter 3 presents the simulation model of the percussion mechanism and development of controller for valve operation. The chapter 4 consists of detailed analysis of the system using idealized valve operation and then using the valve dynamics and pressure losses to check system performance and limits. The modifications to the controller for having broader control strategies are mentioned in chapter 5 and the conclusion of the work is presented in chapter 6.

2. ROCK DRILLS: OVERVIEW

This chapter presents an overview of the rock drilling technology, the systems and functionality of a percussion mechanism in the rock drills.

2.1 General principle of Percussive Rock Drilling

Percussive rock drilling is most commonly used to drill holes (ϕ 20-200mm). In a rock drill, a percussive piston is used to continually hit the drill string. The reciprocating motion of the piston is carried out by a fluid pressure input to the two pressure areas. Each one of these areas are responsible for the corresponding back and forth motion of the piston. The valve is controlling the connections between these pressure areas, system pressure and return line. The piston strikes against the shank of the drill steel during each cycle and this striking is transmitted wholly or partially to the drill steel in the form of a compressive stress wave. This wave passes through the drill steel to the drill bit. The rock surface breaks with the application of a significantly high force. The debris, created as a result of crashed surface, is flushed out of the hole by a flushing fluid. This flushing fluid runs through an axial hole in the drill steel to the drill bit. [2]

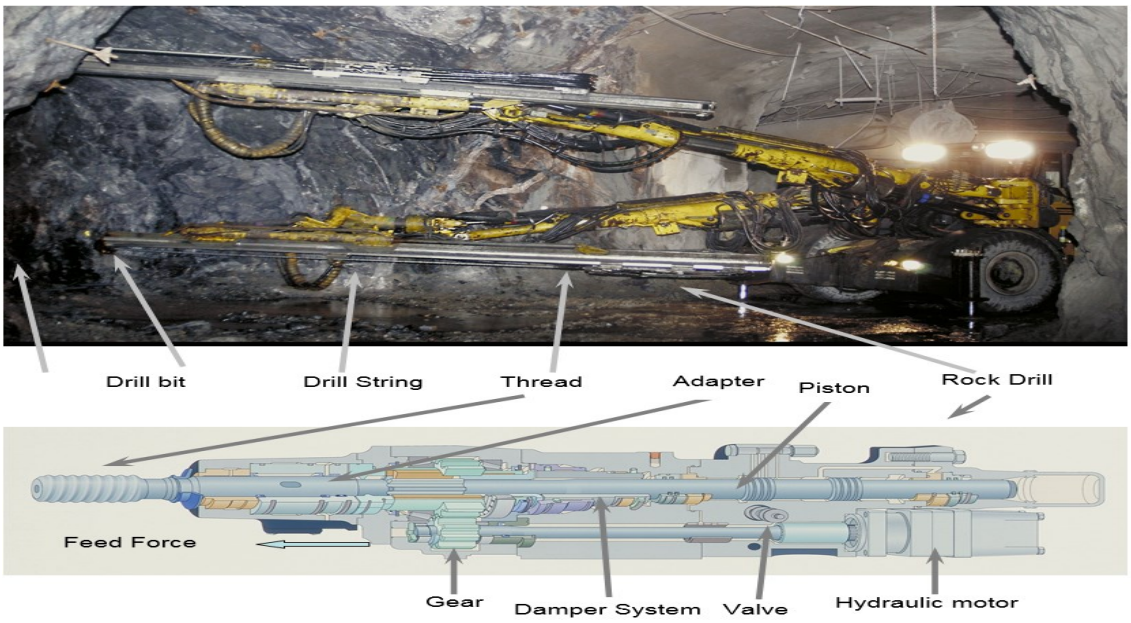

Figure 2. *Main Components in a Rock Drill [15]*

The figure 2 shows important parts in the drilling process. A valve-controlled piston hits the shank adapter that is connected to shank by using threads. A hydraulic motor is used for drill string rotation, acting at the shank through gears. A drill bit is connected to the end of the drill string. A feed cylinder or feed motor is used to move the rock drill and apply a suitable force at the bit acting on the rock. The damper system is used to transfer feed force to the drill string efficiently to make sure that the drill bit is in contact with the rock as efficiently as possible, and to make sure that the shank is at a correct position

when it is hit by the piston, and to protect the rock drill from reflected stresses from the rock [5]. Better controllability and less hole deviation can be attained for straight hole drilling with percussive drilling. [9]

It is important to mention the different percussive rock drilling techniques. The most common methods are Down the Hole (DTH), COPROD and Top Hammer drilling.

2.1.1 Down the Hole (DTH) Drilling

In this drilling technique, there is no drill steel existing in between the rock drill and the drill bit. A cylinder is pushed down the hole in which the rock drill is mounted. A rotation unit is responsible to rotate the drill bit and it is placed outside the hole. The pipes connected to the rock drill are transferring the rotation. Mostly DTH hammers are pneumatic driven and air is used for the purpose of rotation. The use of water as a medium for DTH hammers was investigated by Tuomas et al. (2000). The air functioning the percussion mechanism is directed through the drill bit, so it can flush the debris out of the hole. The benefit with this method is that no stress waves are passing threaded drill steel joints. The tube is rigid, stopping hole deviation. These sorts of hammers are used for holes larger than approximately 120 mm in diameter. [3]

2.1.2 Top Hammer Drilling

In this form of drilling, the rock drill is mounted on drill rig and the rock drill is linked to the drill bit via the drill steel. The drill steel is the source for the transmission of the impact energy and the rotation to the drill bit. The length of the drill steel increases with the increase in the depth of the hole, because of the threaded joints linked to each other. One problem with this system is the use of threads because there is a loss of effective impact energy in each joint due to the distortion of the shock waves. This energy loss can be comparatively greater in case of drilling deep holes using multiple joints. The friction energy generates enough heat to sternly damage the threads therefore it is advisable to properly tighten the joints. This generated heat can also be cause for any harm to the hardening of the steel. The drilling of holes with a maximum dimeter of approximately 140 mm is possible with this type of drilling [3].

2.1.3 COPROD Drilling

The percussive and rotation mechanism are separate in this technique, similar to the DTH drilling, while the rock drill is mounted on a drill rig. The impact energy is transmitted to the drill bit via a drill steel. The transfer of rotation motion is done with a pipe, which is fitted with the steel. An increase in the depth of the hole cause the several pipes to join with threads. The drill steels are arranged on top of each other inside the pipes. The advantage with this method is that the threads do not transfer the shock wave. The loss of

impact energy is smaller as compared to top hammer drilling. Another benefit is to have less hole deviation because the pipes transferring the rotation are stiffer as compared to top hammer drilling [3].

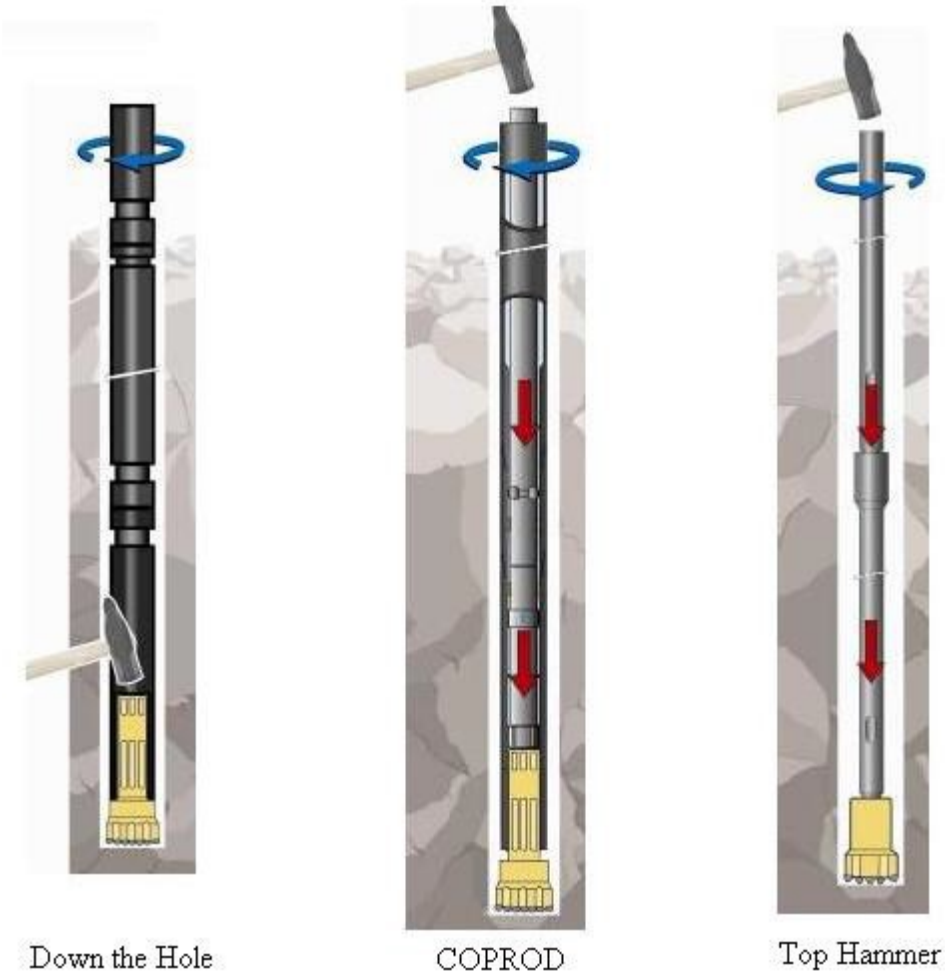

Figure 3. *Techniques of Percussive Rock drilling (a) Down the Hole (b) COPROD (c) Top Hammer [16]*

2.2 Percussion Mechanism

In top hammer drilling, the impact piston accelerates towards the shank adapter to generate the impact force. The shank adapter is connected to the drill steel with a thread joint [2]. The crushing of rock is done by the shock wave generated from the transmission of the impact via drill steel to the drill bit.

Typically, the acceleration distance of the impact piston is few centimeters. To achieve varying striking velocity, the stroke length can be adjusted. This can be done mechanically or hydraulically. The varying flowrate generates shock waves in the inlet and outlet hoses. Mounting pressure accumulators both at the inlet and outlet of the rock drill reduce

this problem. The cavitation problem can arise due to the rapid flowrate variations caused by rapid valve switching. Cavitation can cause leakage or breakdown of the rock drill. [4]

In percussive top-hammer drilling, energy is conveyed from the rock drill via the shank adapter, drill steel and drill bit to the rock, where it is used for crushing. The impact strikes the shank adapter normally 60 times per second, i.e. a frequency of 60 Hz. Impact energy can be defined here as the kinematic energy of one piston blow. The magnitude of the impact energy [J] is based upon the piston, its mass [kg] and blow velocity [m/s]. This is according to the kinematic energy equation $E = 0.5mv^2$. The power [W] equals energy per time unit [J/s], and is the product of energy and frequency, $P_{out} = E\ f$. The use of power magnitude can be puzzling, since a blend of high energy and low frequency can provide equally large power as low energy and high frequency does. In order to get high impact power of the rock drill machine, it is preferred to attain high frequency, but the installed pressure and flow must be adequate. A more concise opinion would be that the energy necessity originates from the rock properties (hardness, softness etc.) and the dimensions of the drilled hole. A higher frequency (and power) will offer high penetration rate as shown in figure 4.

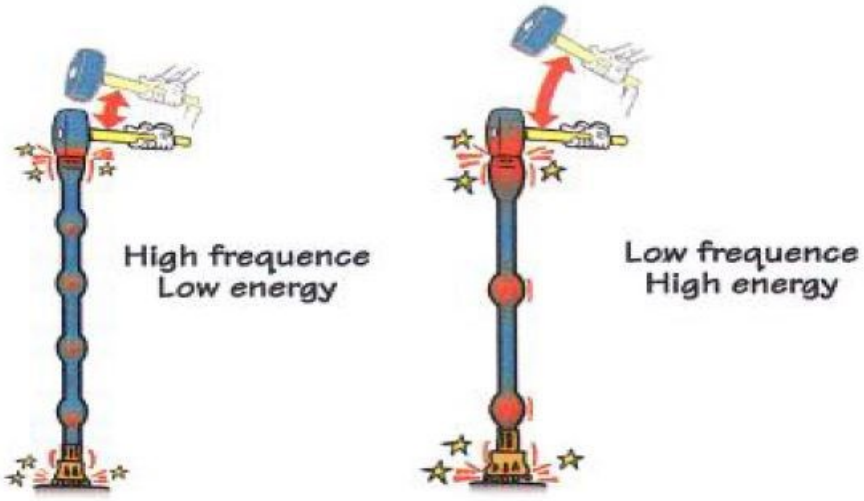

Figure 4. *Basic Principle of a Top Hammer Drill [17]*

3. MODELLING OF THE ROCK DRILL

The simulation model was developed to analyze the dynamic behavior of percussion mechanism. The model is developed in the simulation program HOPSAN, which is briefly described in the following section.

3.1 HOPSAN

Epiroc uses the simulation program HOPSAN (Hydraulisk Och Pneumatisk System Analys) to simulate hydraulic and mechanical systems. The program is developed at the division of Fluid and Mechatronic Systems at Linköping University. HOPSAN has several component libraries comprising of variety of components. It is also possible to develop new components using the programming language C++. [7]

3.2 Requirement Specification

The requirements specify the system functionality and design parameters. Epiroc Rock Drills AB specified all these requirements, and these must have to be taken into consideration for any future development.

The controller

I. Must be adaptable to a variety of rock drills of varying range.
II. Must be able to control the all openings of valves in the rock drill.
III. Must be able to handle percussion pressure variations.
IV. Must be able to control both energy and frequency of rock drill as an input to the machine.
V. Must be able to take into consideration the pressure losses across the valve openings.
VI. Must be able to handle the variations in the dynamic properties of the valve like delay, switching times, maximum velocities etc.

3.3 HOPSAN Model of Percussion Mechanism

This section presents the simulation model of the percussion mechanism and brief introduction of the components. The hydraulic circuit diagram (see figure 5) presents the modelled system. The supply pressure *Ps* is provided using a fixed displacement pump. The two valves 1 and 2 are connected to supply pressure source and two valves 3 and 4 are connected to the tank as shown in figure 6. The chamber A and B of the piston is pressurized using the valves 1, 4 and 2, 3 respectively. The controller is used to send control signal (*Uvalve)* to the valve for switching at their respective opening and closing positions.

Table 1. Components in Hydraulic Circuit Diagram

Sr. No.	Component Name
1,2,3,4.	2-way On-off Valve
5.	Reservoir
6.	Fixed Displacement Pump
7.	Double acting Piston

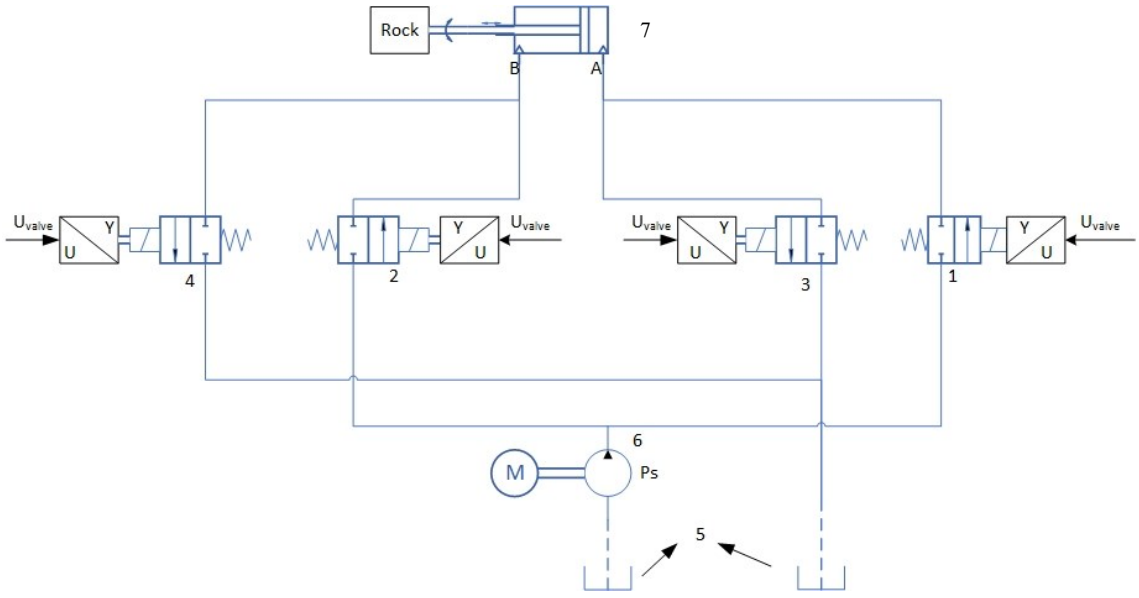

Figure 5. *Hydraulic Circuit Diagram of the modelled system*

Table 1 shows the descriptions of components used for developing the simulation model. A pressure source is providing the constant supply pressure Ps and the controller mechanism is operating the valve openings using the piston position as an input. An SR (Set-Reset) latch is used to control the openings of the valve in order to get the desired stroke of the piston. Valve dynamics consists of the valve properties i.e. delay and switching rate limiter to obtain a realistic valve operation. One end of percussion mechanism is attached to a fixed end while other side is striking the rock component. Figure 6 shows a Hopsan simulation model in which orifice I is opening the path (P→A), which is driving the piston towards the impact position and orifice II is opening the path (A→R) while the orifice III is opening the path (P→B), which is driving the piston in the backward direction and orifice IV is opening the path (B→R). The piston impact [2] on the drill steel is modelled using the following equation.

$$F = \frac{vEA_{ds}}{c\left(1 + \frac{A_{ds}}{A_p}\right)}$$

Where E is the young's modulus (E = 210 GPa), c is the wave velocity (c = 5200 m/s), A_{ds} is the area of the drill steel (A_{ds} = 12 cm^2), v and A_p are the piston impact velocity and piston impact area respectively.

The time required for the impact [2] can be found as

$$t = \frac{2L_p}{c} \quad for\ A_p \leq A_{ds}$$

Where L_p is the length of the piston (L_p = 0.6 m). The compressibility of the oil is 1600 MPa. The fluid channels are modelled as orifices using the equation [14]

$$Q = C_q A \sqrt{\frac{2 \cdot \Delta P}{\rho}}$$

Where A is the valve opening area. ρ is the fluid density (value 890 kg/m^3) and C_q is the flow coefficient (value 0.67).

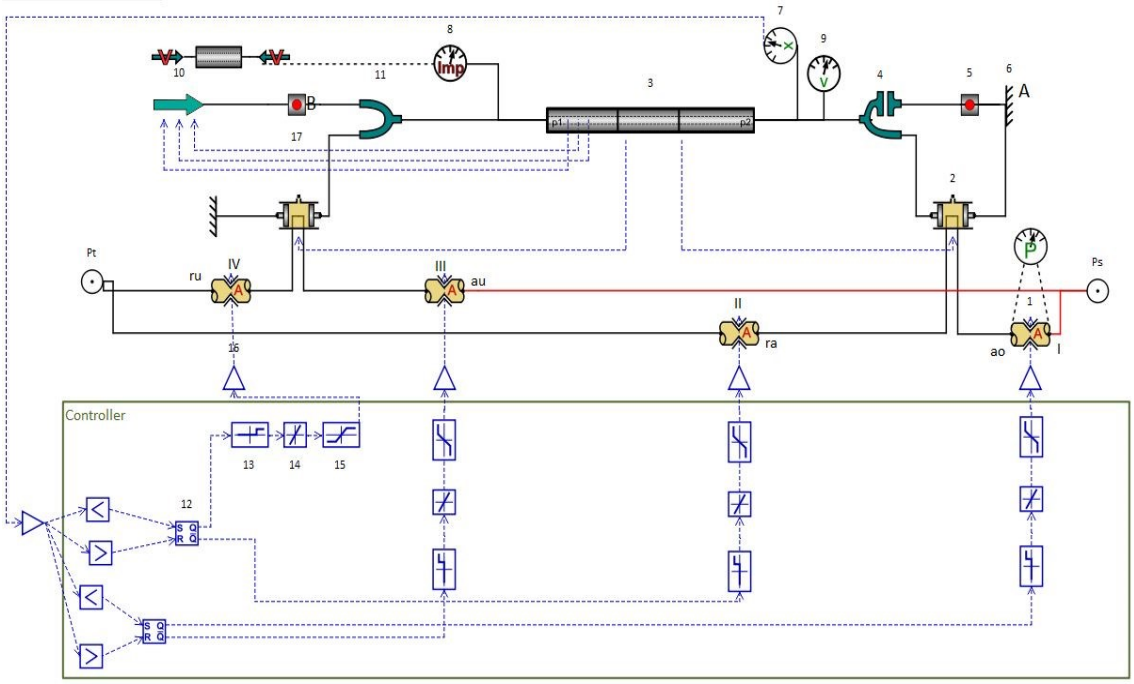

Figure 6. *Hopsan model of the Percussion Mechanism*

The driving areas of the piston are constant, and these areas are provided as an input value to the hydraulic volumes A and B and to the controller. There are four 2-way valves (see figure 6) used for pressurizing the both sides of the piston chambers such that two valves pressurize each piston chamber.

The following simplifications are made in the HOPSAN model:

i. Leakages of the valve are neglected

ii. Hoses are not part of this model

iii. The behaviour of the feed system is not part of this study

iv. Friction between piston and casing is not included in this investigation.

These simplifications are made to investigate the operation and performance of the controller. In this way, the operational limits for the individual properties of the valve dynamics (delay, switching times, and opening rate) with respect to the controller are investigated. It is possible to study the limitations of the modelled controller while controlling the valve operation.

Table 2. Components used in the HOPSAN model

Name	Description	Name	Description
ps	Supply Pressure	8	Impact Calculator
pt	Tank Pressure	9	Velocity Sensor
1	Orifice	10	Rock
2	Variable Volume	11	Connector
3	Piston	12	Logic Controller
4	Connector	13	Delay
5	Short bar	14	Rate Limiter
6	Fixed Position	15	Saturation
7	Position Sensor	16	Gain

3.4 Modelling Controller for Valve Operation

This section presents the modelling of a controller component to regulate the operation of valve in the percussion mechanism. The controller component is built in the programming language C++. The impact velocity is given to the controller as an input while the analytical equations for the piston backward velocity, piston positions for opening and closing of port areas and stroke of the piston will be derived and added to the controller.

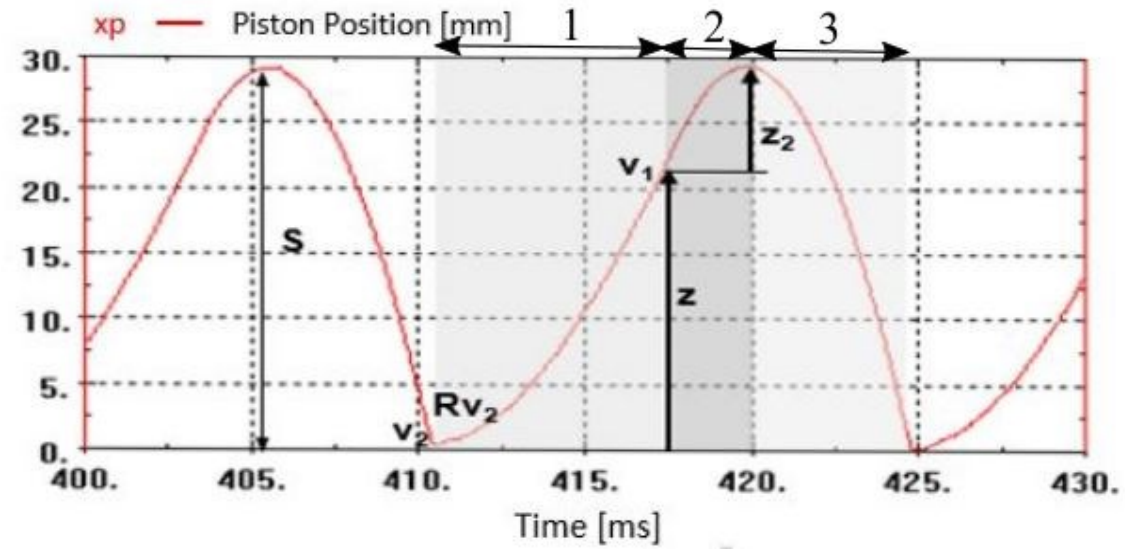

Figure 7. *Piston motion partitioning for valve switching positions*

The following steps will take place in the operation of the controller.

1. The piston starts moving backwards after impact with velocity Rv_2 and reaches maximum backward velocity (v_1) at piston position (z) (see marker 1 in figure 6). At this point the acceleration will be zero, and the areas *ao* and *ra* will be opened while areas *au* and *ru* will be closed (see figure 6).
2. The piston will decelerate from the piston position (z) to the minimum position of the piston and then starts to accelerate towards the maximum stroke position. This piston motion is denoted as z_2 (see marker 2 in figure 7).
3. The piston starts to move towards the impact position and it reaches the impact velocity v_2 (see marker 3 in figure 6). At that point, the areas *ao* and *ra* will close while the areas *au* and *ru* will open (see figure 6).

The piston position (*xp*), piston impact velocity (*vp*) and supply pressure (*Ps*) are the inputs to the controller. The controller calculates the switching position z and v_1 using the derived analytical equations. The ports PB and AR will be opened at the piston's impact position while ports PA and BR will remain closed. The condition for this position (in figure 8) shows that piston position and velocity become greater or equal to the maximum stroke position (*Xstroke*) and reference impact velocity (v_2) respectively. Similarly, the ports PA and BR will be opened at the piston's impact position while ports PB and AR will remain closed. The condition for this switching shows that piston position and velocity become less than or equal to the switching position z and backward velocity (v_1) respectively.

The time required by the piston motion, described in three steps above, must be calculated in order to find the frequency of the mechanism. The equations for the times t_1, t_2 and t_3 for steps 1, 2, and 3 will be derived and added to the controller. In this way, the striking frequency of the mechanism can be compared to the desired value.

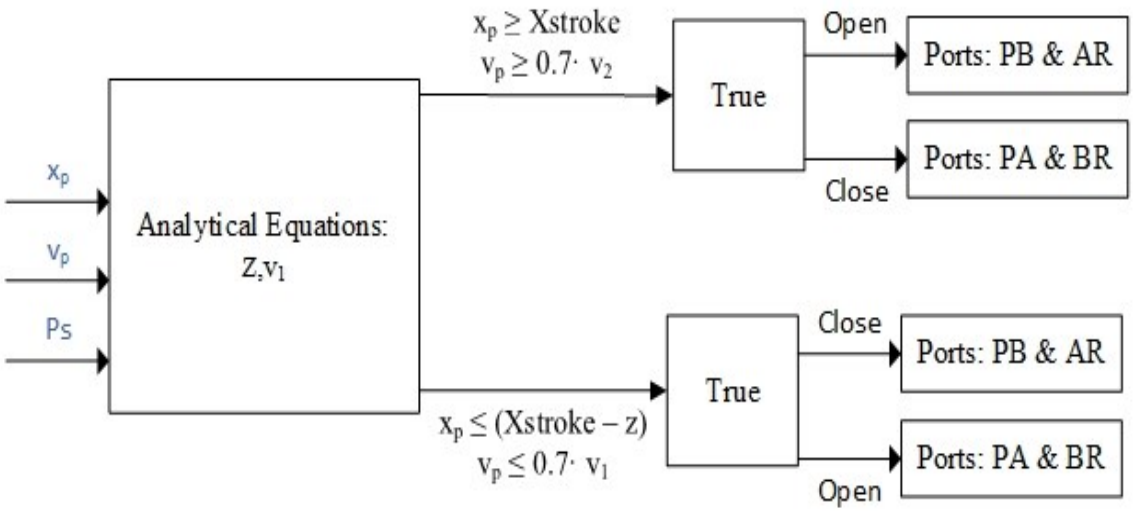

Figure 8. *Diagram of controller structure*

4. ANALYTICAL INVESTIGATION OF PISTON MOTION

The piston motion is divided into three parts as shown in the figure 9. The first part starts right after the stroke, where the piston bounces back and, in this case,, the starting velocity is Rv_2. R is the recoil coefficient, defined as the bouncing velocity divided by striking velocity. The second part begins when the piston reaches the maximum return speed (v_1) and ends when the piston start moving in opposite direction. In the last part, the piston accelerates to the stroke position where the speed is v_2. The piston motion takes place with constant acceleration and the pressure (P) acts on drive areas A_1 and A_2.

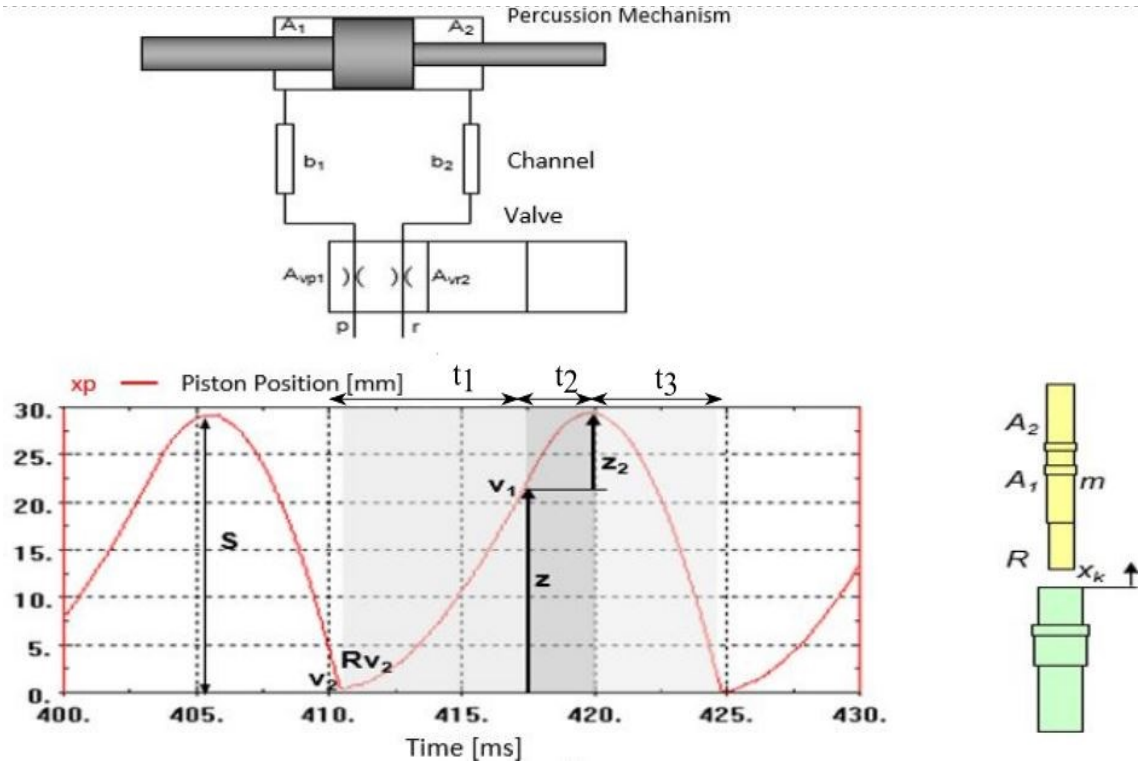

Figure 9. *Piston motion during the stroke in a percussion mechanism*

Newton's laws of motion for constant acceleration [6] in terms of motion from x to y can be written as

$$v_y = v_x + at_{xy} \qquad (1)$$

$$v_y^2 = v_x^2 + 2a(S_y - S_x) \qquad (2)$$

$$S_y - S_x = v_x t_{xy} + \frac{at_{xy}^2}{2} \qquad (3)$$

4.1 Analytical Modelling for Percussion Mechanism

The piston position at point z and maximum stroke position along with maximum return velocity v_1 and impact velocity v_2 are important parameters to know that can help to control the openings of valve. The Newton law can be written as equation (2)

$$v_y^2 = v_x^2 + 2a(S_y - S_x)$$

Start of piston return movement from $x_p = 0 \rightarrow z$

Using equation (2) gives

$$v_1^2 = (Rv_2)^2 + 2\frac{PA_1}{m}z$$

$$v_1 = \sqrt{(Rv_2)^2 + 2\frac{PA_1}{m}z} \qquad (4)$$

Using equation (1) gives

$$v_1 = Rv_2 + \frac{PA_1}{m}t_1$$

$$t_1 = \frac{m(v_1 - Rv_2)}{PA_1} \qquad (5)$$

Deceleration from $x_p = z \rightarrow z+z_2$

Using equation (2), we get

$$0 = v_1^2 - 2\frac{PA_2}{m}z_2$$

$$z_2 = \frac{mv_1^2}{2PA_2} \qquad (6)$$

Using equation (1) gives

$$0 = v_1 - \frac{PA_2}{m}t_2$$

$$t_2 = \frac{mv_1}{PA_2} \qquad (7)$$

Piston motion from start to stroke position, $x_p = z+z_2 \rightarrow 0$

Using equation (2) gives

$$v_2^2 - 0^2 = 2\frac{PA_2}{m}(z + z_2)$$

$$v_2 = \sqrt{\frac{2PA_2(z + z_2)}{m}} \qquad (8)$$

Equation (1) gives

$$v_2 = 0 + \frac{PA_2}{m}t_3$$

$$t_3 = \frac{mv_2}{PA_2} \qquad (9)$$

Solving equations 4, 5, 6, 7, 8 and 9, we will get the equations for stroke length, frequency, energy and power.

$$v_1 = \sqrt{\frac{2Pz(A_1 + R^2A_2)}{m(1 - R^2)}} \qquad (10)$$

Valve switching position:

$$z = \frac{mv_2^2(1 - R^2)}{2P(A_1 + A_2)} \qquad (11)$$

Stroke Length:

$$S = z + z_2 \qquad (12)$$

Frequency:

$$f = \frac{1}{t_1 + t_2 + t_3} \qquad (13)$$

Energy:

$$W = \frac{mv_2{}^2}{2} \qquad (14)$$

Power:

$$P = Wf \qquad (15)$$

In the case of an ideal valve, one of the switching points must coincide with the percussion position. Equations 4, 6 and 8 can be combined to find an expression for the other valve switching position z. Piston position must be measured and given as an input to the controller. Using the piston position, valve switching positions can be determined. The velocity is required because the switching at distance z can only be possible when the piston is moving from the shank. The pressure on both piston chambers is controlled by four valves. The orifice ao and ra control the flow from pressure source to chamber A and

chamber A to return line respectively while au and rb control the flow from pressure source to chamber B and chamber B to return line respectively.

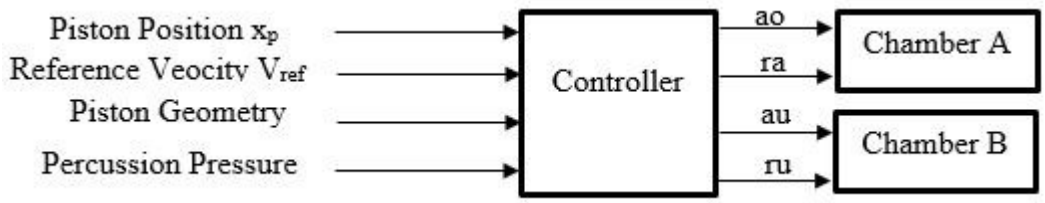

Figure 10. *Input and Output of the Controller*

4.2 Simulation of Piston Motion Using Idealized Valve Operation

The analytical derived expressions mentioned in section 3.1 will be used in this section to verify the results with the help of a Hopsan simulation model. The following parameters are used for the simulation.

Table 3. Simulation Parameters for the HOPSAN model

Type		**Value**	**Unit**
Maximum Piston Stroke Length	xp	120	mm
Piston Mass	M	6.1	kg
Piston Length	L	0.6	m
Piston Rebound Coefficient	R	0.1	-
Supply Pressure	Ps	220	bar
Tank Pressure	Pt	1	bar
Piston Diameter	D_1	42	mm
Piston Diameter	D_2	45	mm
Piston Diameter	D_3	38	mm
Piston Driving Area	A_1	205	mm^2
Piston Driving Area	A_2	456	mm^2

Piston driving area is calculated as

$$A_1 = \frac{\pi}{4} \cdot (D_2^2 - D_1^2)$$

$$A_2 = \frac{\pi}{4} \cdot (D_2^2 - D_3^2)$$

The simulation of the model at three desired impact velocities (6, 8 and 12 m/s) provides the results for the analysis of the system performance. The pressure will be kept constant during the simulation of the model.

4.2.1 Reference Impact Velocity 6 m/s

Figure 11 given below shows the simulation of piston motion at reference impact velocity 6 m/s and the achieved striking velocity was 5.9 m/s. The striking frequency and the striking energy generated was 95.7 Hz and 0.11 kJ respectively.

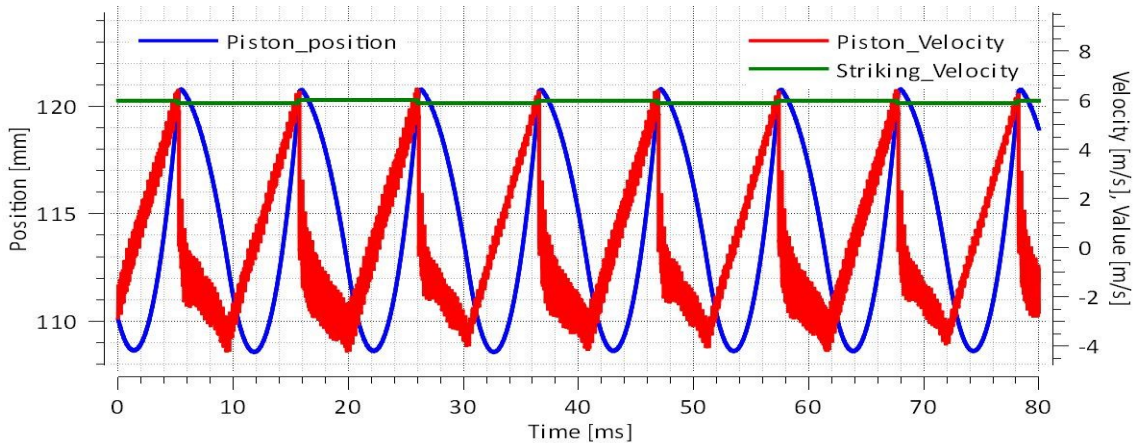

Figure 11. *Piston motion during the stroke along with the piston and striking velocity*

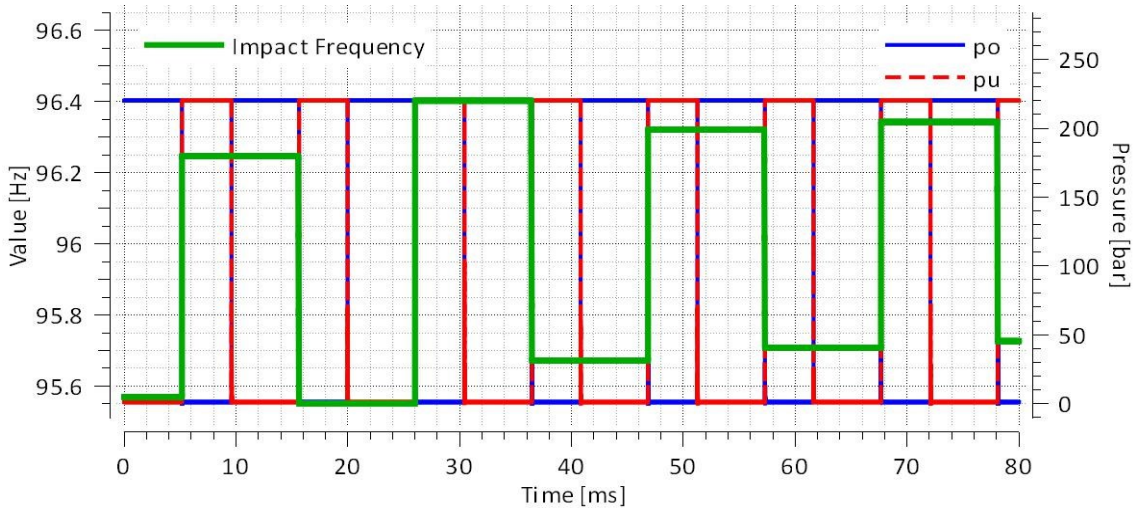

Figure 12. *Impact frequency and piston chamber pressures*

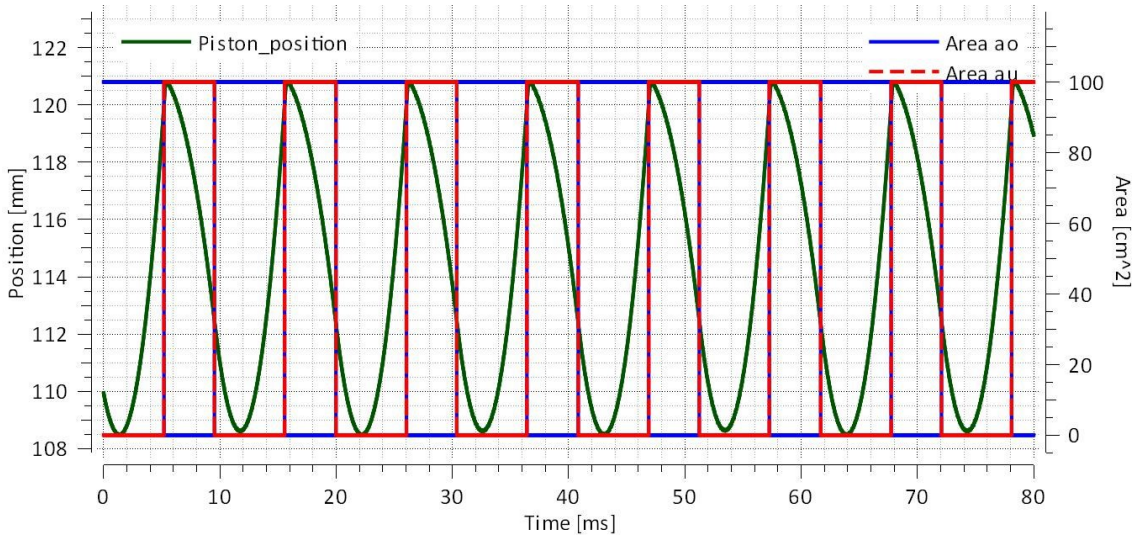

Figure 13. *Valve switching and piston position: ao valve opening between supply pressure and piston chamber A_2 & au valve opening between piston chamber A_1 and return pressure*

4.2.2 Reference Impact Velocity 8 m/s

Figure 14 given below shows the simulation of piston motion at reference impact velocity 8 m/s and the achieved striking velocity was 7.9 m/s. The striking frequency and the striking energy generated was 73.2 Hz and 0.192 kJ respectively. Also, the areas of the valve are opening and closing according to the controller input as shown in figure 16. The stroke length of the piston is 20.4 mm.

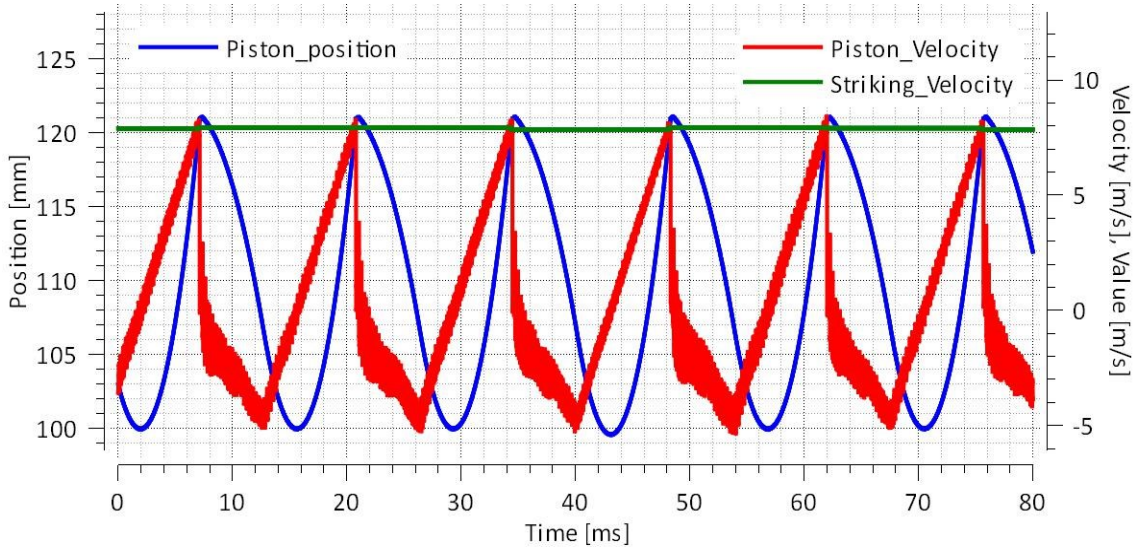

Figure 14. *Piston motion during the stroke along with the piston and striking velocity*

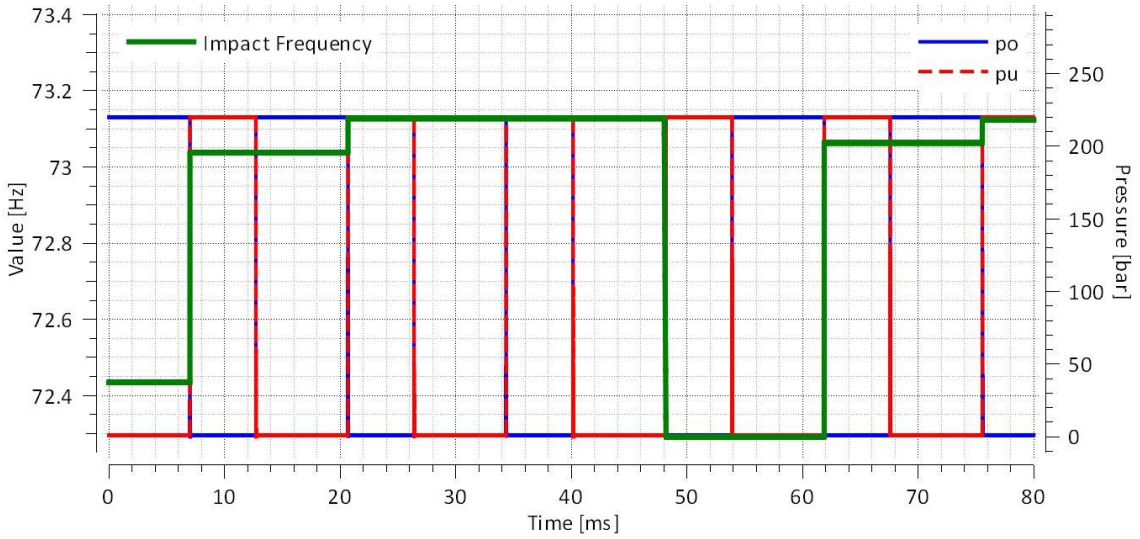

Figure 15. *Impact frequency and piston chamber pressures*

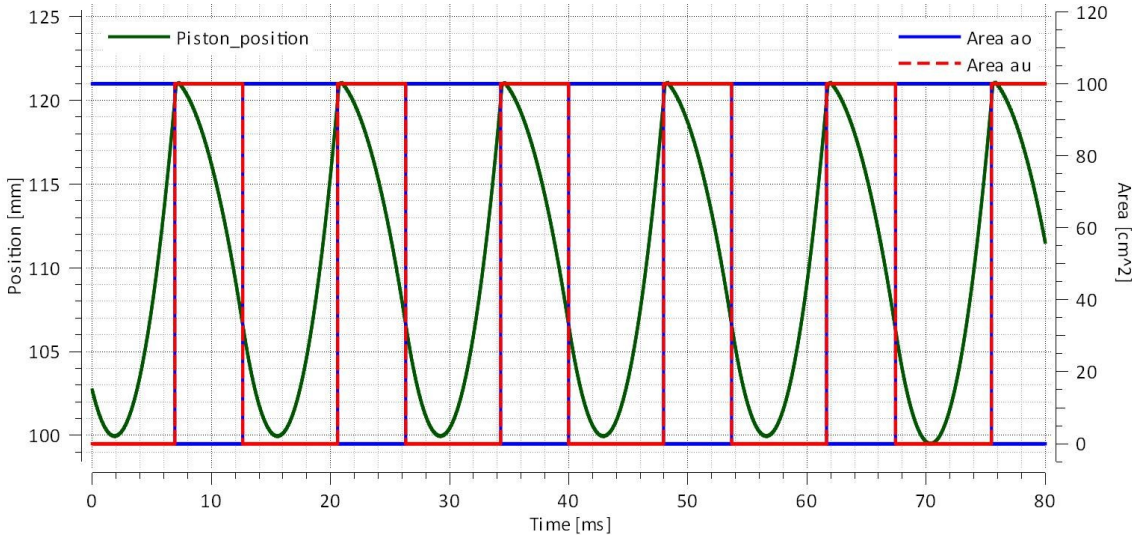

Figure 16. *Valve switching and piston positions: ao valve opening between supply pressure and piston chamber A_2 & au valve opening between piston chamber A_1 and return pressure*

4.2.3 Reference Impact Velocity 10 m/s

Figure 17 given below shows the simulation of piston motion at reference impact velocity 10 m/s and the achieved striking velocity was 9.91 m/s. The striking frequency and the striking energy generated was 58.96 Hz and 0.302 kJ respectively. Also, the areas of the valve are opening and closing according to the controller input as shown in figure 19. The stroke length of the piston is 31.18 mm.

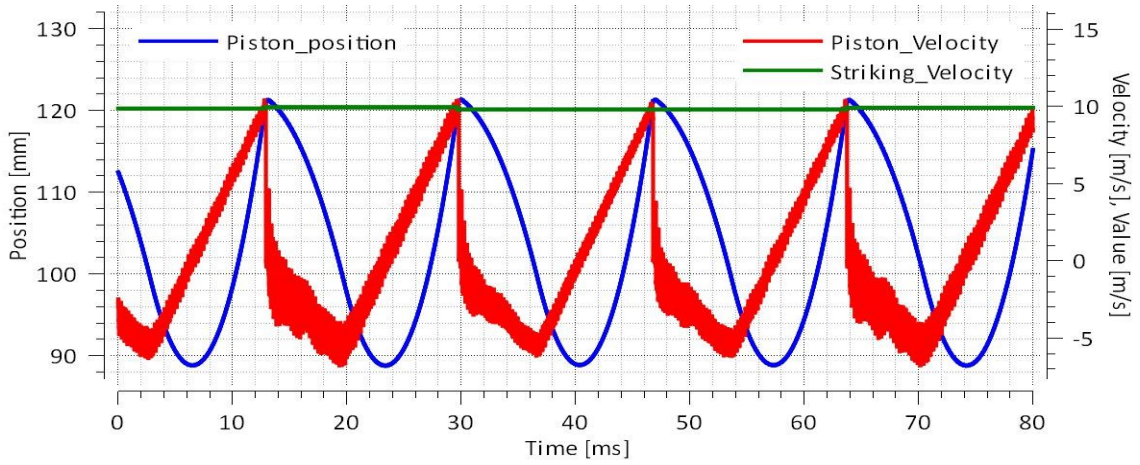

Figure 17. *Piston motion, piston velocity and striking velocity*

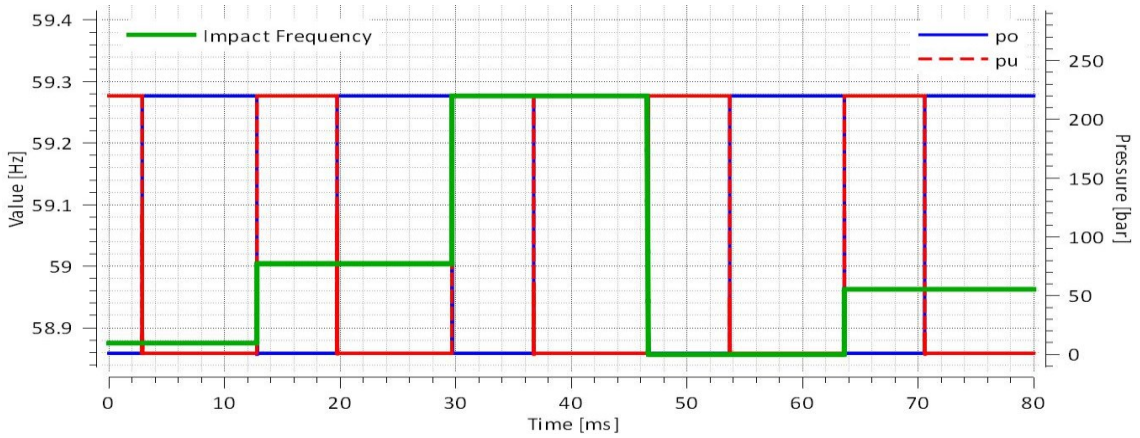

Figure 18. *Impact frequency and piston chamber pressures*

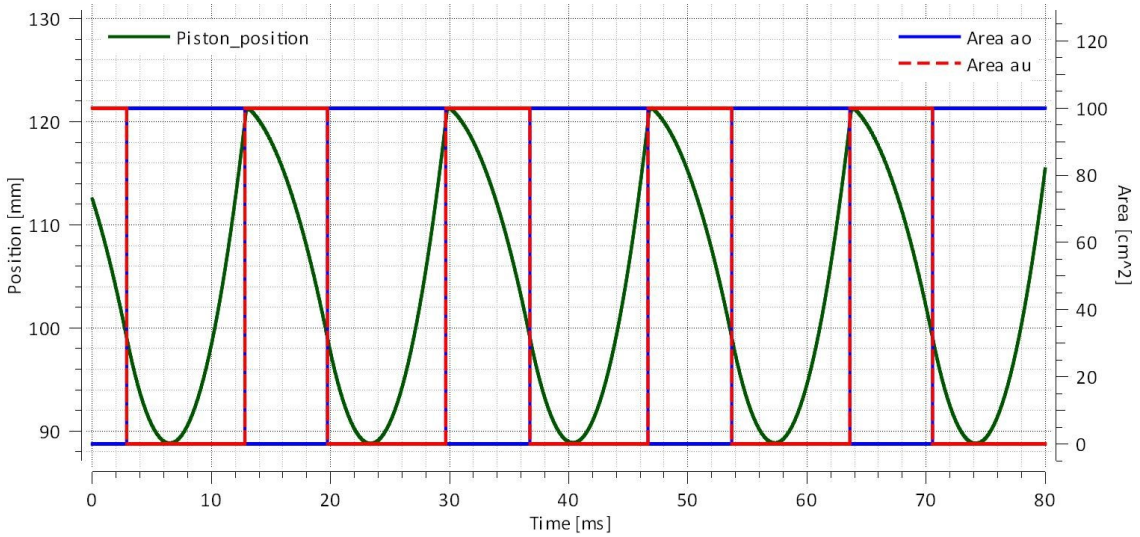

Figure 19. *Valve switching & piston positions: ao valve opening between supply pressure & piston chamber A_2 & au valve opening between piston chamber A_1 & return pressure*

4.2.4 Analysis (At Different Reference Impact Velocities)

The parameters obtained from simulation results at velocities 6 m/s, 8 m/s and 10 m/s in table 4 shows that the higher the impact velocity, the lower will be the frequency of the system. Also, to increase impact velocity, there is an increase in stroke length of the piston movement. Table 4 presents the comparison between the reference and simulated values. The reference values were calculated from the equations 12, 13, 14 and 15 mentioned in the section 4.1. The difference between these values is minimal and simulated values are very closely following the reference values. The small difference in the values is due to the limitation of the controller. It is difficult for the controller to precisely follow the reference piston velocity and piston position simultaneously.

Table 4. Comparison between reference (Ref.) and simulated (Sim.) values of the parameters at reference velocities 6, 8 & 10 m/s

Velocity [m/s]		**Frequency [Hz]**		**Power [kW]**		**Stroke [mm]**		**Energy [J]**	
Ref.	**Sim.**	**Ref.**	**Sim.**	**Ref.**	**Sim.**	**Ref.**	**Sim.**	**Ref.**	**Sim.**
6	5.9	104.7	96.4	11.6	10.4	11.04	11.4	110.8	110
8	7.9	78.5	73.2	15.4	13.9	19.6	19.9	197.1	194
10	9.9	62.8	59.2	19.3	16.9	30.7	30.7	307.8	302

4.2.5 Controller Robustness against Varying Supply Pressure

The change in pressure during the piston motion causes results in an increased piston stroke as shown in figure 20. The percussion pressure is decreased for a time interval 0.5-1.5 ms to obtain the reference percussion velocity, the controller moves the switching position, which result in a longer piston stroke. After this variation, the initial percussion pressure is restored, and the system regains the previous stroke length.

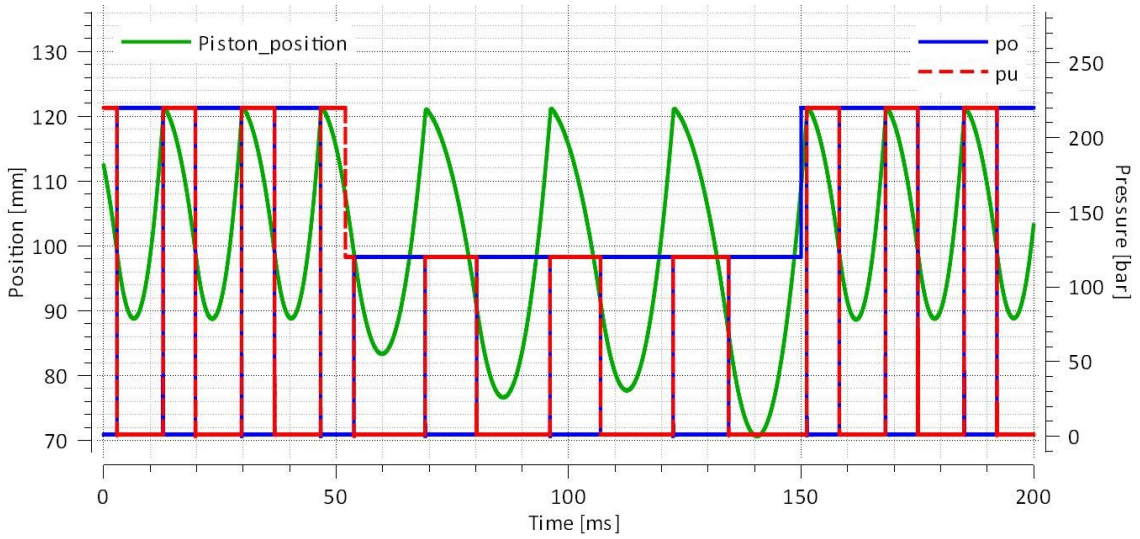

Figure 20. *The change in pressure during the stroke varying the stroke length*

4.2.6 Percussion Operational Range

In figure 21, the solid lines represent performance at varying reference velocities (energies). The green colored lines belong to 260 bar percussion pressure, red lines to 220 bar and blue lines to 160 bar. Figure 22 shows the corresponding input flow, supply pressure and power.

The vertical dashed lines present constant velocity at varying pressure. The velocities 4, 6, 8, 10 and 12 m/s increase from left to right in the figure 21. There are also constant power lines shown as dotted lines in both the energy-frequency and pressure flow figures (figure 21 and 22 respectively). There will be increase in stroke length and decrease in frequency with increase in reference impact velocity at a constant percussion pressure while stroke length decreases and frequency increases with increase in percussion pressure keeping the reference impact velocity constant. The flowrates are increasing with the increase in the percussion pressure as evident in figure 22.

The efficiency of the system remains above 85 % with increase of velocity from 4 to 12 m/s and in a percussion pressure range of 160-260 bar.

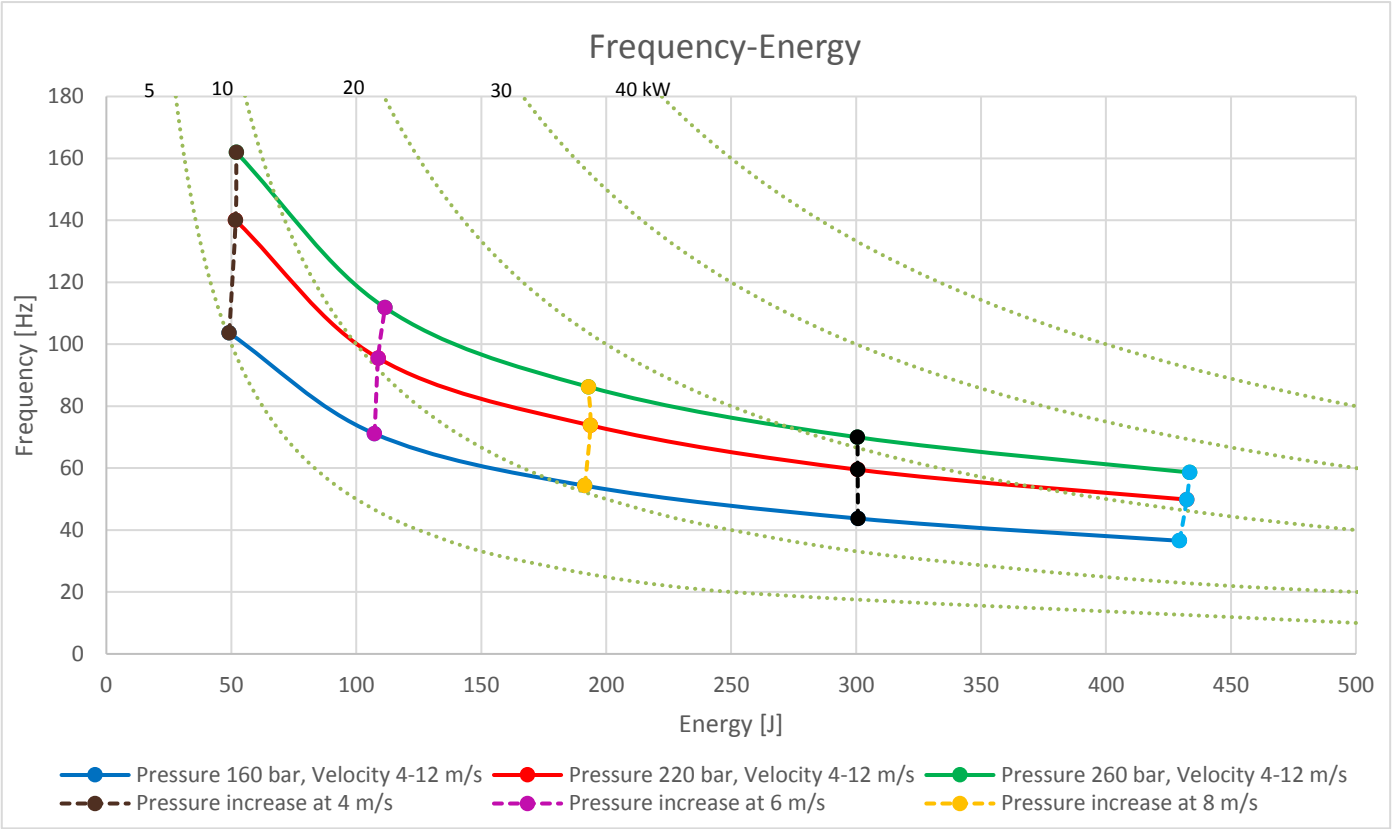

Figure 21. *Horizontal lines show frequency and energy change for different pressure levels (160, 220 and 260 bar) and velocity is changed (from 4 to 12 m/s). Vertical lines show frequency and energy change for different velocities (4, 6, 8, 10 and 12m/s) and pressure is changed (from 160 to 260 bar)*

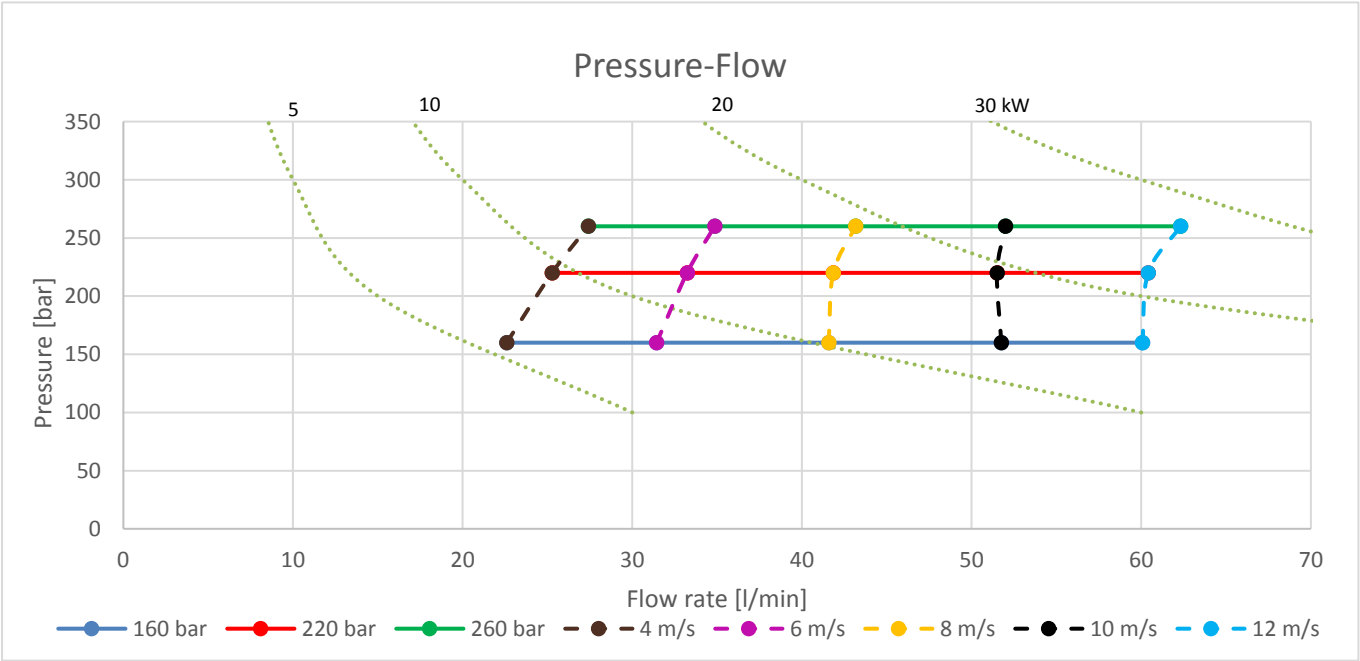

Figure 22. *Horizontal lines show Varying velocities at percussion pressure 160 (blue), 220 (red) and 260 (green) bar, vertical lines present percussion pressure increase from 160 to 260 bar at velocities 4,6,8,10,12 m/s (left to right)*

4.3 Including Valve Delay to Ideal Valve Operation

Two new piston positions z_3 and z_4 as shown in Fig. 23 are introduced in order to include the effect of delay property into consideration during the switching of valve openings. The inputs to the controller are piston position *xp*, piston velocity *vp*, supply pressure *Ps* and valve delay t_d. The controller calculates the switching positions z, z_3, z_4, z_1 along with their corresponding velocities $v_1, v_3,$ *and* v_4. Controller checks the condition and regulate the valve openings accordingly as shown in figure 24.

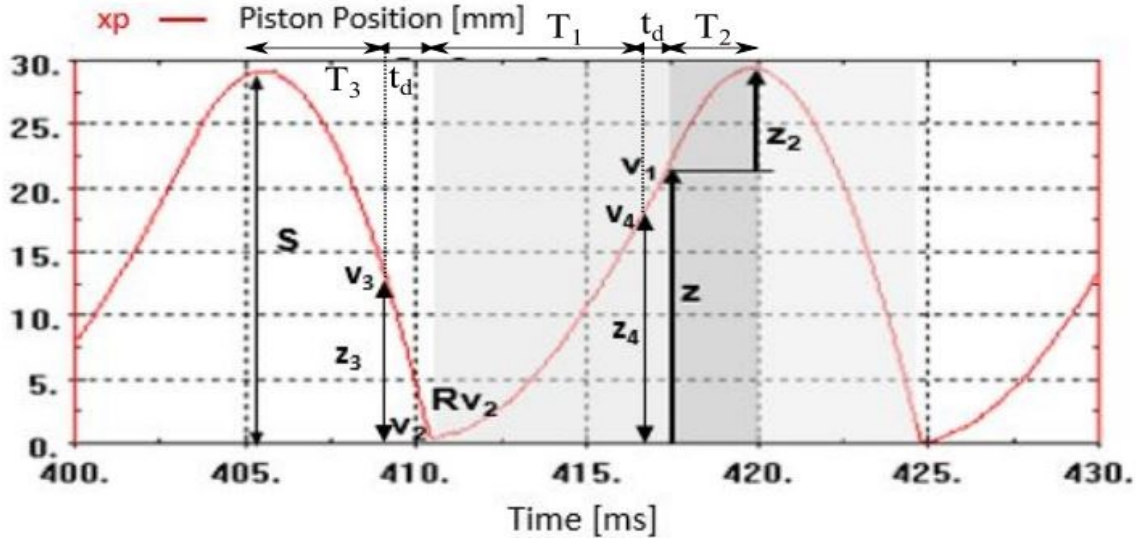

Figure 23. *Introducing the valve delay to the ideal operation*

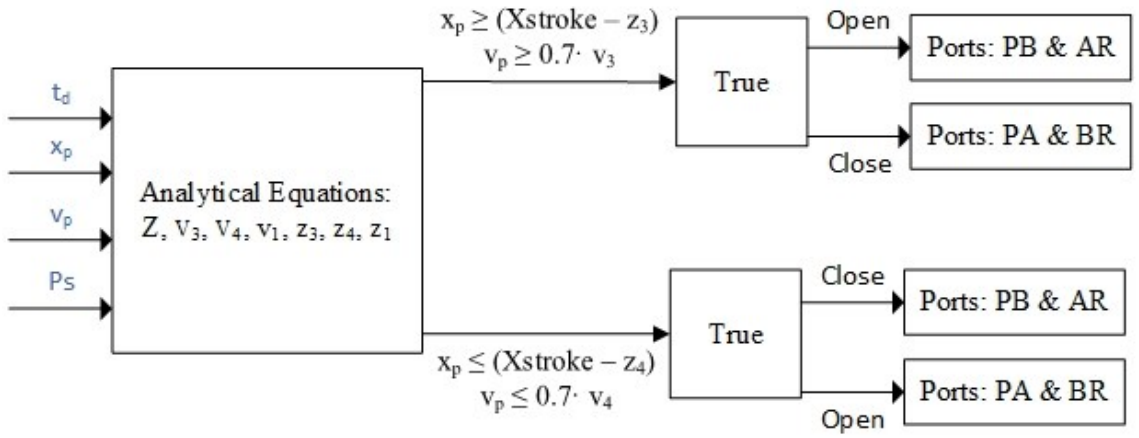

Figure 24. *Controller structure for valve delay operation*

The analytical equations will be derived (see appendix 8.2) and included in the controller for the verification of the simulation model. These points will be the new opening and closing positions for the valve openings (see figure 23) during the simulation of the model. The controller will compensate for the delay time so that the piston strikes the shank at stroke position with the desired impact velocity.

We need equations 1, 2 and 3 to derive the new equations.

$$v_y = v_x + at_{xy}$$

$$v_y^2 = v_x^2 + 2a(S_y - S_x)$$

$$S_y - S_x = v_x t_{xy} + \frac{at_{xy}^2}{2}$$

Piston position, xp = 0→ z_3

Using equation 2, we get

$$\frac{m}{2PA_2}(v_2^2 - v_3^2) = z_3 \qquad (16)$$

Now we can derive velocity at position z_3, using equation 1

$$v_3 = v_2 - \frac{PA_2 t_d}{m} \qquad (17)$$

Now the time taken by piston to reach impact position would be

$$T_3 = t_3 - t_d \qquad (18)$$

Piston position, xp = z_4→z_4+z_1

Using equation 2, we have

$$\frac{PA_1}{m}(z_4 + z_1 - z_4) = \frac{v_1^2}{2} - \frac{v_4^2}{2}$$

$$z_1 = \frac{m}{2PA_1}(v_1^2 - v_4^2) \qquad (19)$$

Now we can derive equation for velocity at this position z_4, we use equation 1

$$v_4 = v_1 - \frac{PA_2 t_d}{m} \qquad (20)$$

Also, the time for the backward motion of piston after impact can be written as

$$T_1 = t_1 - t_d \qquad (21)$$

Solving equations 16, 17, 19 and 20 gives the positions at which the controller must start the valve operations. These positions are presented in equation form as

Valve Switching Positions:

$$z_3 = \frac{m(v_2^2 - v_3^2)}{2PA_2} \qquad (22)$$

$$z_1 = \frac{m(v_1^2 - v_4^2)}{2PA_1} \qquad (23)$$

$$z_4 = z - z_1 \qquad (24)$$

Piston Stroke Length:

$$S = z + z_2$$

Frequency:

$$f = \frac{1}{T_1 + T_2 + T_3 + 2t_d}$$

4.3.1 Analysis

The parameters obtained from simulation results in figure 25 shows that the higher the impact velocity, the lower the frequency and the longer stroke. Table 5 shows that the calculated and simulated values of stroke length and frequency are close enough. This analysis verifies the controller capability to compensate delay into the system.

Table 5. Comparison between reference and simulated parameters

Parameter		**Unit**	**Reference**	**Simulated**
Stroke Length	S	mm	31	31.5
Velocity	V_2	m/s	10	9.8
Frequency	f	Hz	62.8	59
Energy	W	J	307.8	307.4
Power	P	kW	19.3	18.4

The controller is considering any variation in pressure value and adjusting the piston motion according to the percussion pressure as shown in figure 26. The change in pressure results in longer stroke and decrease in frequency which shows the operation of controller is smooth. The valve delay is 1.5 ms, initial percussion pressure is 220 bar and reference impact velocity is 10 m/s in this analysis.

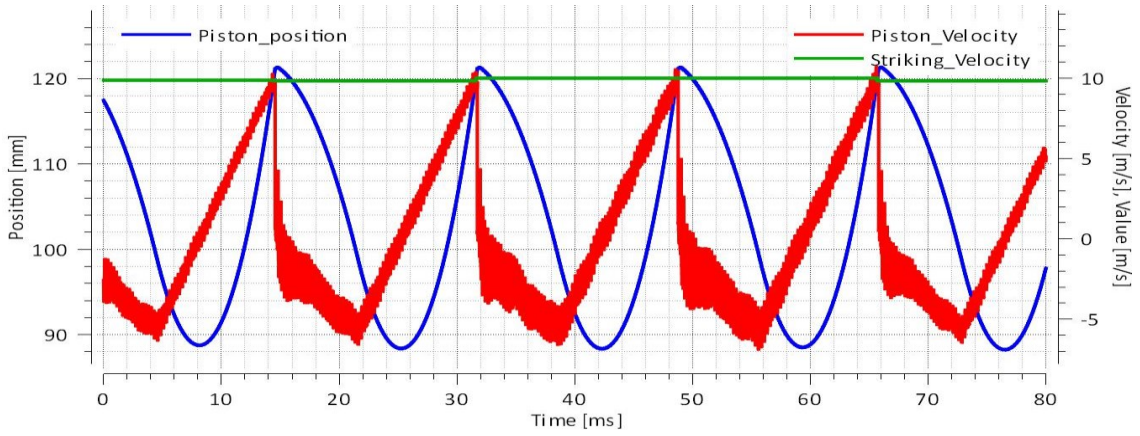

Figure 25. *Piston motion, piston velocity and striking velocity*

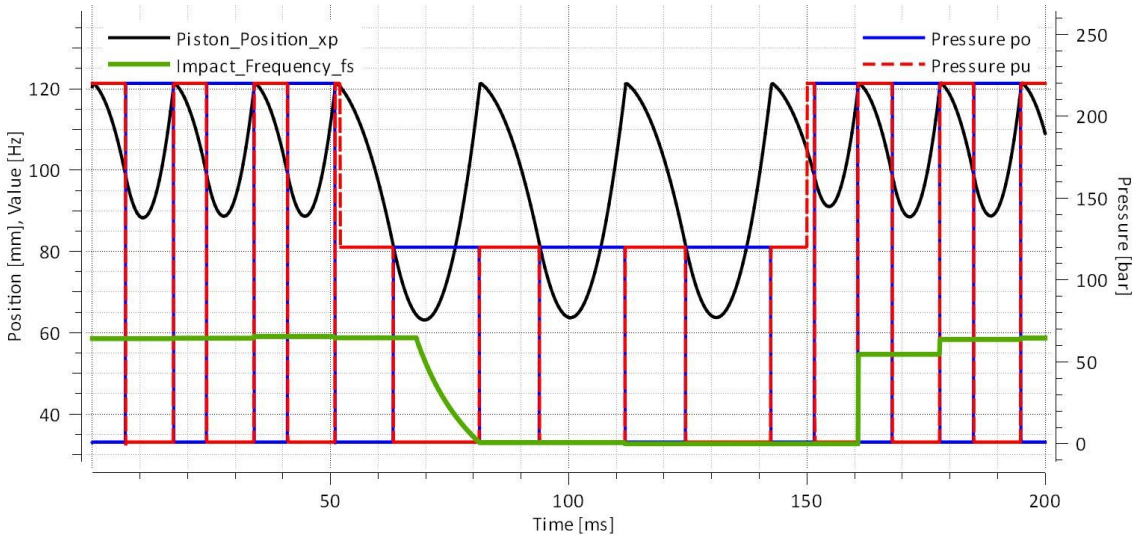

Figure 26. *Impact frequency and stroke variation with change in pressure during operation*

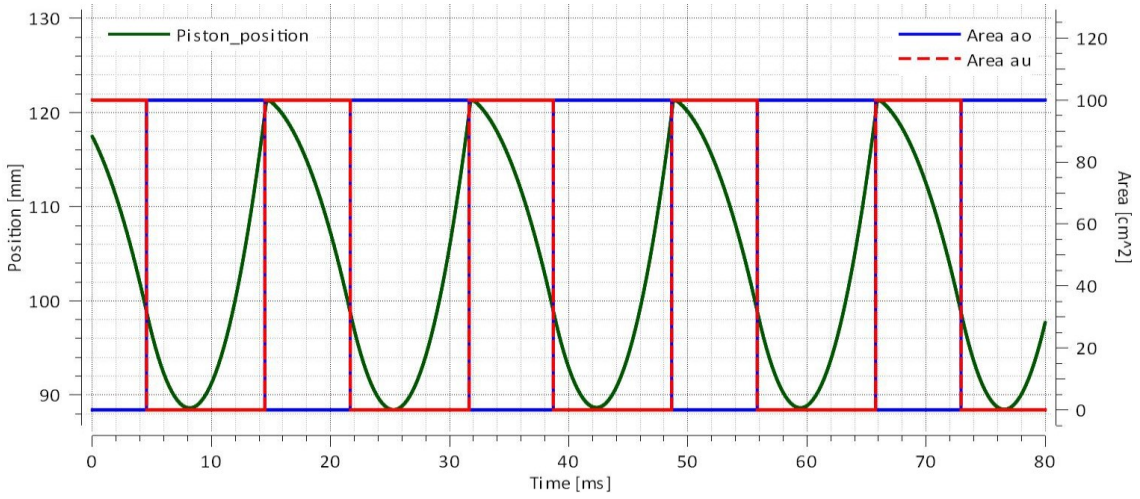

Figure 27. *Valve switching at impact position and backward motion of piston*

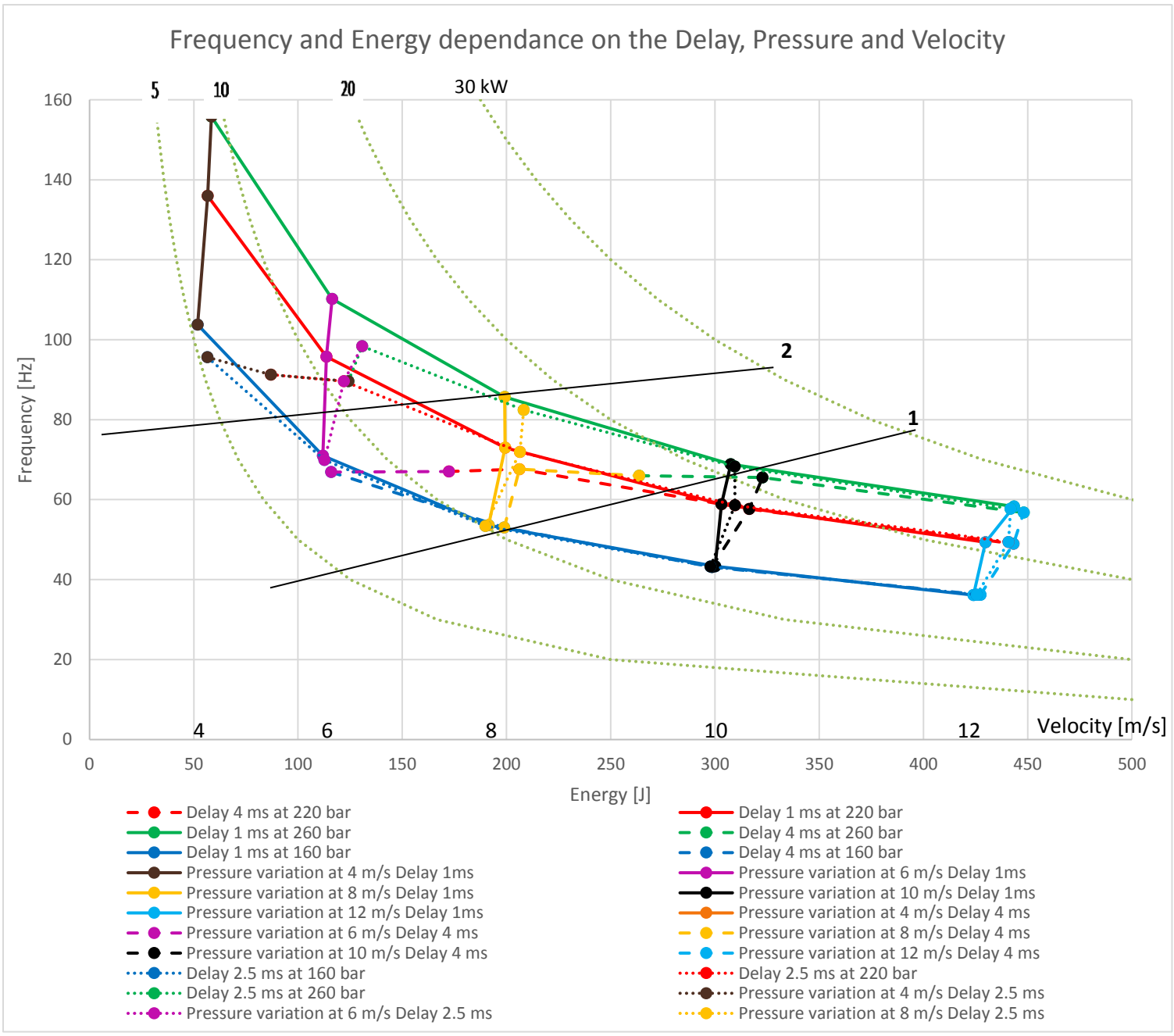

Figure 28. *Horizontal lines show frequency and energy change for different pressure levels (160, 220 and 260 bar) and velocity is changed (from 4 to 12 m/s). Vertical lines show frequency and energy change for different velocities (4, 6, 8, 10 and 12 m/s) and pressure is changed (from 160 to 260 bar)*

In figure 28, the horizontal lines represent performance at varying reference velocities (energies). The green colored lines belong to 260 bar percussion pressure, red lines to 220 bar and blue lines to 160 bar.

There are also three types of lines. Solid lines belong to 1 ms delay between control signal and valve action, dotted lines 2.5 ms and dashed lines 4 ms. Of course, the delay will be more difficult to handle running at higher frequencies. Looking at the performance curves from high energies towards lower, the solid lines follow the expected path very well. The

dashed lines (4 ms delay) fail to follow the expected path at lower frequencies and higher energies than the dotted lines (2.5 ms delay).

1. Marker 1 (see figure 28) shows the limit of the 4 ms delay while varying impact velocity and supply pressure. The marker 1 shows that the 4 ms delay is not suitable for the velocities below 10 m/s and pressure above 220 bar. But 4 ms delay can work for pressure values around 160 bar and impact velocity ≥ 8 m/s. The reason for this limitation is due to the time dependency of the opening areas of the valve. The following statements are true for this case.

i) If $t_d > T_1$ such that $T_1 \leq 0$ (figure 29), then the controller will provide some unrealistic values of time for piston motion that is not desirable.

ii) Or if $t_d > T_3$ such that $T_3 \leq 0$ (figure 29), it is not possible for controller to provide accurate results. It is evident in figure 3 and 4 that at a velocity of 10 m/s and 260 bar pressure, there is not much increase in flow rate but slight increase in energy. The delay t_d is greater than T_3 so that the controller is pushing the piston beyond the impact position to compensate the delay and this result in higher value of impact velocity. The switching of the valve openings is happening after the impact point.

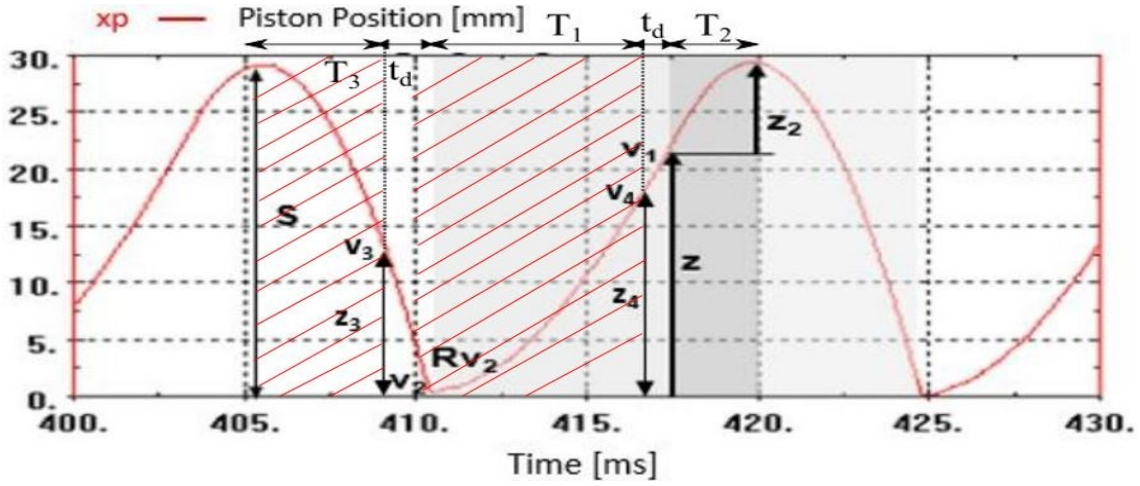

Figure 29. *Valve delay and switching time limits for controller*

2. Marker 2 presented in figure 28 shows the operation for 2.5 ms delay. It can be seen in the figure 3 that with the increase in supply pressure and impact velocity, it has a broader working range than the 4 ms delay. Again, we can say that

i) If $t_d > T_1$ such that $T_1 \leq 0$ (figure 29), then the controller will provide some unrealistic values of time for piston motion that is not desirable.

ii) Or if $t_d > T_3$ such that $T_3 \leq 0$ (figure 29), it is not possible for controller to perform accurately under these conditions. It can be seen in figure 3 and 4 that at a velocity of 6 m/s and 260 bar pressure, there is not much increase in flow rate and slight increase in energy. The delay t_d is greater than T_3 so that the controller is pushing the piston beyond the impact position to compensate the delay and this result in higher value of impact velocity.

It can be concluded from the figure 28 that the smaller will be the delay values (< 2 ms), the easier to achieve high frequencies. The energy and frequency output of the system increase with increase in input velocity and supply pressure of the system respectively. Also, the piston stroke will increase with decrease in frequency and vice versa. The controller is successfully compensating the pressure variations during the operation. This result in a larger piston stroke during that percussion pressure variation as shown in figure 26. All of the results in the figure are in the range of 5-30 kW power output. Power generated is increasing with increase in impact velocity and the frequency will decrease if percussion pressure is kept constant. The figure 28 depicts that there is increase in power consumption at higher values of percussion pressure and impact velocity of the piston. There is an increase in flow rate with increase in percussion pressure from 160 bar to 260 bar as shown in the figure 30. The increase in flowrate can also be seen, when we are changing the valve delay from 1 ms to 4 ms at a constant percussion pressure. Higher valve delay (4 ms) with a higher percussion pressure (260 bar) is not suitable for operation at smaller velocities (< 6 m/s) because of the controller limitation explained above.

Limitation: This investigation only considers the opening and closing delay of the valve and pressure losses are ignored in this case.

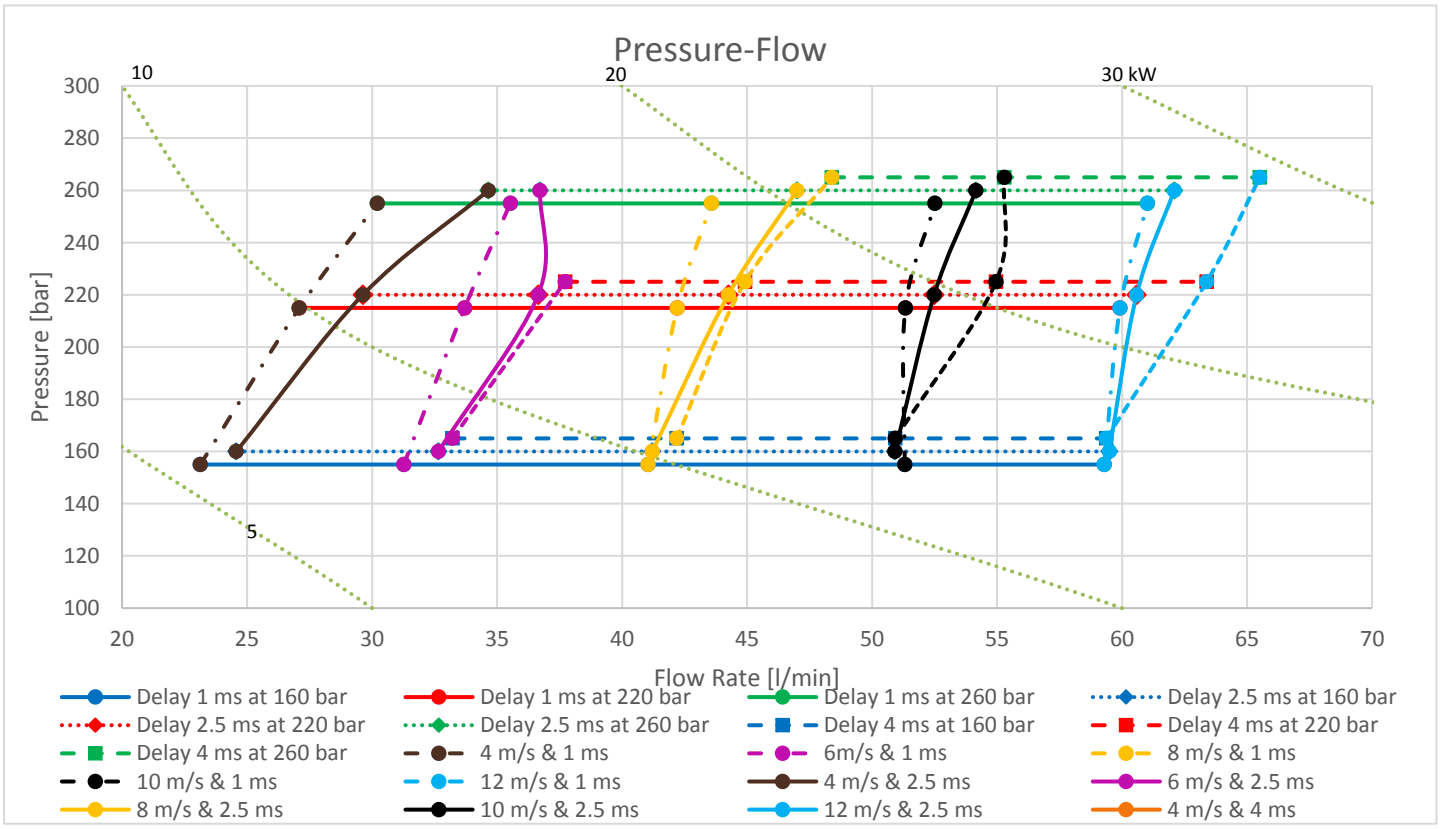

Figure 30. *Horizontal lines show Varying velocities at percussion pressure 160 bar (blue), 220 bar (red) and 260 bar (green), vertical lines present percussion pressure increase from 160 to 260 bar at velocities 4, 6, 8, 10, 12 m/s (left to right)*

4.4 Analysis including Pressure Losses

This section explains the percussion mechanism including the pressure losses of valve. The mechanism is tested with three different area (A_v) sizes of the valve openings i.e. 0.5 cm^2, 1 cm^2 and 1.5 cm^2. The controller inputs (see fig. 31) are piston position *xp*, piston velocity *vp,* supply pressure *Ps* and valve area *Av.* The controller calculates pressure losses, switching position *z* and backward velocity v_1 using the analytical equations. Then, the controller regulates the openings of valve according to the respective conditions as shown in figure 31.

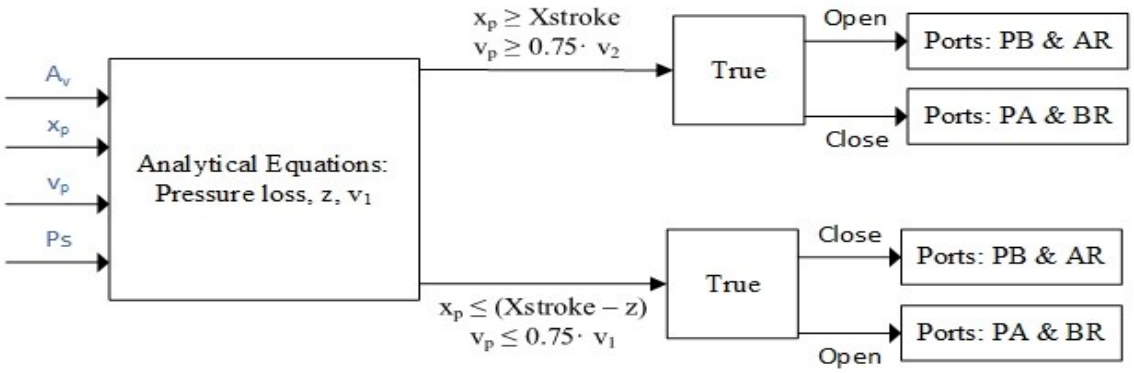

Figure 31. *Controller structure including Pressure losses*

The equation for the pressure loss [13] in general form is

$$\Delta P = \left(\frac{q_v \cdot \sqrt{\rho}}{\sqrt{2} \cdot C_q \cdot A_v} \right)^2 \qquad (25)$$

Where q_v can be approximated to

$$q_v = \frac{V_p A_p}{\sqrt{2}} \qquad (26)$$

Where v_p and A_p are the velocity and area of the piston respectively and A_v is the valve opening area. ρ is the fluid density (value 890 kg/m^3) and C_q is the flow coefficient (value 0.67).

The analytical expressions for pressure losses are derived (see appendix 8.3) and taken into consideration in the operation of the controller.

$$v_1 = \frac{\sqrt{(m \cdot R^2 \cdot v_2^2 + 2 \cdot P \cdot z \cdot A_1) \cdot (2 \cdot z \cdot K \cdot A_1^3 - 2 \cdot z \cdot K \cdot A_2^2 + m)}}{(2 \cdot z \cdot K \cdot A_1^3 - 2 \cdot z \cdot K \cdot A_2^3 + m)} \qquad (27)$$

$$z_2 = \frac{2 \cdot z \cdot P \cdot A_1 \cdot m + m \cdot R^2 \cdot v_2^2}{2 \cdot (2 \cdot K \cdot P \cdot z \cdot A_1^3 \cdot A_2 - K \cdot m \cdot R^2 \cdot v_2^2 \cdot A_2^3 - 2 \cdot K \cdot P \cdot z \cdot A_1 \cdot A_2^3 + 2 \cdot K \cdot P \cdot z \cdot A_2^4 + P \cdot m \cdot A_2)} \qquad (28)$$

Stroke length: $S = z + z_2$

Frequency:

$$f = \frac{1}{T_1 + T_2 + T_3}$$

The figure 32 and 33 shows that the variation in opening areas from 0.5 cm^2 to 1.5 cm^2, while keeping the same reference velocity 8 m/s and percussion pressure 160 bar, result in a decrease in stroke length of the piston while the striking frequency eventually increases. Overall, there must be increase in stroke length to compensate the pressure losses, so the desired velocity can be achieved. The impact velocity of the mechanism is very close to the input value which shows that system is generating energy at a steady rate.

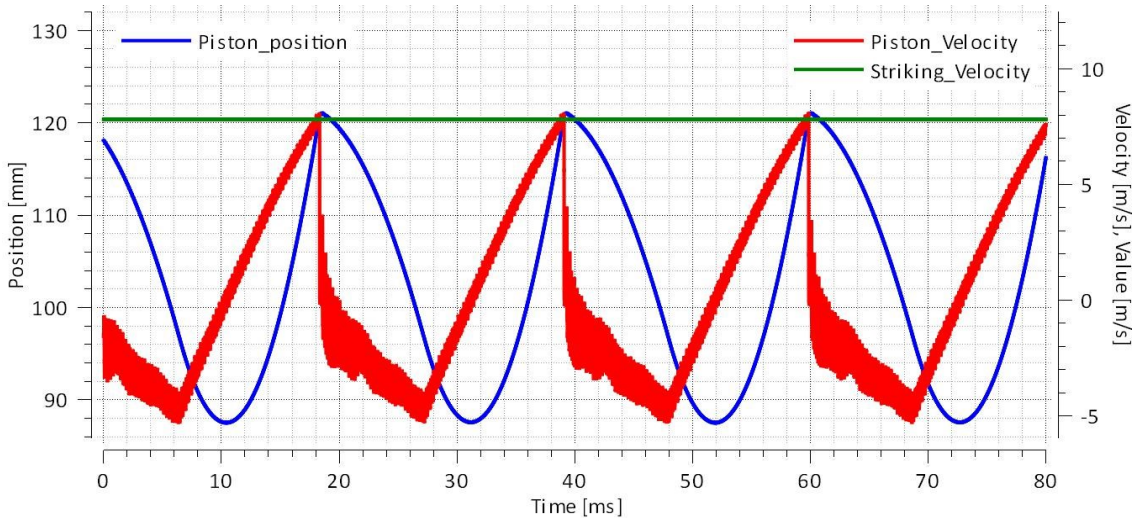

Figure 32. *Piston motion and velocity at 0.5 cm^2 valve size*

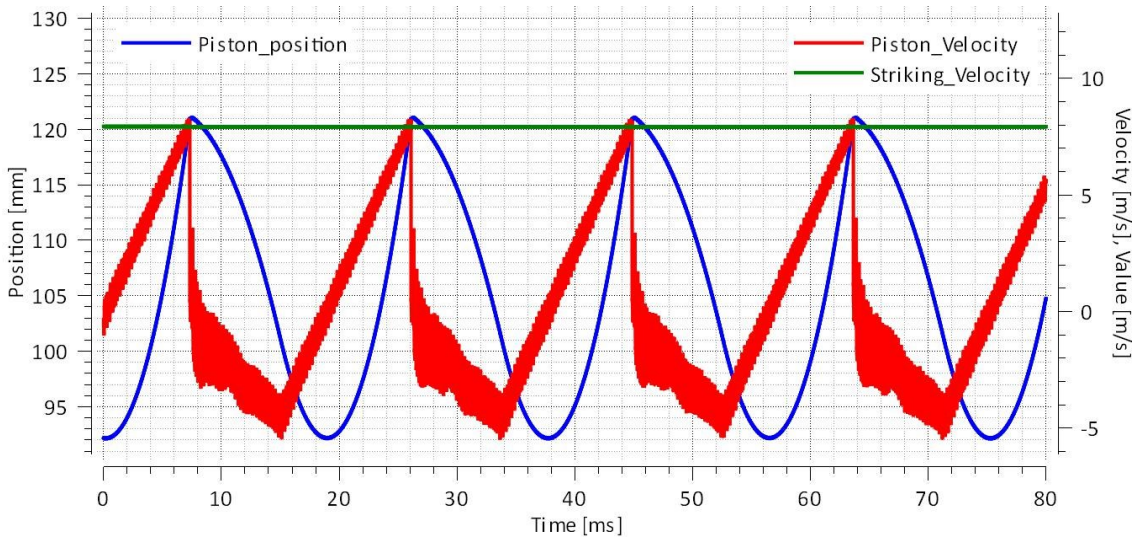

Figure 33. *Piston motion and velocity at 1.5 cm^2 valve size*

The velocity is kept at 8 m/s and pressure 160 bar for both of the following calculations. The change in the flow rate is visible when we increase the size of the valve opening area from 0.5 cm^2 to 1.5 cm^2 as shown in figure 34 and 35. The flowrate increases with increase in valve losses and vice versa.

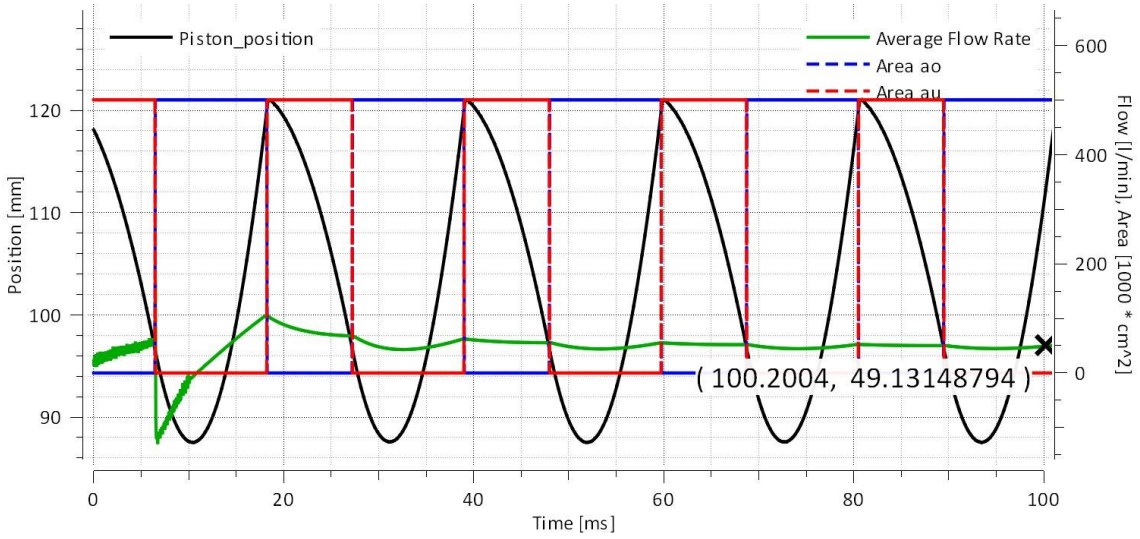

Figure 34. *Valve switching with opening area 0.5 cm^2*

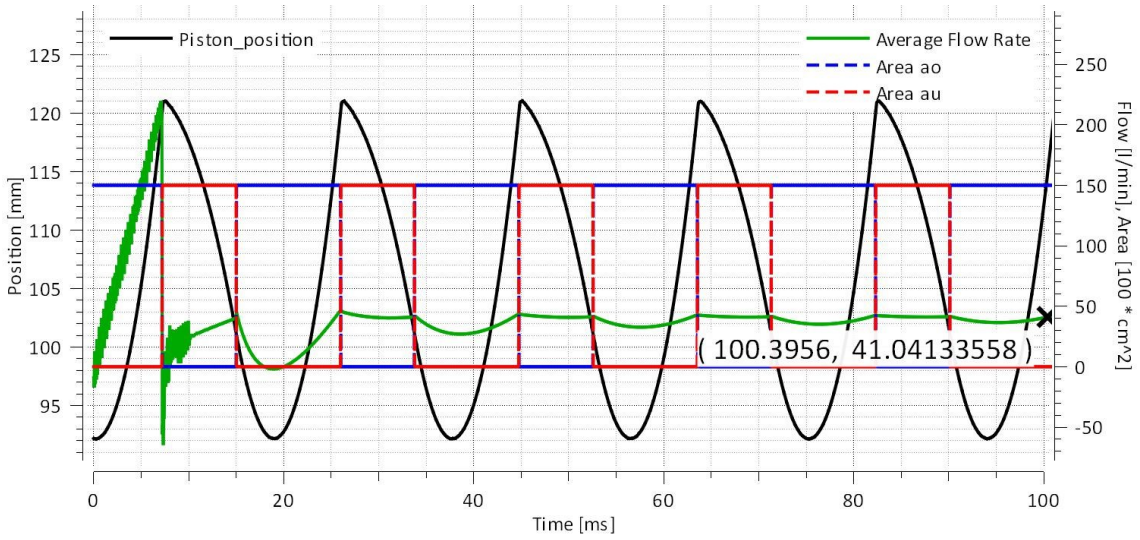

Figure 35. *Valve switching with opening area 1.5 cm^2*

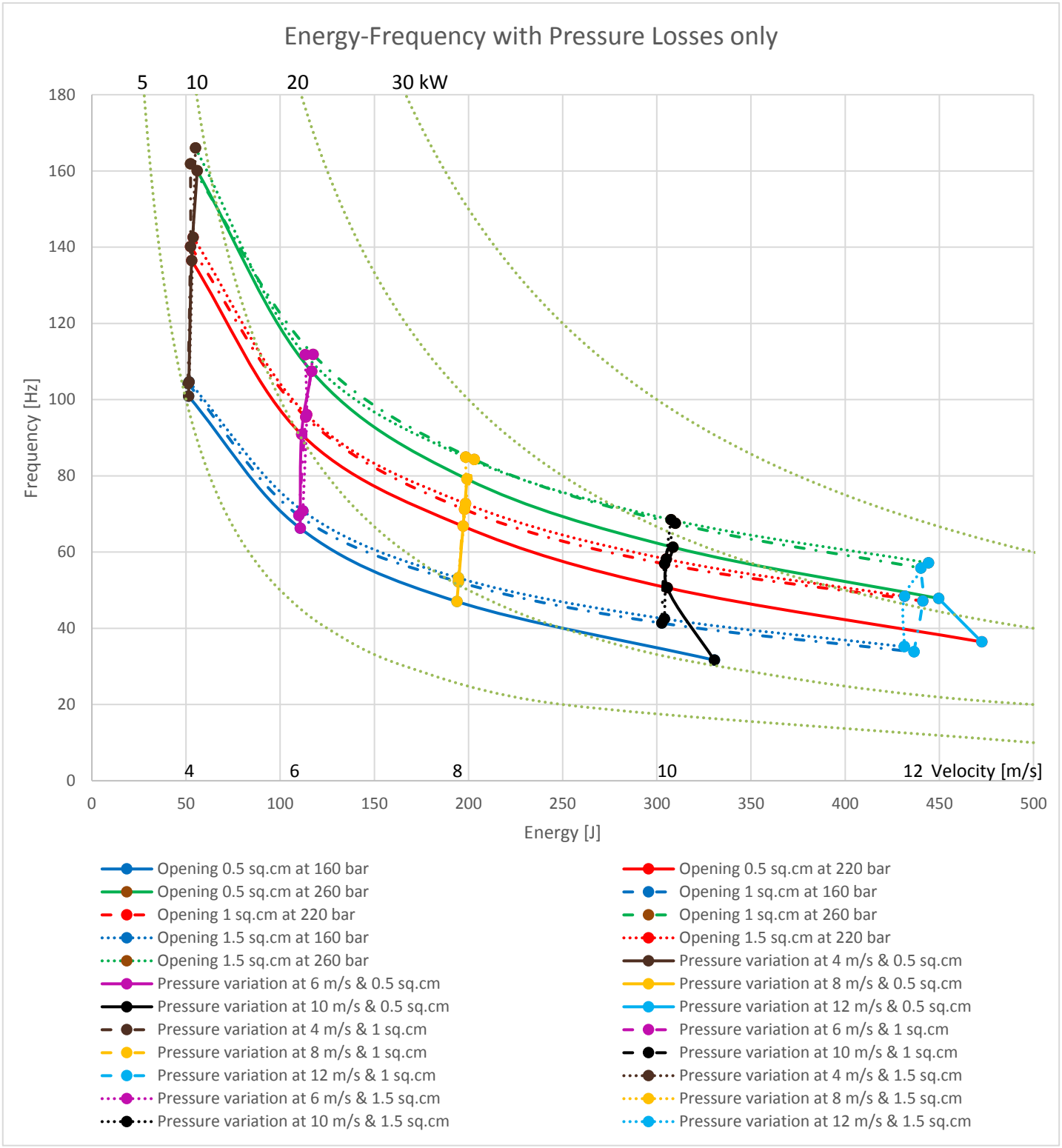

Figure 36. *Horizontal lines show Varying velocities at percussion pressure 160 bar (blue), 220 bar (red) and 260 bar (green), vertical lines present percussion pressure increase from 160 to 260 bar at velocities 4,6,8,10,12 m/s (left to right)*

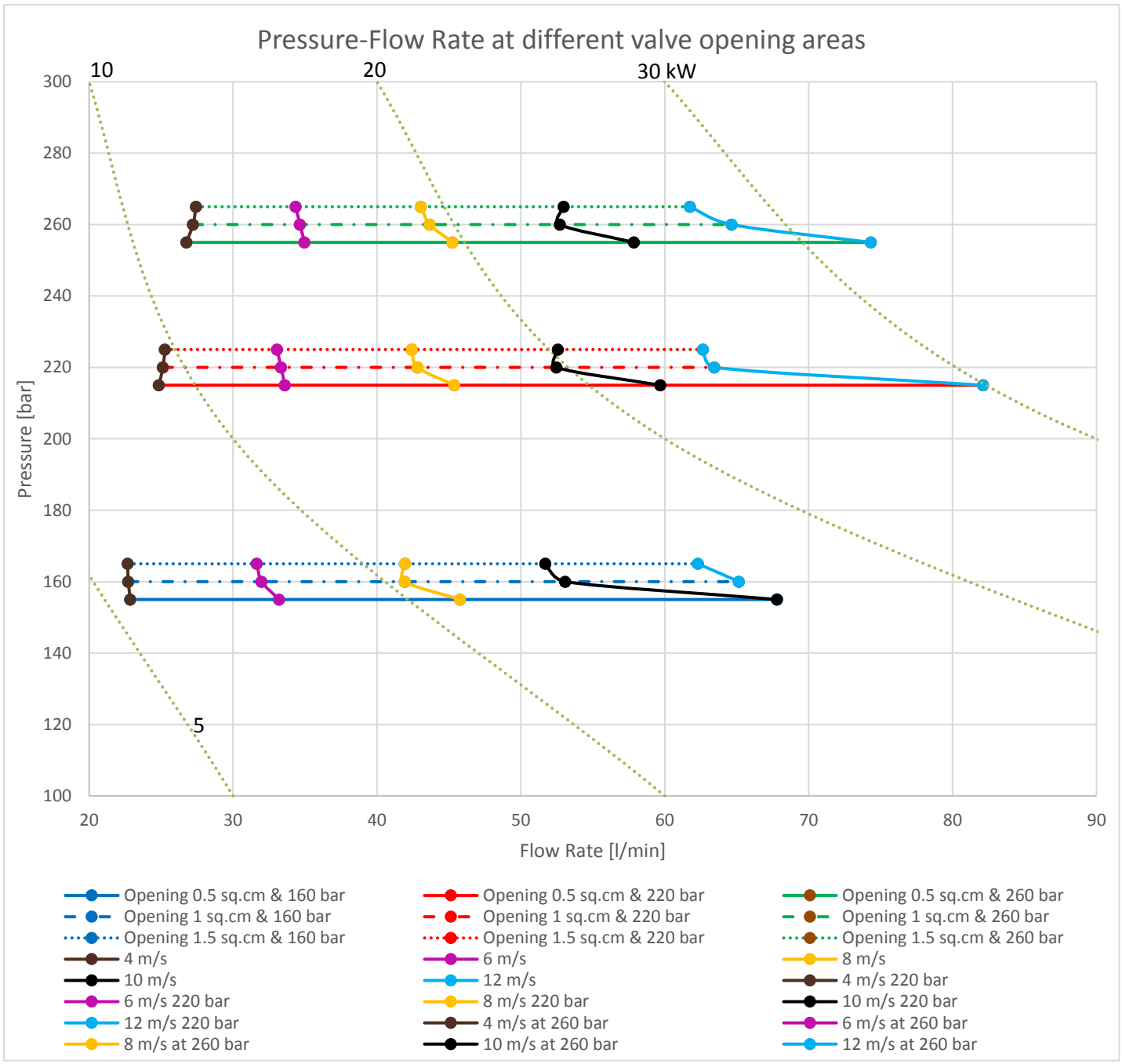

Figure 37. *Horizontal lines showing varying velocities at percussion pressure 160 bar (blue), 220 bar (red) and 260 bar (green), vertical lines present percussion pressure increase from 160 to 260 bar at velocities 4,6,8,10,12 m/s (left to right). Offset of constant pressure curves were added for improved readability.*

In figure 36, solid lines represent performance at varying reference velocities (energies). The green colored lines (solid, dashed-dot & dot) belong to 260 bar percussion pressure, red lines (solid, dashed-dot & dot) to 220 bar and blue lines (solid, dashed-dot & dot) to 160 bar.

There are also three types of lines. Solid lines belong to 0.5 cm^2 opening area of the valve, dashed-dotted lines 1 cm^2 and dotted lines 1.5 cm^2. Of course, the small opening areas will be more difficult to handle running at lower percussion pressures (see 160 bar at higher energy). Looking at the performance curves from high energies towards lower, the dashed-dot and dotted lines follow the expected path very well. The solid line (160 bar) fail to follow the expected path at higher energies than the other lines. To compensate for pressure losses, the stroke length must increase in order to obtain the desired striking velocity. This will also lead to decreased frequency, which can be seen in the figure 36. Totally, the flow rate will increase with valve losses as shown in figure 37.

Limitation:

The pressure losses of the valve are taken into consideration in this section. The valve dynamics properties are ignored for this analysis.

4.5 Analysis using Valve Dynamics and Pressure Losses

The controller structure (see fig. 38) consists of inputs such as piston position *xp*, piston velocity *vp*, supply pressure *Ps*, valve opening area A_v and valve delay t_d. The controller uses the analytical equations 29, 30, 31, 32 and 33 to calculate the pressure losses, switching positions z, z_1, z_3, z_4 and corresponding switching velocities v_1, v_3 and v_4. The valve openings are regulated by controller according to the conditions shown in the figure 38.

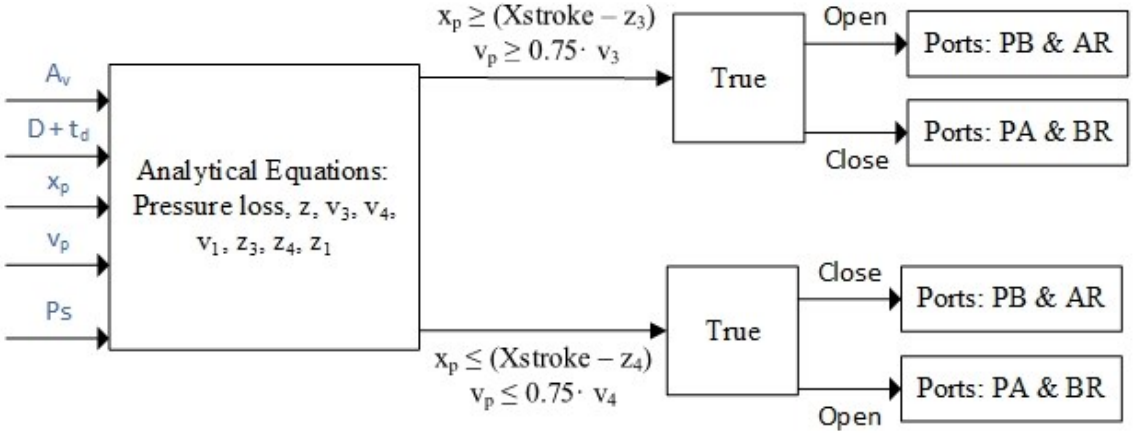

Figure 38. *Controller structure including valve delay and pressure losses*

The figures 43 and 44 depicts the results for the simulation of the percussion mechanism while taking into consideration the pressure losses across the valve openings and the valve

dynamics properties. The values used for valve opening area is 0.75 cm^2, the opening and closing delay of 2.5 ms and opening rate is 0.9 ms in this analysis. The simulation of the mechanism is done for reference impact velocities 4, 6, 8, 10 and 12 m/s and percussion pressure of 160, 220 and 260 bar. The table 6 shown below presents the values of other parameters used during the simulation process. The derived equations (see appendix 8.4) for this analysis utilize both the pressure losses and valve delay during the simulation.

$$z_3 = \frac{m \cdot (v_2^2 - v_3^2)}{2 \cdot ((P - \Delta P_{2i}) \cdot A_2 - \Delta P_{1i} \cdot A_1)} \tag{29}$$

$$v_3 = v_2 - \frac{[(P - \Delta P_{2i}) \cdot A_2 - \Delta P_{1i} \cdot A_1] \cdot t_d}{m} \tag{30}$$

$$z_1 = \frac{m \cdot (v_1^2 - v_4^2)}{2 \cdot ((P - \Delta P_1) \cdot A_1 - \Delta P_2 \cdot A_2)} \tag{31}$$

$$v_4 = v_1 - \frac{[(P - \Delta P_1) \cdot A_1 - \Delta P_2 \cdot A_2] \cdot t_d}{m} \tag{32}$$

$$z_4 = z - z_1 \tag{33}$$

$$f = \frac{1}{T_1 + T_2 + T_3 + 2 \cdot t_d} \tag{34}$$

Table 6. Simulation parameters

Type		**Value**	**Unit**
Piston Stroke Length	xp	0.12	m
Piston Mass	M	6.16	kg
Piston Length	L	0.6	m
Piston Rebound Coefficient	R	0.1	-
Tank Pressure	Pt	1	bar
Piston Diameter	D1	42	mm
Piston Diameter	D2	45	mm
Piston Diameter	D3	38	mm
Piston Driving Area	A1	205	mm^2
Piston Driving Area	A2	456	mm^2

Pressure variation at reference impact velocity 10 m/s

The increase in pressure result in an increased flow rate from 71 l/min at 160 bar to 78 l/min at 220 bar. The figure 39 and 40 verify the changes in stroke length of the piston such that the increase in flowrate as a result of pressure rise is forcing the system to perform on a higher frequency and consequently it causes a decline in the piston stroke length.

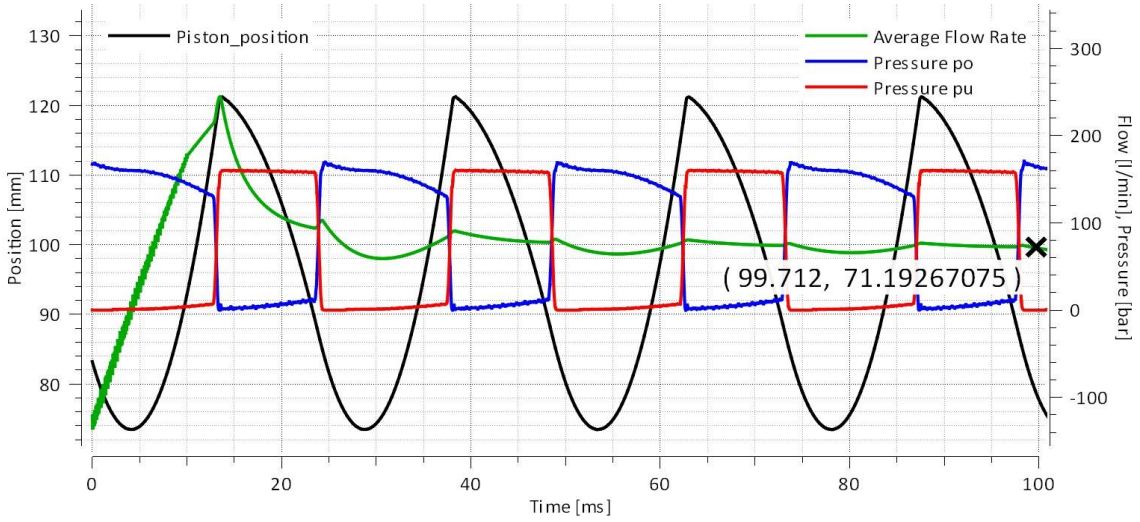

Figure 39. *Piston motion involving valve delay and pressure losses at 160 bar*

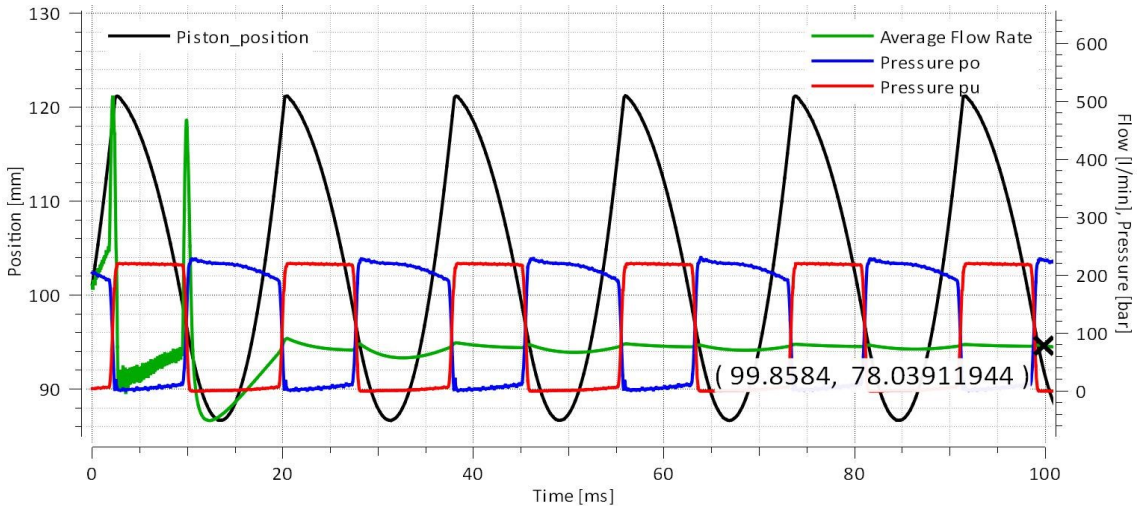

Figure 40. *Piston motion involving valve delay and pressure losses at 220 bar*

Also, this is evident from the figures 41 and 42 that the mechanism is generating energy at a steady rate and the impact velocity is reaching very close to the reference value of the velocity.

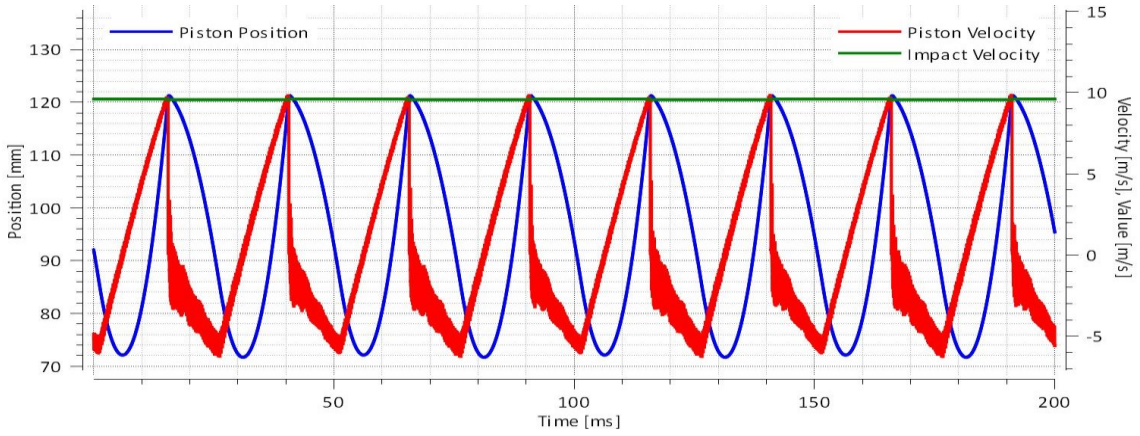

Figure 41. *Piston motion along piston and striking velocity at 160 bar*

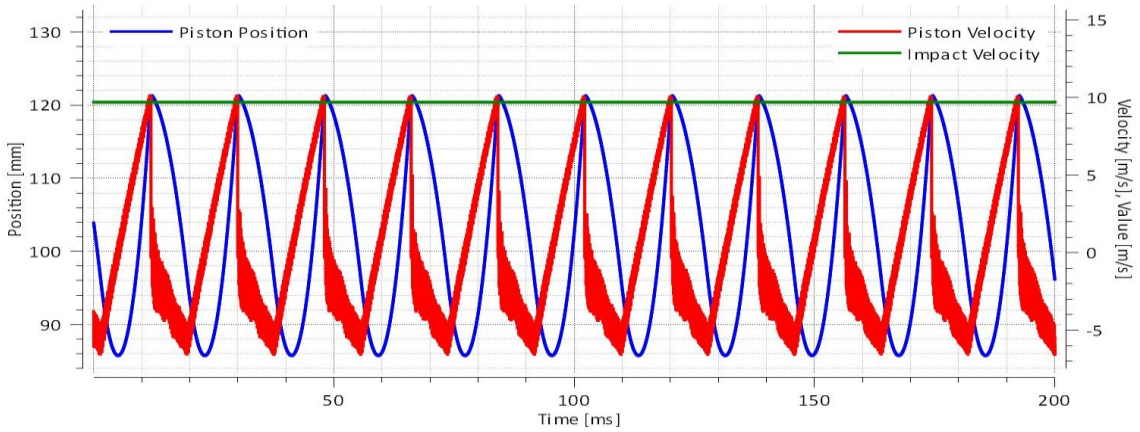

Figure 42. *Piston motion along piston and striking velocity at 220 bar*

- **Power consumption**

The power consumption and output of the mechanism is presented in the figures 43 and 44. The input power of the system is between 18- 38 kW at velocity 10 m/s and pressure change from 160 bar to 260 bar. At same velocity and pressure range, the power output is in the range of 11-19 kW. It shows that varying pressure to higher values is decreasing the efficiency of the system from 61 % to 50 %.

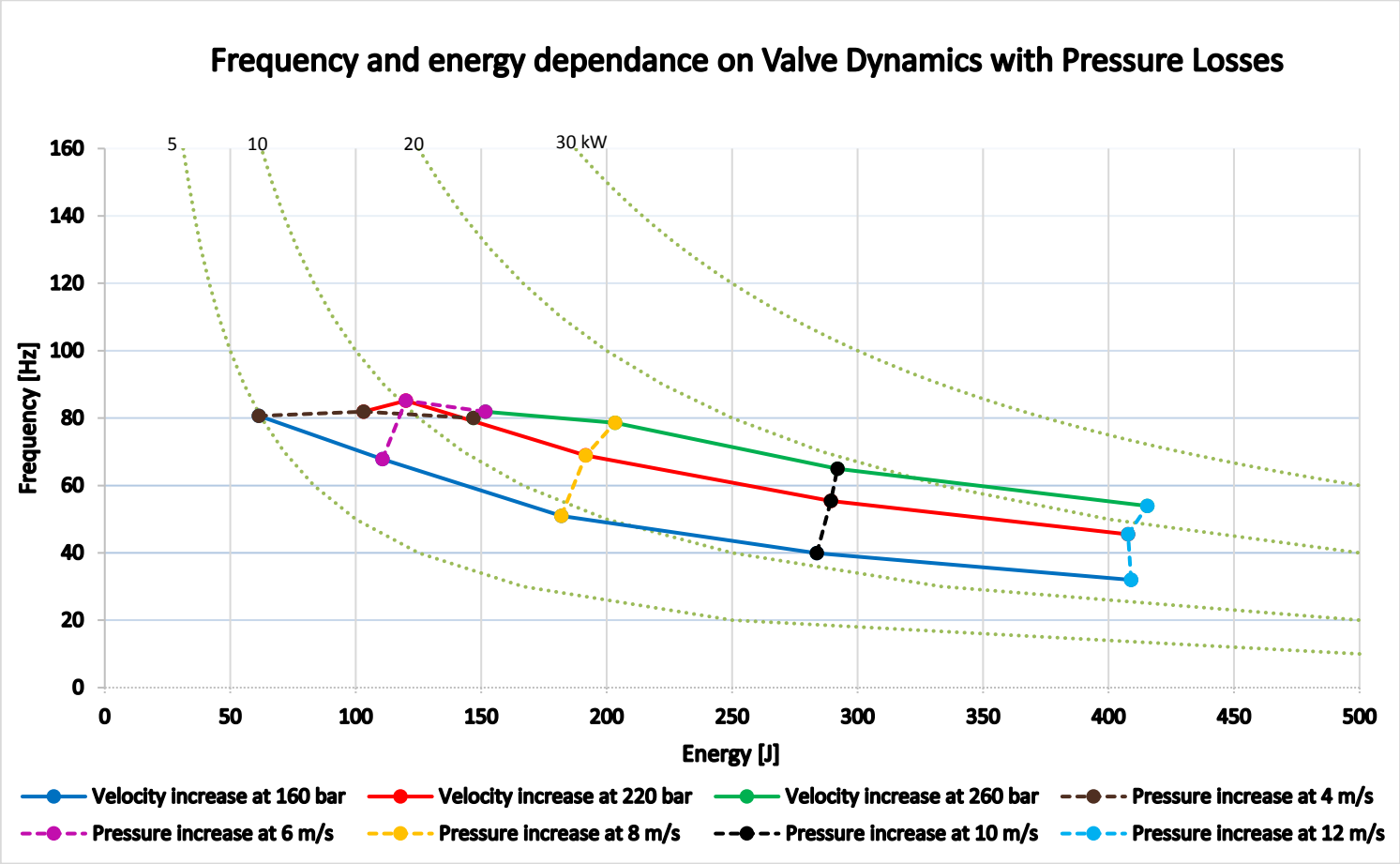

Figure 43. *Horizontal lines show Varying velocities at percussion pressure 160 bar (blue), 220 bar (red) and 260 bar (green), vertical lines present percussion pressure increase from 160 to 260 bar at velocities 4,6,8,10,12 m/s (left to right)*

In figure 43, the solid lines represent performance at varying reference velocities (energies). The green colored lines belong to 260 bar percussion pressure, red lines to 220 bar and blue lines to 160 bar.

The vertical dashed lines demonstrate the constant velocity lines and percussion pressure is varying from 160 bar to 260 bar. There are constant power lines shown as dotted lines in the background (see figure 43 and 44). Frequency is presented on the Y-axis while energy is on the x-axis.

The output energy is increasing with the increase in the impact velocity from 4 m/s to 12 m/s as shown in figure 43. The results are explained as follows.

i) Varying pressure at 4 m/s:

The increase in pressure from 160 to 220 bar aiming at keeping the impact velocity constant at 4 m/s fails. The energy increases while there is not much change in the frequency of the piston motion. This is because the time T_1 and T_3 required by the piston to move

backwards after impact and to move to impact point respectively is becoming negative. So, the value of delay is bigger than the T_1 and T_3 ($t_d > T_1$ & $t_d > T_3$) which is not realistic in this case. This cause the piston to move beyond the impact position and result in a higher impact velocity that generate higher energy value. This phenomenon is clearly visible in figure at 220 bar and 260 bar pressure curves.

ii) Varying pressure at 6 m/s:

The mechanism is performing better at 160 and 220 bar keeping velocity at 6 m/s. The piston stroke decreases and there is an increase in the frequency of the system on these pressures. At 260 bar, the delay value is becoming greater than T_1 and T_3, which makes the system fail.

iii) Varying Pressure at 8 m/s:

Piston stroke is decreasing with increase in pressure from 160 bar to 260 bar. Consequently, there is rise in the value of frequency of the system while energy generated during that period is slightly increased. This is due to the reason that system is trying to reach maximum impact velocity with a smaller piston stroke and with increase in supply pressure, it gets closer to the input velocity value.

iv) Varying Pressure at 10 m/s:

The performance of the mechanism at 10 m/s with increasing pressure from 160 bar to 260 bar remains very stable and the frequency of the system increase with a decline in the value of the piston stroke. The output energy values are very close and output power range for this case is 10-20 kW.

v) Varying Pressure at 12 m/s:

There is a steady rise in the value of frequency when switching from 160 bar to 220 bar and the output energy remains the same. At 260 bar pressure, there is more time T_3 for the piston before impact which help the piston to reach higher velocity. This result in a slight increase in output energy.

The flow rate increases increasing percussion pressure from 160 to 260 bar as evident from figure 44. The controller is more smoothly operating at higher velocities (> 6 m/s) due to the limits defined in the section 4.3.1. The power consumption is in the range of 15-40 kW while the output power generated is in the range 5-25 kW.

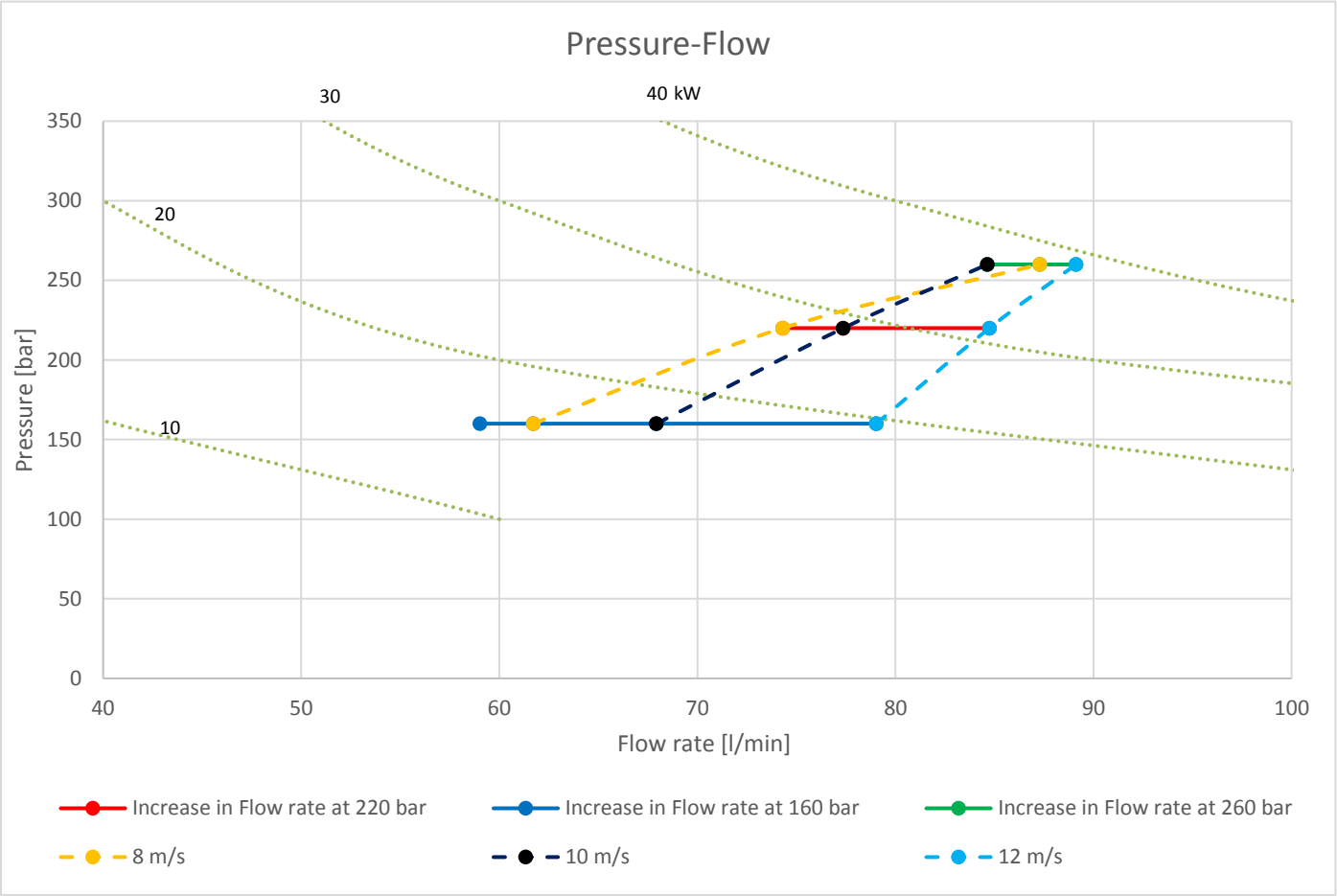

Figure 44. *Horizontal lines show Varying velocities at percussion pressure 160 bar (blue), 220 bar (red) and 260 bar (green), vertical lines present percussion pressure increase from 160 to 260 bar at velocities 4,6,8,10,12 m/s (left to right)*

5. CONTROL STRATEGY

This chapter describes the control strategy of a percussion mechanism by using both frequency and velocity as a reference to the system. The behavior and the analysis of the system will be briefly presented along with the advantage of this control technique.

5.1 Reference Velocity and Frequency

The Hopsan simulation model and controller structure used for the analysis is presented in the figure 45 and 46 respectively. The controller structure (see fig. 46) consists of inputs such as piston position *xp*, piston velocity *vp*, supply pressure *Ps*, valve opening area A_v valve opening rate *D,* reference frequency f_{ref} and valve delay t_d. The controller uses the analytical equations 29, 30, 31, 32 and 33 to calculate the pressure losses, switching positions z, z_1, z_3, z_4 and corresponding switching velocities v_1, v_3 and v_4. The controller is compensating the variations in the supply pressure during the operation.

The velocity and frequency will be used as a reference to the controller and it controls the valve openings. Also, percussion pressure will be controlled in order to achieve both desired energy and frequency. The simulation parameters for this analysis is same as presented in the table 2. Valve delay, opening rate and opening area for this analysis are 2.5 ms, 0.9 ms and 0.75 cm^2.

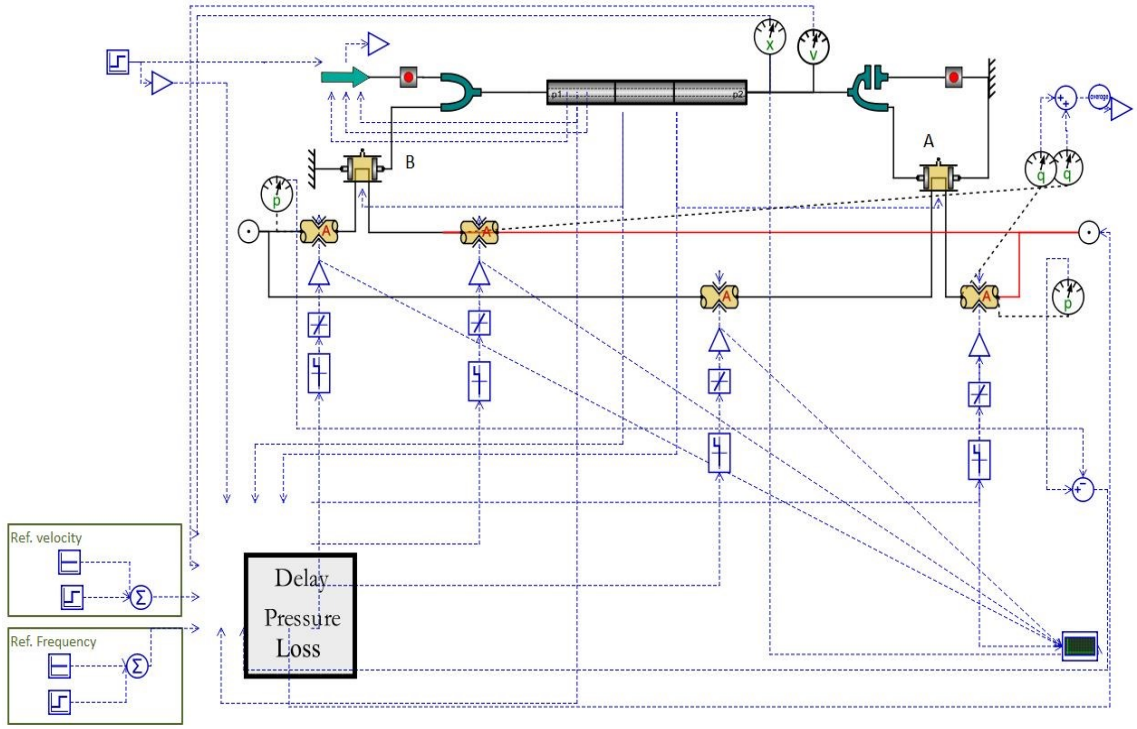

Figure 45. *Overview of the simulation model with reference velocity and frequency*

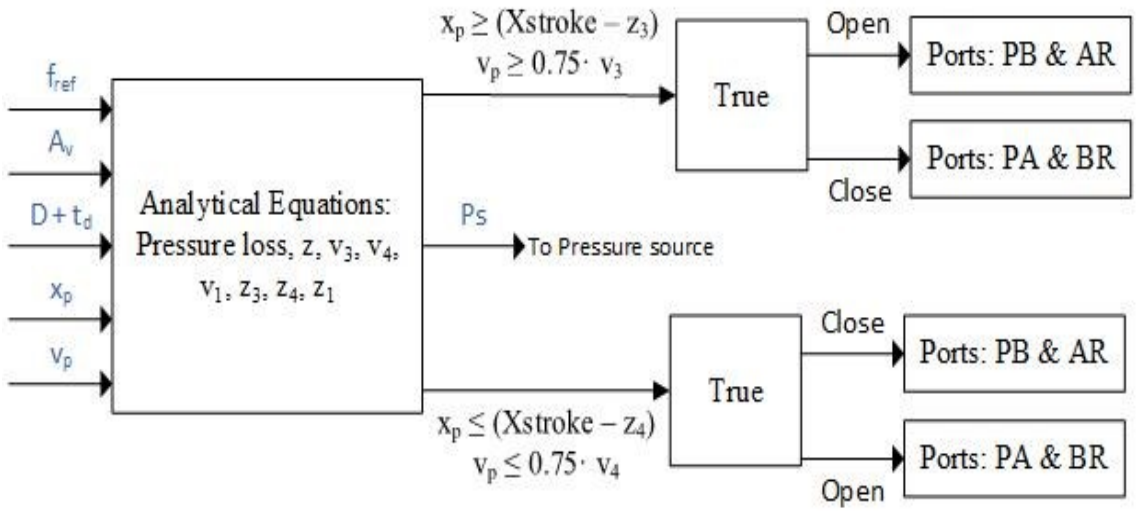

Figure 46. *Controller structure for simultaneous control strategy of reference velocity and frequency*

5.2 Analysis

The simulation model presented in section 5.1 will be tested with different reference velocities and frequencies and the simulation results will be compared to the reference data. The comparison between the reference and simulated parameters is presented in the table 7.

Table 7. Comparison between simulated and reference parameters

Test No.	**Impact Velocity [m/s]**		**Impact Frequency [Hz]**		**Stroke [mm]**	**Figure**
	Reference	**Simulated**	**Reference**	**Simulated**		
1.	4	3.9	40	38	20	31 & 32
2.	6	6	50	47	24.7	33 & 34
3.	8	7.9	30	29.9	52.5	35 & 36
4.	10	9.9	60	58.7	34.1	37 & 38
5.	12	11.8	70	69	35.6	39 & 40

5.2.1 Test 1

The simulated impact velocity and impact frequency is very closely following the reference velocity and frequency respectively as shown in the figure 47 and 48 respectively.

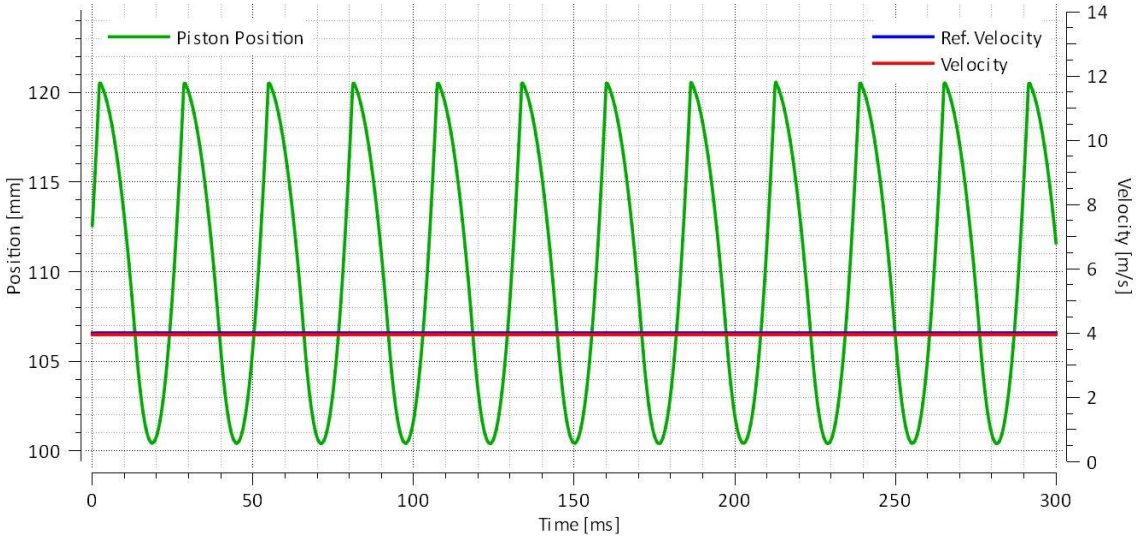

Figure 47. *Reference and Simulated striking velocity*

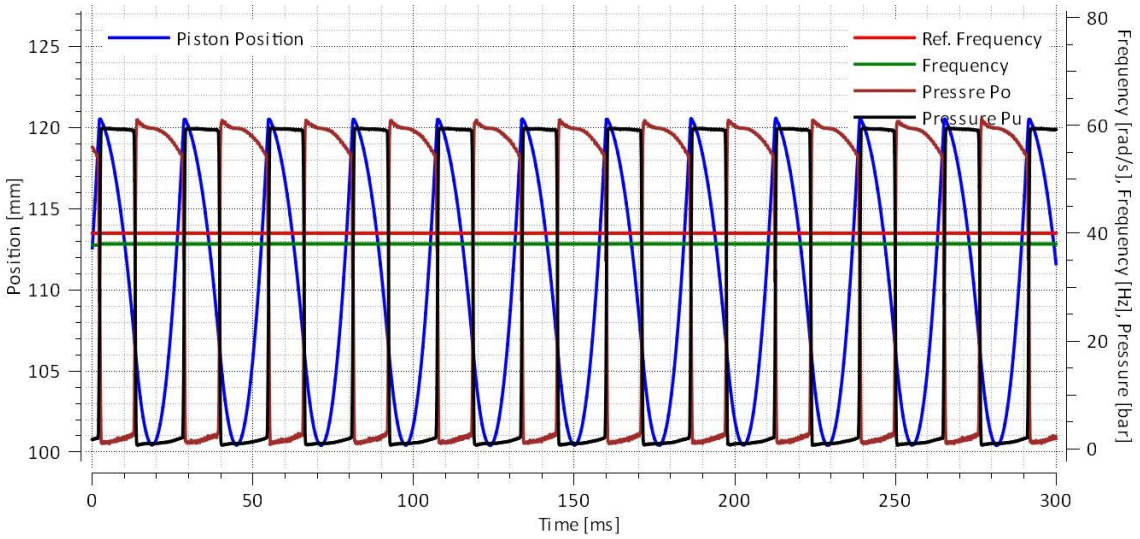

Figure 48. *Reference and Simulated Frequency*

5.2.2 Test 2

The increase in reference impact velocity to 6 m/s and frequency to 50 Hz generates a stroke of 24.72 mm. It is more than the case 1 while the simulated impact velocity is

almost same as reference velocity while there is a slight difference in the simulated frequency value to the reference frequency as shown in figure 49 and 50.

.

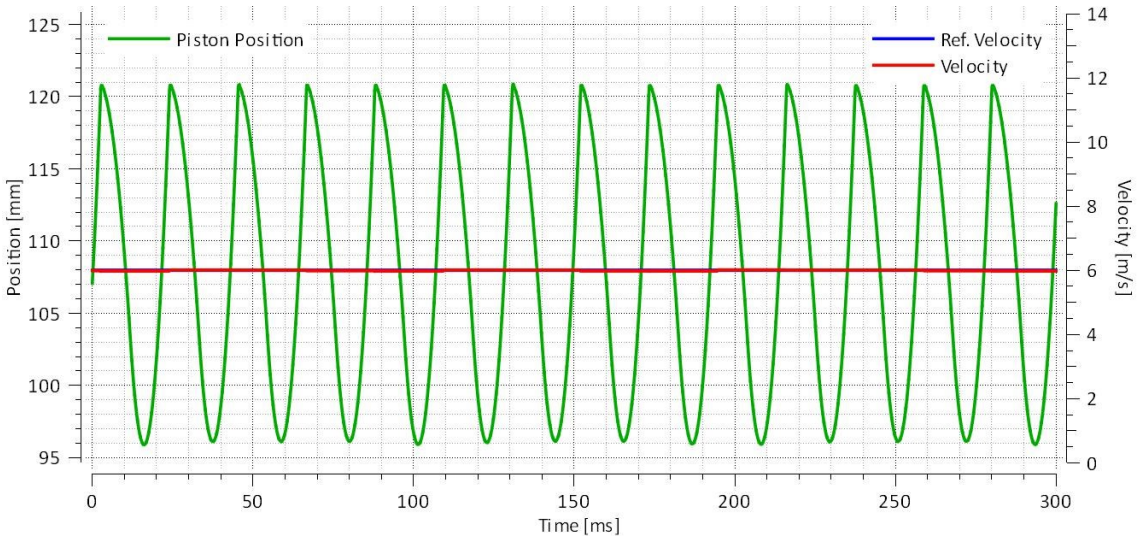

Figure 49. *Reference and Simulated striking Velocity*

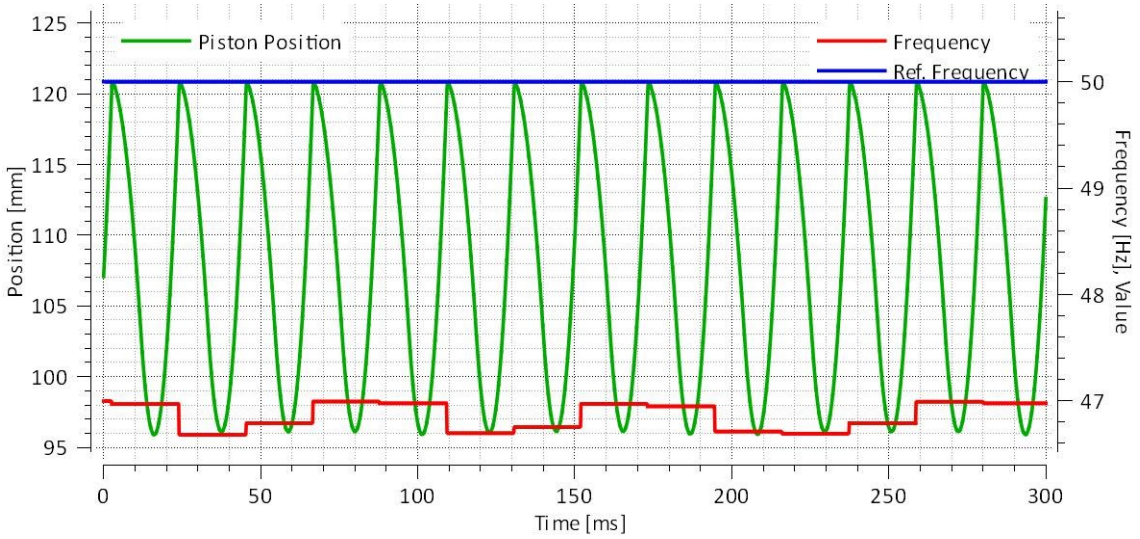

Figure 50. *Reference and Simulated Frequency*

5.2.3 Test 3

The reference velocity is increased to 8 m/s while reference frequency is kept at a low value of 30 Hz to observe the behavior of the system. There is a marginal difference between reference and simulated impact velocity while impact frequency is almost same according to figure 51 and 52 respectively. The increase in reference impact velocity and decrease in impact frequency results in a longer piston stroke.

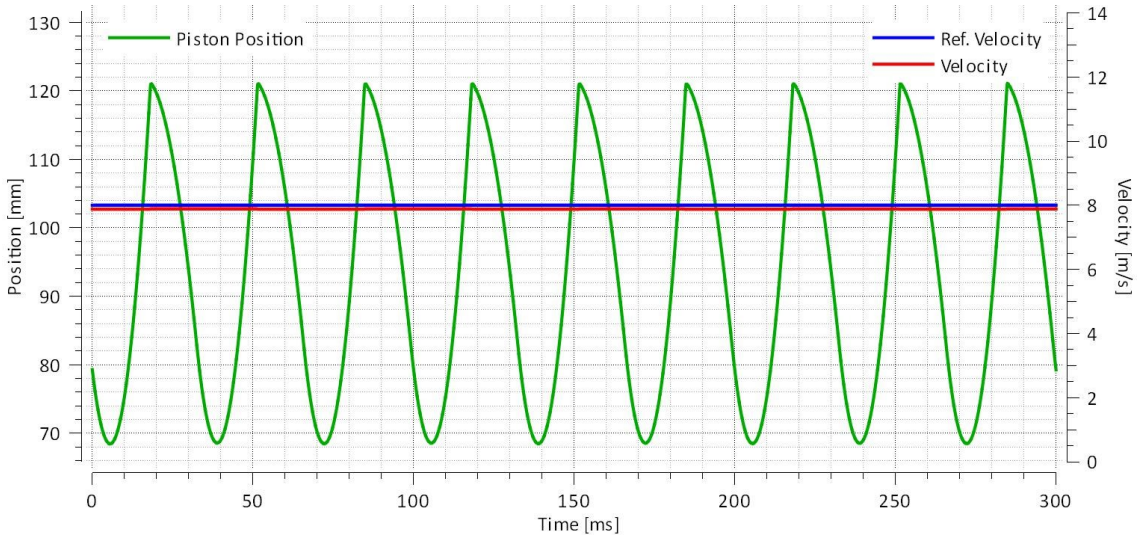

Figure 51. *Reference and Simulated striking Velocity*

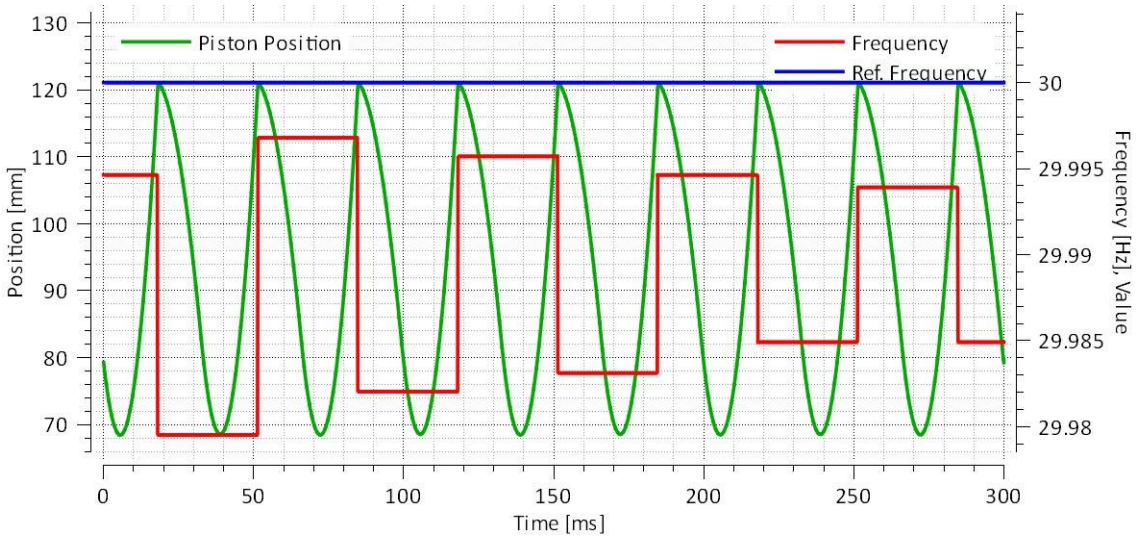

Figure 52. *Reference and Simulated Frequency*

5.2.4 Test 4

Due to increase in both reference impact velocity and frequency, there is a considerable decrease in piston stroke shown in table 7. The reference and simulated values of impact velocity and frequency are almost same and there is very marginal error (see fig. 53 and 54).

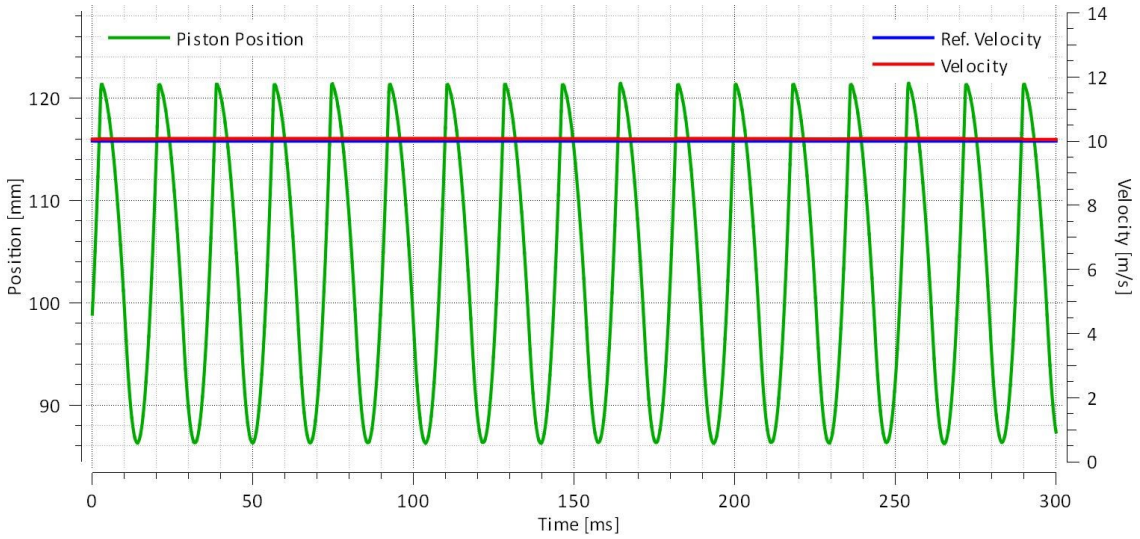

Figure 53. *Reference and Simulated striking Velocity*

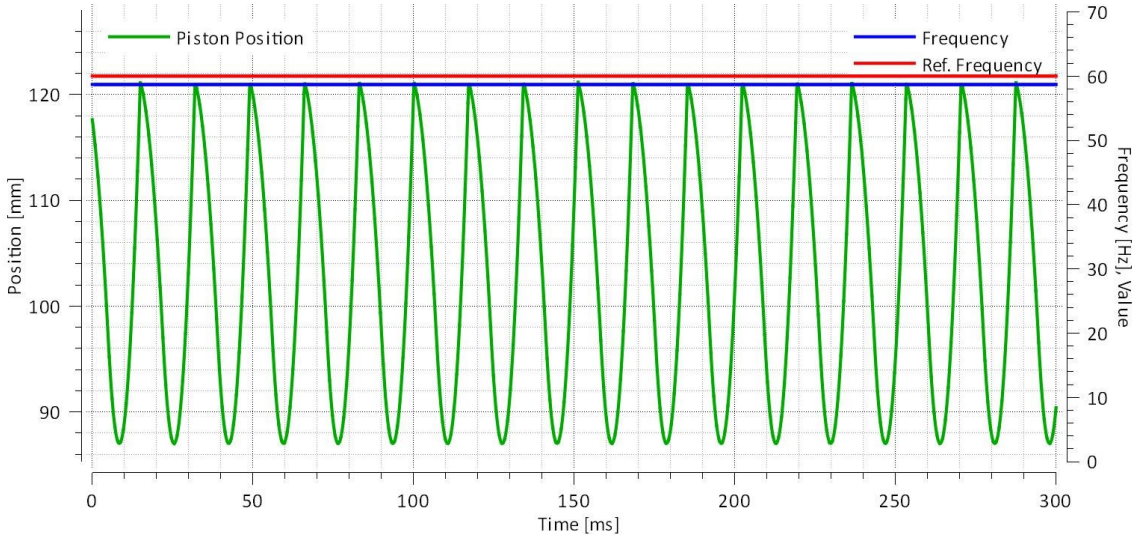

Figure 54. *Reference and Simulated Frequency*

5.2.5 Test 5

There is a slight increase in the piston stroke (see table 7) as compared to previous case since we are increasing both the reference impact velocity and frequency. The reference and simulated values of the impact velocity and frequency are close enough with a very marginal error evident from the figures 55 and 56.

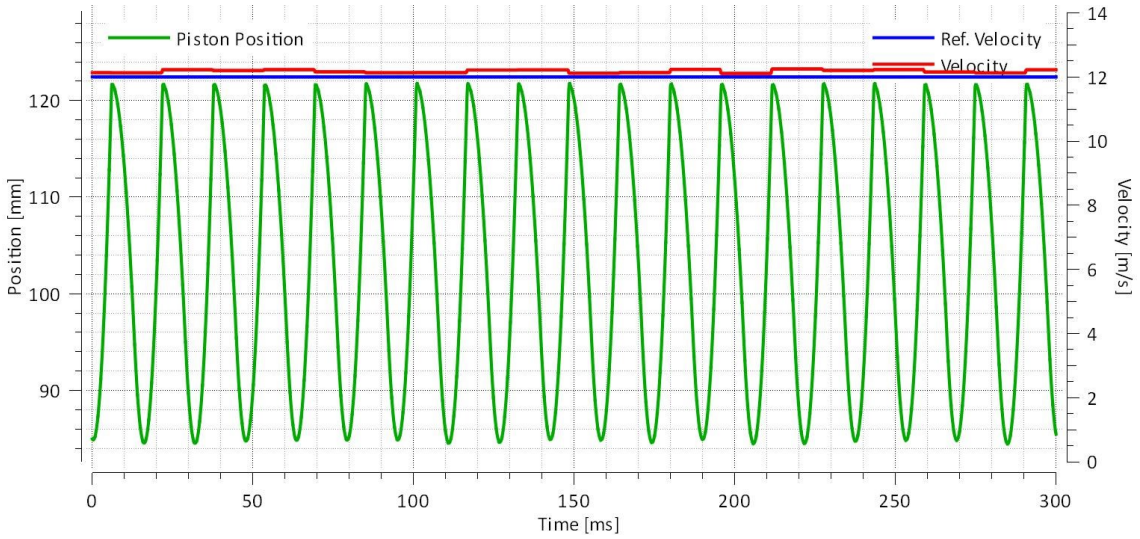

Figure 55. *Reference and simulated striking velocity*

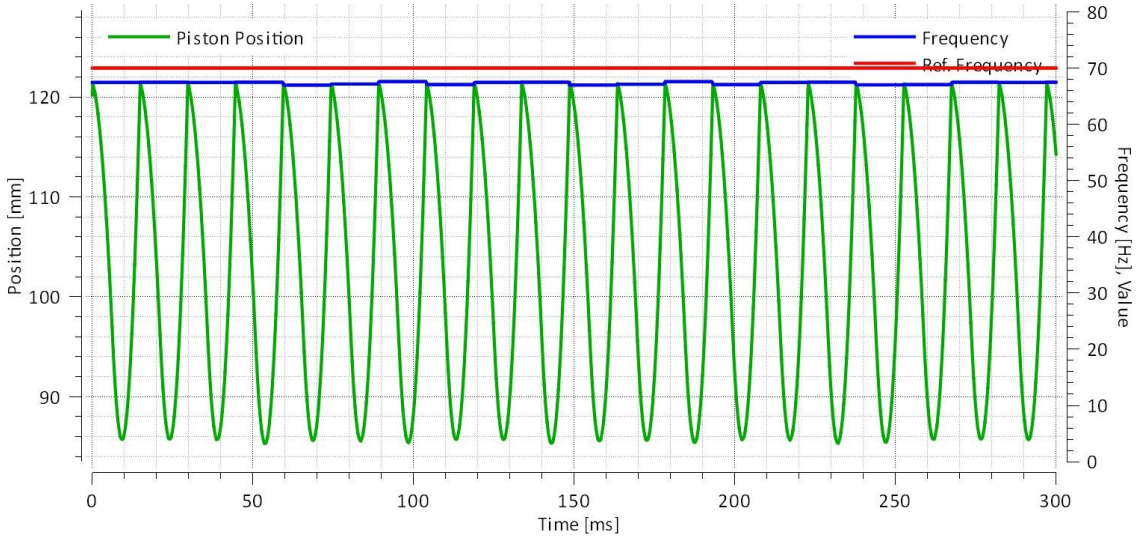

Figure 56. *Reference and Simulated Frequency*

5.2.6 Analysis

In figure 57, each marker represents a specific value of impact velocity and frequency. For instance, the brown marker represents the energy and frequency of the mechanism at 4 m/s and 40 Hz respectively in figure 57 while the brown marker shows the pressure and flowrate at same data in figure 58. The constant power lines are shown in the background of both figures.

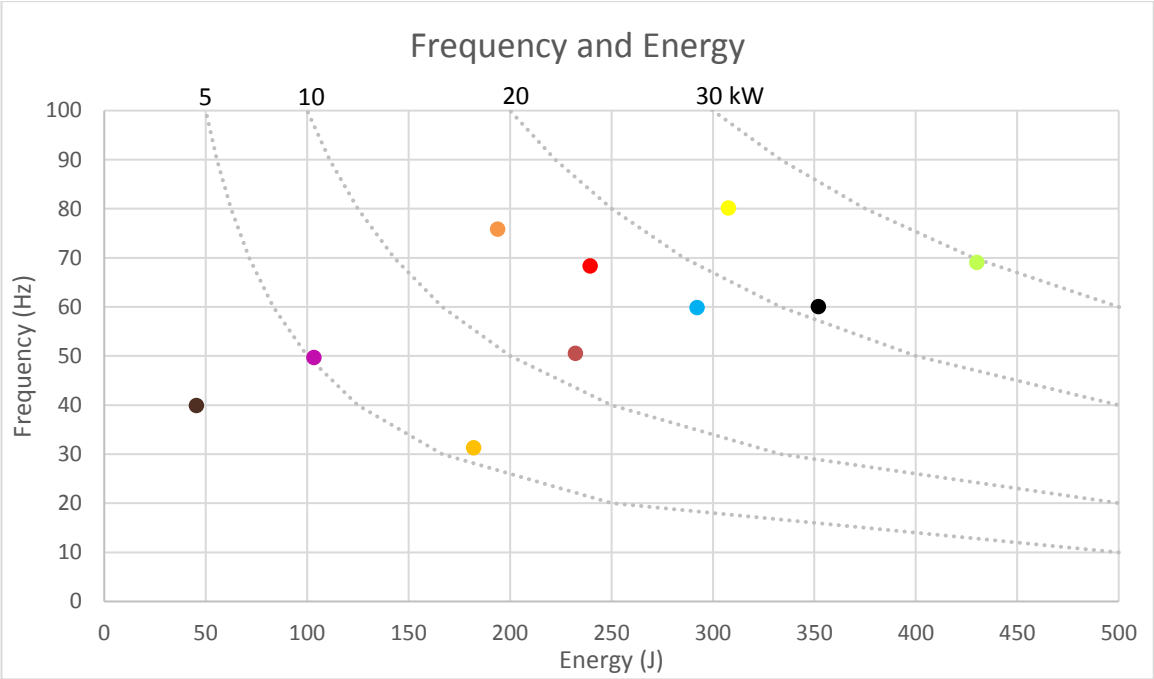

Figure 57. *System performance using reference velocity and frequency together*

The controller is performing normally for the simultaneous reference velocity and frequency. Several combinations of values were used to verify the performance of the system. The efficiency can be defined as the ratio between output power and input power. In this case the piston rebound is negligible, and the efficiency can be written as

$$\eta = \frac{E \cdot f}{P \cdot Q} \quad where\ E = \frac{m \cdot v_2^2}{2}$$

Where P is the supply pressure, Q is the flow rate, E is the impact energy and f is the frequency in above equation. Flow losses occur in valve openings, and compression losses in volumes with varying pressure. Other losses, such as leakage in the rock drill and supply system pressure drop are not considered, since it is a conceptual survey.

The efficiency value is in the range of 45-60 % for this analysis. The efficiency is lower for higher values of frequencies (more than 60 Hz). The best possible efficiency can be achieved with a reference frequency of 50 Hz and reference velocity 8-10 m/s.

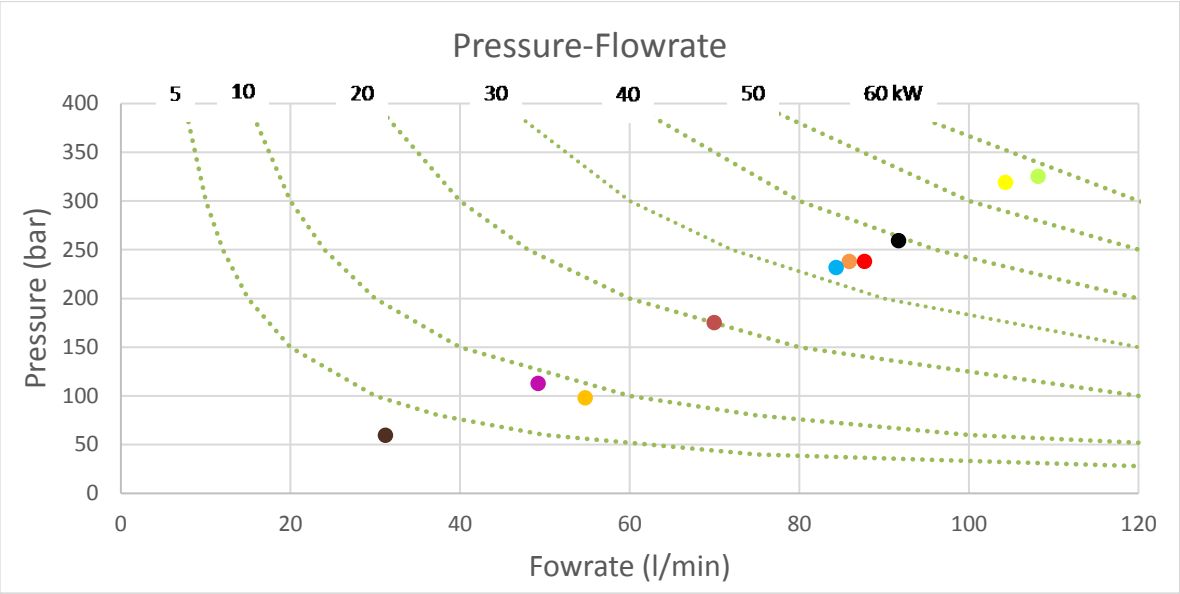

Figure 58. *Pressure flowrate variation with simultaneous reference velocity and frequency*

5.3 Controller Test with Changes in Reference Input

This section comprises the verification of the controller's tendency to cope with the variations in the reference input during the operation. Initial reference velocity and frequency values were set at 7 m/s and 40 Hz in the beginning. The increase in initial values was done by using a step input of 3 m/s and 10 Hz at 0.1 ms and 0.2 ms respectively. The controller considers these variations and smoothly switch to the new values such that the difference between reference and simulated values is minimal (see figure 59). The stroke length of the piston is changing accordingly to the variations in the reference values of velocity and frequency. This behavior is evident in figure 59 so that the increase in reference velocity results in a longer piston stroke. At the same time, there is a slight decrease in frequency due to change in piston stroke length, but the controller restores the frequency according to the reference and then the increase in reference frequency at 0.2 ms cause a shorter piston stroke. The changes in piston stroke and efficiency due to changes in reference velocity and frequency during the operation can be observed in table 8.

Table 8. Stroke and Efficiency variations with changes in reference velocity and frequency

Reference Velocity [m/s] & Frequency [Hz]	**Piston Stroke [mm]**	**Efficiency %**
7:40	35.1	55.4

10:40	48.6	63.4
10:50	39.2	56.8
9:45	40.4	70.6
6:45	27.8	53.5
6:35	25.3	64.6

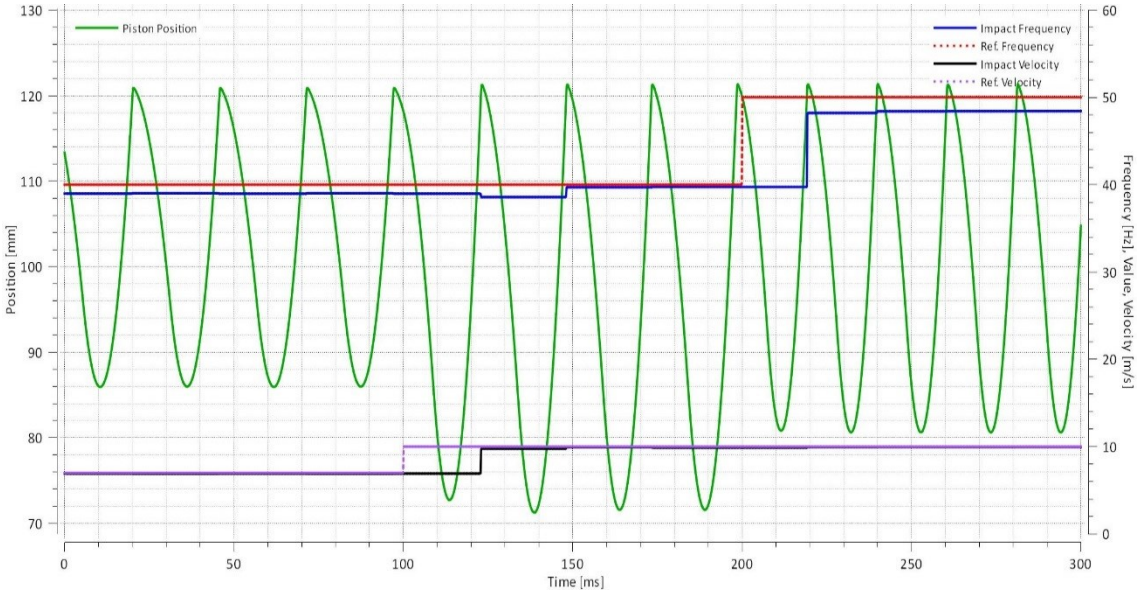

Figure 59. *Variation in piston stroke with increase in reference velocity and frequency*

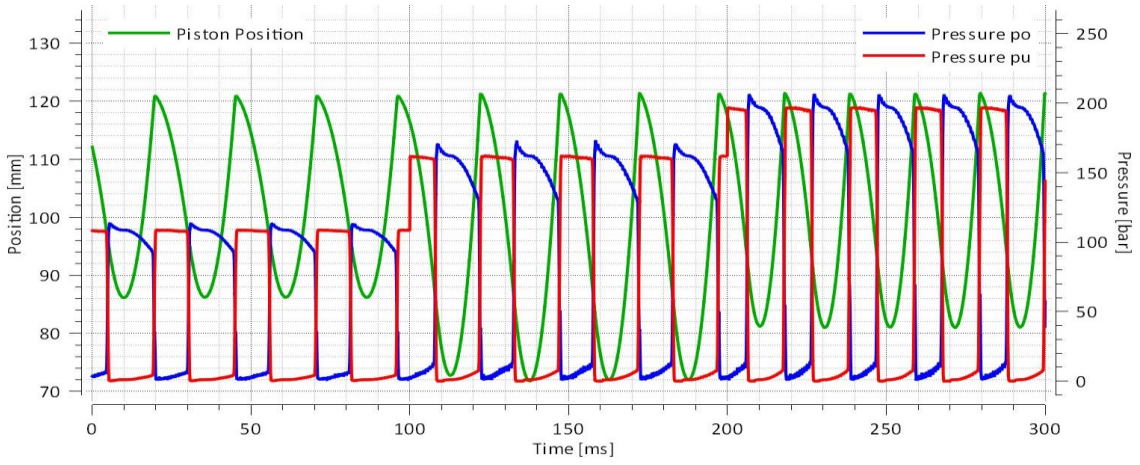

Figure 60. *Variation in percussion pressure as a result of increase in reference velocity and frequency*

Also, the variations in the reference input result in the controller to adjust the percussion pressure during the operation and figure 60 depicts smooth transition in percussion pressure during the variations. The controller changes twice the percussion pressure according to the increase in reference velocity and reference frequency at 0.1 ms and 0.2 ms respectively.

The same behavior can be observed in another way by decreasing the reference velocity and reference frequency during operation. Reference velocity and reference frequency were set initially at 9 m/s and 45 Hz respectively and decrease in these values was done from 9 m/s to 6 m/s and 45 Hz to 35 Hz at 0.1 ms and 0.2 ms respectively. The velocity and frequency obtained from simulation model were closely following the reference values as mentioned in the figure 61. First, a decline in velocity takes place at 0.1 ms causing the impact frequency to slightly decrease due to a change in piston stroke but the controller sooner restores back frequency to the reference frequency. It is clear (see figure 61) that decrease in reference velocity results in shorter piston stroke until there is a decrease in reference frequency at 0.2 ms causing an increase in piston stroke.

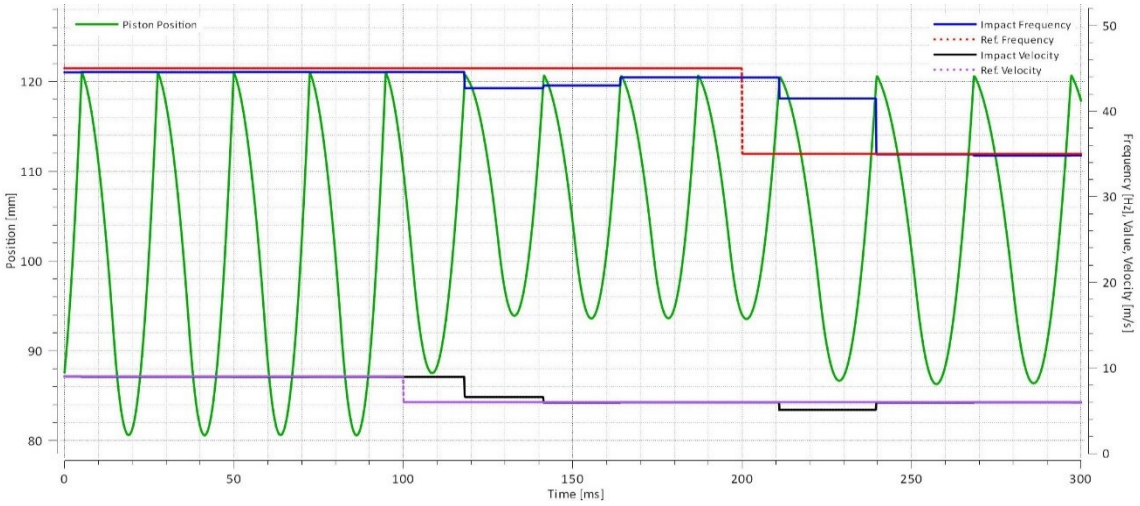

Figure 61. *Variations in piston stroke with increase in reference velocity and frequency*

The decrease in reference inputs effect the percussion pressure and the controller efficiently adjusts the percussion pressure according to new reference input values as presented in figure 62. The percussion pressure drops twice at 0.1 ms and 0.2 ms due to an effective drop in reference velocity and reference frequency respectively.

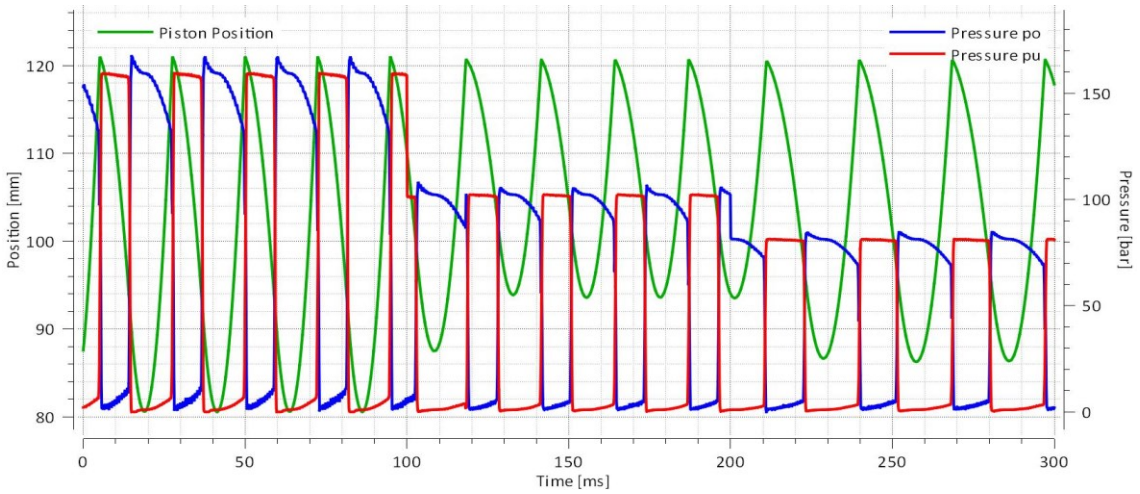

Figure 62. *Variations in percussion pressure due to decrease in the reference velocity and frequency*

5.4 Back-Hammering Operation

According to Gunnar [8], back-hammering is used when the drill steel is stuck in the drilled hole. Back-hammering is done in order to get the drill steel out from the hole if there is no drill steel extractor present at the front end of the hammer.

This section demonstrates the ability of the controller to adapt swiftly in case of back-hammering. The HOPSAN simulation model is tested with the same parameters as mentioned in section 5.3. The initial reference velocity and frequency was set at 10 m/s and 40 Hz respectively. The back-hammering caused the shank position 25 mm away from piston impact position at time 0.1 ms while the reference velocity was set to drop from 10 m/s to 6 m/s at time 0.1 ms to observe the behavior of the controller. The simulated velocity and frequency are closely following the reference velocity and frequency values respectively as shown in figure 63. The piston impact position changes from 120 m to 145 mm due to the change in shank position. The controller adjusts the piston position according to new shank position at 0.1 ms while there is a drop-in reference velocity at the same time. This decrease in velocity results in a shorter piston stroke and the increase in reference frequency (from 40 Hz to 50 Hz at 0.2 ms) further reduce the piston stroke. The variations in percussion pressure at time 0.1 ms and 0.2 ms are evident in the figure 64. The first pressure changes at 0.1 ms is due to the decrease in reference velocity while increase in reference frequency at 0.2 ms results in a small increase in the percussion pressure. It is important to note that there is a small decrease in frequency when we decrease the reference impact velocity (at 0.1 ms) but the controller restores it back to the reference value.

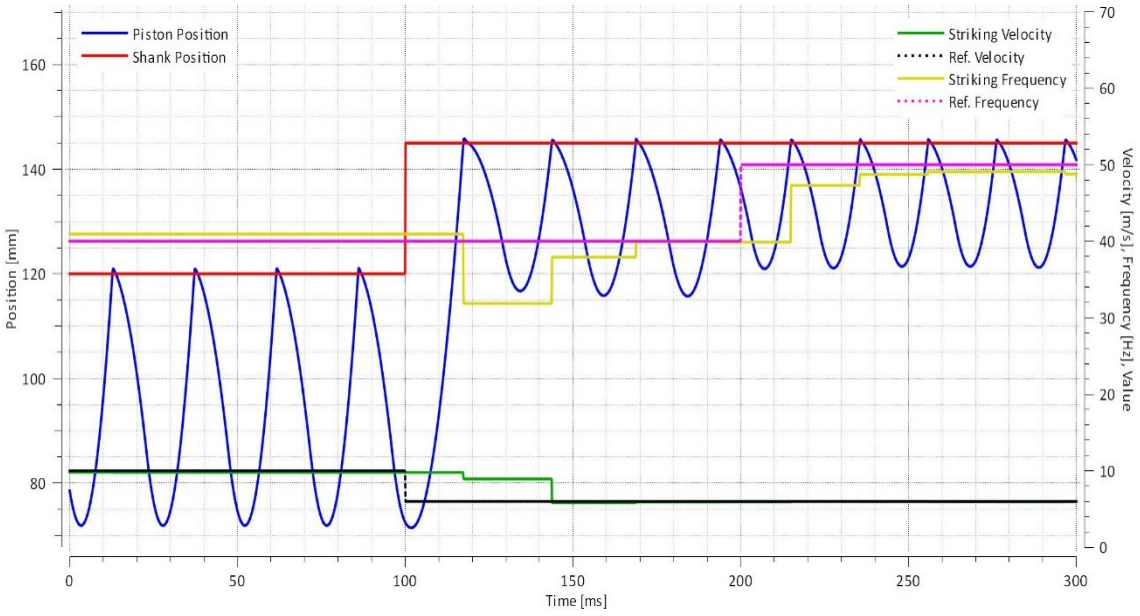

Figure 63. *Controller adjusting piston impact position in case of Back-Hammering*

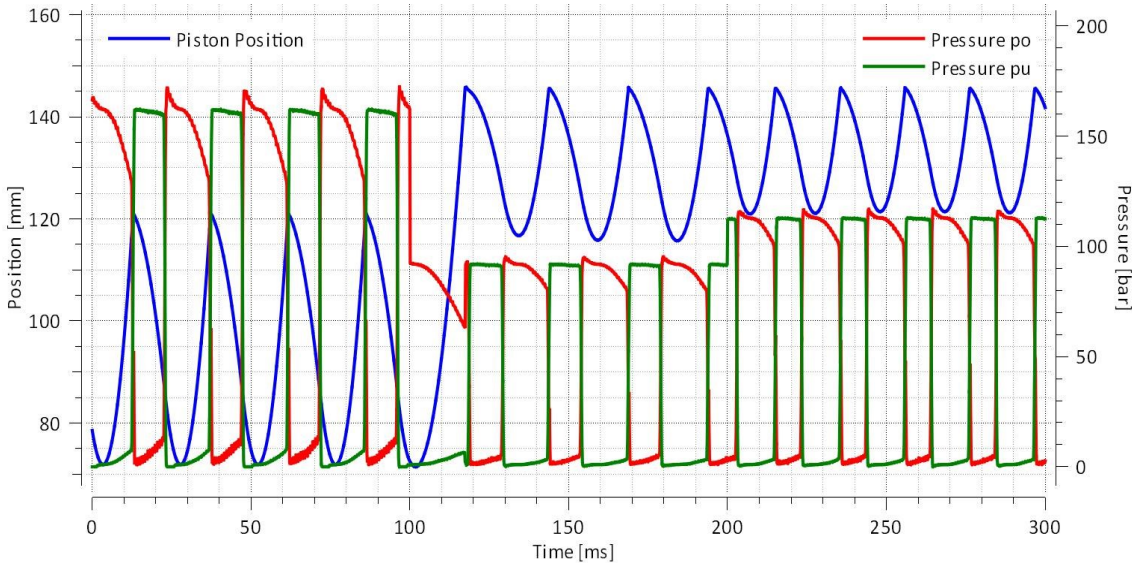

Figure 64. *Variations in percussion pressure due to Back-Hammering and change in reference impact velocity and frequency*

Advantage: Since the piston position is measured, the valve regulating control can easily be adopted to the new striking position. There is a hydraulic brake used to slow down the piston in case of back-hammering. With the possibility of controlling the impact velocity and frequency to adjust the piston stroke and percussion pressure, there is no need for the hydraulic brake.

5.5 Discussion

The rock drill simulation model was simplified, and the supply system was not included. The results therefore show an estimation of the possibilities that could be achieved using the concept. More detailed simulation models are normally used to determine geometry during rock drill development and agree well with measurements.

6. CONCLUSIONS

The master thesis has resulted in a conceptual design of an electrically controlled hydraulic rock drill. Electric control provides a great opportunity to control the percussion mechanism according to various demands. One important aspect was to investigate the performance range using different valve size and valve switching dynamics.

A simplified model of a rock drill with electric valves was used to study the performance during the development of controllers. Analytical models of piston motion were derived and utilized in the controller algorithms. The algorithm also comprised and compensated for delay in valve switching and valve flow losses.

The efficiency of the electrically controlled rock drill was comparable to a standard rock drill. The controller was capable to adjust the striking velocity during operation. Also, simultaneous control of frequency and velocity were achievable if also percussion pressure was controlled. The operational range was broad, both energy and frequency could be varied at least +/- 50%.

During drilling, the bit might get stuck. To come loose, the rock drill is fed backwards, and a reduced impact velocity is desired. Using the electric controller, this velocity reduction is easily provided without any need of piston hydraulic braking device.

To make a realistic design, a more detailed model of the drill and supply system must be utilized. Then laboratory tests can be done, verifying the performance. One scope would be to adopt energy and frequency to rock conditions. Also, robustness of valve, and piston measurement must be improved.

7. REFERENCES

1. Epiroc Photo Archive, https://www.atlascopco.com/content/products/sv/mrba/drill-rigs/face-drill-rigs/face-drill-rigs/boomer-282.html

2. Gunnar Wijk, Percussive Rock Drilling, Epiroc Rock Drills AB

3. Gunnar Wijk (1996), Total Rock Drilling Technology, Orebro, Atlas Copco Rock Drills AB

4. Johan Aleberg, Andreas Wiberg (2007), Designing a Hydraulic Energy Absorber for Endurance Tests of Percussive Rock Drills

5. Thesis Problem Statement, Epiroc Document

6. J. L. Meriam, L. G. Kraige. Engineering Mechanics Dynamics (7th Edition)

7. User's guide to HOPSAN

8. Gunnar Wijk, Hammer Theory and Practice, Epiroc Rock Drills AB

9. Terralog Technologies Inc (USA), Fundamental Research on Percussion Drilling: Improved rock mechanics analysis, advanced simulation technology, and full-scale laboratory investigations, Final Report 2nd Edition, pp 18-19.

10. Tuomas G., Nordell B (2000). Down-Hole Water Driven Hammer Drilling for BTES Applications. Proc. Terrastock 2000, 8th International Conference on Thermal Energy Storage, August 28-September 1, 2000, Stuttgart, Germany.

11. Johannes Reuter, Sebastian Maerkl & Matthias Jaekle (2010) Optimized Control Strategies for Fast Switching Solenoid Valves, International Journal of Fluid Power, 11:3, 23-33.

12. David T. Branson III, John H. Lumkes Jr., Kitti Wattananithiporn & Frank J. Fronczak (2008) Simulated and Experimental Results for a Hydraulic Actuator Controlled by two High-Speed on\off Solenoid Valves, International Journal of Fluid Power, 9:2, 47-56.

13. M. Hyvönen, Modelling of Fluid Power Components, Course Study Guide, unpublished, Laboratory of Automation and Hydraulics (AUT), Tampere University of Technology, Tampere, Finland, 2015.

14. Formelsamling, Hydraulik och Pneumatik. Ämnesområdet hydraulik och pneumatik. Institutionen för Konstrucktions och Productionsteknik, Linköping Tekniska Högskola

15. Epiroc Photo Archive, Types of rock drilling

16. Epiroc Photo Archive, Main components in a rock drill

17. Epiroc Photo Archive, Top Hammer Drill

8. APPENDICIES

Appendix I: Percussion Mechanism

8.1 Derivation of Analytical equations for Piston Position

$$\int a \cdot ds = \int v \cdot dv \qquad (I.1)$$

- **Start of piston return movement from $x_p = 0 \rightarrow z$**

$$\int_0^z a \cdot ds = \int_{Rv_2}^{v_1} v \cdot dv$$

$$\frac{v_1^2}{2} - \frac{(Rv_2)^2}{2} = \frac{PA_1}{m}(z - 0)$$

$$v_1^2 = (Rv_2)^2 + 2\frac{PA_1}{m}z$$

$$v_1 = \sqrt{(Rv_2)^2 + 2\frac{PA_1 z}{m}} \qquad (I.2)$$

$$v_1 = Rv_2 + \frac{PA_1}{m}t_1$$

$$t_1 = \frac{m(v_1 - Rv_2)}{PA_1}$$

- **Deceleration from $x_p = z \rightarrow z + z_2$**

Using equation (A), we get

$$\int_z^{z+z_2} a \cdot ds = \int_{v_1}^{0} v \cdot dv$$

$$0 - \frac{v_1^2}{2} = -\frac{PA_2}{m}(z + z - z_2)$$

$$0 = v_1^2 - 2\frac{PA_2}{m}z_2$$

$$z_2 = \frac{mv_1^2}{2PA_2} \qquad (I.3)$$

$$0 = v_1 - \frac{PA_2}{m} t_2$$

$$t_2 = \frac{mv_1}{PA_2}$$

- **Piston motion from start to stroke position, $x_p = z+z_2 \rightarrow 0$**

Putting the limits in equation (A), we have

$$\int_{z+z_2}^{z} a \cdot ds = \int_{0}^{v_2} v \cdot dv$$

$$v_2^2 - 0^2 = 2\frac{PA_2}{m}(z + z_2)$$

$$v_2 = \sqrt{\frac{2PA_2(z + z_2)}{m}} \qquad (I.4)$$

$$v_2 = 0 + \frac{PA_2}{m} t_3$$

$$t_3 = \frac{mv_2}{PA_2}$$

Putting the value of z_2 and v_2 from equation I. 2 and I. 3 in equation I. 1, so that

$$v_1^2 = R^2 \left(\frac{2PA_2 \left(z + \frac{mv_1^2}{2PA_2} \right)}{m} \right) + 2\frac{PA_1}{m} z$$

$$v_1^2 = R^2 \left(\frac{2PA_2 z + mv_1^2}{m} \right) + 2\frac{PA_1}{m} z$$

$$v_1^2 = R^2 \left(\frac{2PA_2 z}{m} + v_1^2 \right) + 2\frac{PA_1}{m} z$$

$$v_1^2 = \frac{2R^2 PA_2 z}{m} + Rv_1^2 + \frac{2PA_1 z}{m}$$

$$v_1^2 - R^2 v_1^2 = \frac{2Pz}{m}(R^2 A_2 + A_1)$$

$$v_1^2(1-R^2) = \frac{2Pz}{m}(R^2A_2 + A_1)$$

$$v_1^2 = \frac{2Pz(R^2A_2 + A_1)}{m(1-R^2)}$$

$$v_1 = \sqrt{\frac{2Pz(A_1 + R^2A_2)}{m(1-R^2)}} \qquad (I.5)$$

8.2 Analytical equations including Delay

- **Piston position, xp = 0→ z_3**
  Applying limits to equation (A), we have

$$\int_0^{z_3} a \cdot ds = \int_{v_3}^{v_2} v \cdot dv$$

$$\frac{v_2^2}{2} - \frac{v_3^2}{2} = \frac{PA_2}{m} z_3$$

$$\frac{m}{2PA_2}(v_2^2 - v_3^2) = z_3 \qquad (I.6)$$

$$S_y - S_x = v_x t_{xy} + \frac{at_{xy}^2}{2}$$

Solving above equation, so that we have equation of v_3,

$$z_3 - 0 = v_3 t_d + \frac{at_d^2}{2}$$

$$z_3 = v_3 t_d + \frac{PA_2 t_d^2}{2\,m} \qquad (I.7)$$

Putting the value of z_3 in equation 3.5, we get

$$\frac{m}{2PA_2}(v_2^2 - v_3^2) = v_3 t_d + \frac{PA_2 t_d^2}{2\,m}$$

$$v_2^2 - v_3^2 = \frac{2PA_2 t_d v_3}{m} + \frac{2PA_2}{m}\frac{PA_2 t_d^2}{2\,m}$$

$$v_2^2 = v_3^2 + \frac{2PA_2t_dv_3}{m} + \frac{P^2{A_2}^2t_d^2}{m^2}$$

$$v_2^2 = \left(v_3^2 + \frac{PA_2t_d}{m}\right)^2$$

$$v_2 = v_3 + \frac{PA_2t_d}{m}$$

$$v_3 = v_2 - \frac{PA_2t_d}{m} \qquad (I.8)$$

- **Piston position, xp = $z_4 \rightarrow z_4+z_1$**
  Applying limits to equation (A), we have

$$\int_{z_4}^{z_4+z_1} a \cdot ds = \int_{v_4}^{v_1} v \cdot dv$$

$$\frac{PA_1}{m}(z_4 + z_1 - z_4) = \frac{v_1^2}{2} - \frac{v_4^2}{2}$$

$$z_1 = \frac{m}{2PA_1}(v_1^2 - v_4^2) \qquad (I.9)$$

Solving 3.8 and 3.3, we have the values of v_4,

$$z_4 + z_1 - z_4 = v_4t_d + \frac{at_d^2}{2}$$

$$z_1 = v_4t_d + \frac{PA_1t_d^2}{2\,m} \qquad (I.10)$$

Putting the value of z_1 in equation 3.8, we get

$$\frac{m}{2PA_1}(v_1^2 - v_4^2) = v_4t_d + \frac{PA_1t_d^2}{2\,m}$$

$$v_1^2 - v_4^2 = \frac{2PA_1t_dv_4}{m} + \frac{2PA_1}{m}\frac{PA_1t_d^2}{2\,m}$$

$$v_1^2 = v_4^2 + \frac{2PA_1t_dv_4}{m} + \frac{P^2{A_1}^2t_d^2}{m^2}$$

$$v_1^2 = \left(v_4^2 + \frac{PA_1t_d}{m}\right)^2$$

$$v_1 = v_4 + \frac{PA_1 t_d}{m}$$

$$v_4 = v_1 - \frac{PA_1 t_d}{m} \qquad (I.11)$$

8.3 Analytical equations including Pressure Losses

We know from equation I.1,

$$\int a \cdot ds = \int v \cdot dv$$

First, we derive the equations for z, z_2 and v_1 by taking into account the pressure losses and valve dynamics.

- **Piston position, xp = 0→ z**

$$\int_0^z a \cdot ds = \int_{Rv_2}^{v_1} v \cdot dv$$

$$\frac{v_1^2}{2} - \frac{(Rv_2)^2}{2} = \frac{[(P - \Delta P_1) \cdot A_1 - \Delta P_2 \cdot A_2] \cdot z}{m}$$

In this case, the pressure losses can be defined as

$$\Delta P_1 = \left(\frac{v_\mathrm{p} \cdot A_1 \cdot \sqrt{\rho}}{2 \cdot C_q \cdot A_v}\right)^2$$

$$\Delta P_2 = \left(\frac{v_\mathrm{p} \cdot A_2 \cdot \sqrt{\rho}}{2 \cdot C_q \cdot A_v}\right)^2$$

It is assumed that during the piston motion from shank to position z and then z_2, the approximated flow will be according to the piston velocity defined below.

$$v_p = \frac{v_1}{\sqrt{2}}$$

We can define constant terms in above equation as new constant K,

$$K = \left(\frac{\sqrt{\rho}}{2 \cdot C_q \cdot A_v}\right)^2$$

So, we can write pressure loss in this case as

$$\Delta P_1 = K \cdot v_1^2 \cdot A_1^2$$

$$\Delta P_2 = K \cdot v_1^2 \cdot A_2^2$$

Then we can write,

$$\frac{v_1^2}{2} - \frac{(Rv_2)^2}{2} = \frac{[(P - K \cdot v_1^2 \cdot A_1^2) \cdot A_1 - K \cdot v_1^2 \cdot A_2^2 \cdot A_2] \cdot z}{m} \qquad (I.12)$$

Now, we use the following equation to find the time taken to reach the position z by the piston, we have

$$S_y - S_x = v_x t_{xy} + \frac{a t_{xy}^2}{2}$$

$$z = R \cdot v_2 \cdot T_1 + \frac{[(P - \Delta P_1) \cdot A_1 - \Delta P_2 \cdot A_2] \cdot T_1^2}{2 \cdot m}$$

Putting the value of z in I.12, we get the value of time T_1

$$T_1 = \frac{m \cdot (v_1 - R \cdot v_2)}{P \cdot A_1 - K \cdot A_1^3 \cdot v_1^2 - K \cdot A_2^3 \cdot v_1^2} \qquad (I.13)$$

- **Piston position, xp = z→z+z_2**

$$\int_{z}^{z+z_2} a \cdot ds = \int_{v_1}^{0} v \cdot dv$$

$$0 - \frac{v_1^2}{2} = -\frac{[(P + \Delta P_2) \cdot A_2] \cdot (z + z - z_2)}{m}$$

$$0 = v_1^2 - 2\frac{[(P + \Delta P_2) \cdot A_2] \cdot z_2}{m}$$

$$z_2 = \frac{m \cdot v_1^2}{2 \cdot [(P + \Delta P_2) \cdot A_2]}$$

Then we can write,

$$z_2 = \frac{m \cdot v_1^2}{2 \cdot [(P + K \cdot v_1^2 \cdot A_2^2) \cdot A_2]} \qquad (I.14)$$

Now, we use the following equation to find the time taken to reach the position z_2 by the piston, we have

$$S_y - S_x = v_x t_{xy} + \frac{a t_{xy}^2}{2}$$

$$z_2 = v_1 \cdot T_2 + \frac{[(P + \Delta P_2) \cdot A_2] \cdot T_2^2}{2 \cdot m}$$

Putting the value of z_2 in I.14, we get the value of time T_2

$$T_2 = \frac{m \cdot v_1}{P \cdot A_2 + K \cdot A_2^3 \cdot v_1^2} \qquad (I.15)$$

- **Piston position, xp = z+z_2→0**

$$\int_{z+z_2}^{z} a \cdot ds = \int_{0}^{v_2} v \cdot dv$$

$$v_2^2 - 0^2 = 2\frac{[(P - \Delta P_{2i}) \cdot A_2 - \Delta P_{1i} \cdot A_1] \cdot (z + z_2)}{m}$$

$$v_2 = \sqrt{\frac{2 \cdot [(P - \Delta P_{2i}) \cdot A_2 - \Delta P_{1i} \cdot A_1] \cdot (z + z_2)}{m}}$$

Here the pressure loss equation will be

$$\Delta P_{1i} = \left(\frac{v_2 \cdot A_1 \cdot \sqrt{\rho}}{2 \cdot C_q \cdot A_v}\right)^2$$

$$\Delta P_{2i} = \left(\frac{v_2 \cdot A_2 \cdot \sqrt{\rho}}{2 \cdot C_q \cdot A_v}\right)^2$$

It is assumed that during the piston motion from position z_2 to shank, the approximated flow will be according to the piston velocity defined below.

$$v_p = \frac{v_2}{\sqrt{2}}$$

Therefore, the equation

$$v_2 = \sqrt{\frac{2 \cdot [(P - K \cdot v_2^2 \cdot A_2^2) \cdot A_2 - K \cdot v_2^2 \cdot A_1^3] \cdot (z + z_2)}{m}} \qquad (I.16)$$

Now, we use the following equation to find the time taken to reach the strike position by the piston, we have

$$S_y - S_x = v_x t_{xy} + \frac{a t_{xy}^2}{2}$$

$$z + z_2 = \frac{[(P - K \cdot v_2^2 \cdot A_2^2) \cdot A_2 - K \cdot v_2^2 \cdot A_1^3] \cdot T_3^2}{2.m}$$

Putting the value of $z+z_2$ in equation I.16, we get the value of time T_3

$$T_3 = \frac{m \cdot v_2}{P \cdot A_2 - K \cdot v_2^2 \cdot A_2^3 - K \cdot v_2^2 \cdot A_1^3} \qquad (I.17)$$

Solving equations I.12, I.14 and I.16 together provide the equations of z, z_2 and v_1 as follows I.18, I.19, I.20 for piston position z, z_2 and velocity v_1 respectively.

$$z = -\frac{m \cdot (\sqrt{K^4 \cdot R^4 \cdot A_1^4 \cdot A_2^6 \cdot v_2^8 - 2 \cdot K^4 \cdot R^4 \cdot A_1^2 \cdot A_2^8 \cdot v_2^8 + K^4 \cdot R^4 \cdot A_2^{10} \cdot v_2^8} -}{4 \cdot K^2 \cdot P \cdot A_1^4 \cdot A_2^2 \cdot v_2^2 + 12 \cdot K^2 \cdot P \cdot A_1^3 \cdot A_2^3 \cdot v_2^2 +} \ldots$$

$$\ldots \frac{\sqrt{2 \cdot K^3 \cdot P \cdot R^4 \cdot A_1^3 \cdot A_2^5 \cdot v_2^6 + 2 \cdot K^3 \cdot P \cdot R^4 \cdot A_1^2 \cdot A_2^6 \cdot v_2^6 + 2 \cdot K^3 \cdot P \cdot R^4 \cdot A_1 \cdot A_2^7 \cdot v_2^6}}{4 \cdot K^2 \cdot P \cdot A_1^2 \cdot A_2^4 \cdot v_2^2 - 4 \cdot K^2 \cdot P \cdot A_1 \cdot A_2^5 \cdot v_2^2 -} \ldots$$

$$\ldots \frac{\sqrt{-2 \cdot K^3 \cdot P \cdot R^4 \cdot A_2^8 \cdot v_2^6 - 6 \cdot K^3 \cdot P \cdot R^2 \cdot A_1^5 \cdot A_2^3 \cdot v_2^6 - 18 \cdot K^3 \cdot P \cdot R^2 \cdot A_1^4 \cdot A_2^4 \cdot v_2^6 -}}{4 \cdot K \cdot P^2 \cdot A_1^3 \cdot A_2 - 8 \cdot K \cdot P^2 \cdot A_1^2 \cdot A_2^2 + 4 \cdot K \cdot P^2 \cdot A_1 \cdot A_2^3} \ldots$$

$$\ldots \frac{\sqrt{8 \cdot K^3 \cdot P \cdot R^2 \cdot A_1^3 \cdot A_2^5 \cdot v_2^6 + 4 \cdot K^3 \cdot P \cdot R^2 \cdot A_1^2 \cdot A_2^6 \cdot v_2^6 - 2 \cdot K^3 \cdot P \cdot R^2 \cdot A_1 \cdot A_2^7 \cdot v_2^6}}{-} \ldots$$

$$\ldots \frac{\sqrt{-2 \cdot K^3 \cdot P \cdot R^2 \cdot A_2^8 \cdot v_2^6 + K^2 \cdot P^2 \cdot R^4 \cdot A_1^2 \cdot A_2^4 \cdot v_2^4 - 2 \cdot K^2 \cdot P^2 \cdot R^4 \cdot A_1 \cdot A_2^5 \cdot v_2^4 +}}{-} \ldots$$

$$\ldots \frac{\sqrt{K^2 \cdot P^2 \cdot R^4 \cdot A_2^6 \cdot v_2^4 + 10 \cdot K^2 \cdot P^2 \cdot R^2 \cdot A_1^4 \cdot A_2^2 \cdot v_2^4 + 22 \cdot K^2 \cdot P^2 \cdot R^2 \cdot A_1^3 \cdot A_2^3 \cdot v_2^4 -}}{-} \ldots$$

$$\ldots \frac{\sqrt{2 \cdot K^2 \cdot P^2 \cdot R^2 \cdot A_1^2 \cdot A_2^4 \cdot v_2^4 - 2 \cdot K^2 \cdot P^2 \cdot R^2 \cdot A_1 \cdot A_2^5 \cdot v_2^4 + 4 \cdot K^2 \cdot P^2 \cdot R^2 \cdot A_2^6 \cdot v_2^4 +}}{-} \ldots$$

$$\frac{\sqrt{K^2 \cdot P^2 \cdot A_1^6 \cdot v_2^4 + 6 \cdot K^2 \cdot P^2 \cdot A_1^5 \cdot A_2 \cdot v_2^4 + 7 \cdot K^2 \cdot P^2 \cdot A_1^4 \cdot A_2^2 \cdot v_2^4 - 4 \cdot K^2 \cdot P^2 \cdot A_1^3 \cdot A_2^3 \cdot v_2^4}}{-} \ldots$$

$$\ldots \frac{\sqrt{+3 \cdot K^2 \cdot P^2 \cdot A_1^2 \cdot A_2^4 \cdot v_2^4 + 6 \cdot K^2 \cdot P^2 \cdot A_1 \cdot A_2^5 \cdot v_2^4 + K^2 \cdot P^2 \cdot A_2^6 \cdot v_2^4 -}}{-} \ldots$$

$$\ldots\frac{\sqrt{4\cdot K\cdot P^3\cdot R^2\cdot A_1^3\cdot A_2\cdot v_2^2-6\cdot K\cdot P^3\cdot R^2\cdot A_1^2\cdot A_2^2\cdot v_2^2+4\cdot K\cdot P^3\cdot R^2\cdot A_1\cdot A_2^3\cdot v_2^2-}}{-}\ldots$$

$$\ldots\frac{\sqrt{2\cdot K\cdot P^3\cdot R^2\cdot A_2^4\cdot v_2^2-2\cdot K\cdot P^3\cdot A_1^4\cdot v_2^2-4\cdot K\cdot P^3\cdot A_1^3\cdot A_2\cdot v_2^2-8\cdot K\cdot P^3\cdot A_1\cdot A_2^3\cdot v_2^2}}{-}\ldots$$

$$\ldots\frac{\sqrt{2\cdot K\cdot P^3\cdot A_2^4\cdot v_2^2+P^4\cdot A_1^2+2\cdot P^4\cdot A_1\cdot A_2+P^4\cdot A_2^2)}-P^2\cdot A_2-P^2\cdot A_1-}{-}\ldots$$

$$\ldots\frac{K^2\cdot R^2\cdot A_2^5\cdot v_2^4+K\cdot P\cdot A_1^3\cdot v_2^4+K\cdot P\cdot A_2^3\cdot v_2^4+K^2\cdot R^2\cdot A_1^2\cdot A_2^3\cdot v_2^4+}{-}\ldots$$

$$\ldots\frac{K\cdot P\cdot R^2\cdot A_2^3\cdot v_2^4+K\cdot P\cdot A_1\cdot A_2^2\cdot v_2^2+3\cdot K\cdot P\cdot A_1^2\cdot A_2\cdot v_2^2-K\cdot P\cdot R^2\cdot A_1\cdot A_2^2\cdot v_2^2}{-}$$

If we ignore the terms with rebound coefficient R, we have

$$z=-\frac{m\cdot(\sqrt{K^2\cdot P^2\cdot A_1^6\cdot v_2^4+6\cdot K^2\cdot P^2\cdot A_1^5\cdot A_2\cdot v_2^4+7\cdot K^2\cdot P^2\cdot A_1^4\cdot A_2^2\cdot v_2^4-}}{4\cdot K^2\cdot P\cdot A_1^4\cdot A_2^2\cdot v_2^2+12\cdot K^2\cdot P\cdot A_1^3\cdot A_2^3\cdot v_2^2+}$$

$$\ldots\frac{\sqrt{4\cdot K^2\cdot P^2\cdot A_1^3\cdot A_2^3\cdot v_2^4+3\cdot K^2\cdot P^2\cdot A_1^2\cdot A_2^4\cdot v_2^4+6\cdot K^2\cdot P^2\cdot A_1\cdot A_2^5\cdot v_2^4+}}{4\cdot K^2\cdot P\cdot A_1^2\cdot A_2^4\cdot v_2^2-4\cdot K^2\cdot P\cdot A_1\cdot A_2^5\cdot v_2^2-}\ldots$$

$$\ldots\frac{\sqrt{K^2\cdot P^2\cdot A_2^6\cdot v_2^4-2\cdot K\cdot P^3\cdot A_1^4\cdot v_2^2-4\cdot K\cdot P^3\cdot A_1^3\cdot A_2\cdot v_2^2-8\cdot K\cdot P^3\cdot A_1\cdot A_2^3\cdot v_2^2}}{4\cdot K\cdot P^2\cdot A_1^3\cdot A_2-8\cdot K\cdot P^2\cdot A_1^2\cdot A_2^2+4\cdot K\cdot P^2\cdot A_1\cdot A_2^3}\ldots$$

$$\ldots\frac{\sqrt{-2\cdot K\cdot P^3\cdot A_1^4\cdot v_2^2-4\cdot K\cdot P^3\cdot A_1^3\cdot A_2\cdot v_2^2-8\cdot K\cdot P^3\cdot A_1\cdot A_2^3\cdot v_2^2}}{-}\ldots$$

$$\ldots\frac{\sqrt{2\cdot K\cdot P^3\cdot A_2^4\cdot v_2^2+P^4\cdot A_1^2+2\cdot P^4\cdot A_1\cdot A_2+P^4\cdot A_2^2)}-P^2\cdot A_2-P^2\cdot A_1}{-}\ldots$$

$$\ldots\frac{+K\cdot P\cdot A_1^3\cdot v_2^4+K\cdot P\cdot A_2^3\cdot v_2^4+K\cdot P\cdot A_1\cdot A_2^2\cdot v_2^2+3\cdot K\cdot P\cdot A_1^2\cdot A_2\cdot v_2^2}{-}$$

Equation of z_2:

$$z_2=\frac{2\cdot z\cdot P\cdot A_1\cdot m+m\cdot R^2\cdot v_2^2}{2\cdot(2\cdot K\cdot P\cdot z\cdot A_1^3\cdot A_2-K\cdot m\cdot R^2\cdot v_2^2\cdot A_2^3-2\cdot K\cdot P\cdot z\cdot A_1\cdot A_2^3+2\cdot K\cdot P\cdot z\cdot A_2^4+P\cdot m\cdot A_2)}$$

Equation of v_1:

$$v_1 = \frac{\sqrt{(m \cdot R^2 \cdot v_2^2 + 2 \cdot P \cdot z \cdot A_1) \cdot (2 \cdot z \cdot K \cdot A_1^3 - 2 \cdot z \cdot K \cdot A_2^2 + m)}}{(2 \cdot z \cdot K \cdot A_1^3 - 2 \cdot z \cdot K \cdot A_2^3 + m)}$$

Frequency equation:

$$f = \frac{1}{T_1 + T_2 + T_3}$$

8.4 Analytical equations including Valve Dynamics and Pressure Losses

Now we can calculate the pressure losses by taking into account the opening and closing delay property of the valve. Thus, we derive equations for piston position point z_3 and z_4, along with velocities v_3 and v_4 at these positions.

- **Piston position, xp = 0→ z_3**
  Applying limits to equation (I.1), we have

$$\int_0^{z_3} a \cdot ds = \int_{v_3}^{v_2} v \cdot dv$$

$$\frac{v_2^2}{2} - \frac{v_3^2}{2} = \frac{[(P - \Delta P_{2i}) \cdot A_2 - \Delta P_{1i} \cdot A_1]}{m} z_3 \qquad (I.21)$$

The general form of pressure losses is

$$\Delta P = \left(\frac{\mathrm{v}_p \cdot \mathrm{A}_p \cdot \sqrt{\rho}}{\sqrt{2} \cdot C_q \cdot A_v} \right)^2$$

The piston velocity in this case will be derived according to the following equation,

$$v_p = \frac{v_2 + \frac{2}{3} \cdot v_2}{2}$$

Here pressure losses will be

$$\Delta P_{1i} = K \cdot v_2^2 \cdot A_1^2$$

$$\Delta P_{2i} = K \cdot v_2^2 \cdot A_2^2$$

Now,

$$S_y - S_x = v_x t_{xy} + \frac{a \cdot t_{xy}^2}{2}$$

Solving above equation, so that we have equation of v_3,

$$z_3 - 0 = v_3 \cdot t_d + \frac{a \cdot t_d^2}{2}$$

$$z_3 = v_3 \cdot t_d + \frac{[(P - \Delta P_{2i}) \cdot A_2 - \Delta P_{1i} \cdot A_1]}{m} t_d^2 \qquad (I.22)$$

Putting the value of z_3 in equation I.21, we get

$$v_3 = v_2 - \frac{[(P - \Delta P_{2i}) \cdot A_2 - \Delta P_{1i} \cdot A_1] \cdot t_d}{m} \qquad (I.23)$$

- **Piston position, xp = $z_4 \rightarrow z_4 + z_1$**
  Applying limits to equation (A), we have

$$\int_{z_4}^{z_4+z_1} a \cdot ds = \int_{v_4}^{v_1} v \cdot dv$$

$$\frac{[(P - \Delta P_1) \cdot A_1 - \Delta P_2 \cdot A_2] \cdot (z_4 + z_1 - z_4)}{m} = \frac{v_1^2}{2} - \frac{v_4^2}{2}$$

$$z_1 = \frac{m \cdot (v_1^2 - v_4^2)}{2[(P - \Delta P_1) \cdot A_1 - \Delta P_2 \cdot A_2]} \qquad (I.24)$$

The piston velocity in this case will be derived according to the following equation,

$$v_p = \frac{v_1 + \frac{2}{3} \cdot v_1}{2}$$

Here pressure losses will be

$$\Delta P_1 = K \cdot v_1^2 \cdot A_1^2$$

$$\Delta P_2 = K \cdot v_1^2 \cdot A_2^2$$

Now we solve the equation given below, so we have the values of v_4,

$$S_y - S_x = v_x t_{xy} + \frac{a \cdot t_{xy}^2}{2}$$

$$z_4 + z_1 - z_4 = v_4 t_d + \frac{a \cdot t_d^2}{2}$$

$$z_1 = v_4.t_d + \frac{[(P - \Delta P_1) \cdot A_1 - \Delta P_2 \cdot A_2] \cdot t_d^2}{2\,m} \qquad (I.25)$$

Putting the value of z_1 in equation I.24, we get

$$v_4 = v_1 - \frac{[(P - \Delta P_1) \cdot A_1 - \Delta P_2 \cdot A_2] \cdot t_d}{m} \qquad (I.26)$$

$$z_4 = z - z_1 \qquad (I.28)$$

Equation for Frequency:

The equation for frequency will be modified after adding the pressure losses and valve dynamics. So we can write

$$f = \frac{1}{T_1 + T_2 + T_3 + 2 \cdot t_d} \qquad (I.28)$$